Generation of an *in vitro* embryo model based on cellular reprogramming paradigms in embryonic stem cells

Dissertation

zur

Erlangung des Doktorgrades (Dr. rer. nat.)

der

Mathematisch-Naturwissenschaftlichen Fakultät

der

Rheinischen Friedrich-Wilhelms-Universität Bonn

vorgelegt von

Jan Michael Langkabel

aus

Köln-Porz

Bonn, 2021

Angefertigt mit Genehmigung der Mathematisch-Naturwissenschaftlichen Fakultät der Rheinischen Friedrich-Wilhelms-Universität Bonn

1. Gutachter: Prof. Dr. Hubert Schorle
2. Gutachterin: Prof. Dr. Marieta Toma
Tag der Promotion: 20.05.2022
Erscheinungsjahr: 2022

Eidesstattliche Erklärung

Hiermit versichere ich, dass diese Dissertation von mir selbst und ohne unerlaubte Hilfe angefertigt wurde. Es wurden keine anderen als die angegebenen Hilfsmittel benutzt. Ferner erkläre ich, dass die vorliegende Arbeit an keiner anderen Universität als Dissertation eingereicht wurde.

Teile dieser Arbeit wurden bereits oder werden in folgenden Originalpublikationen veröffentlicht:

Langkabel, J., Horne, A., Bonaguro, L., Holsten, L. Hesse, T., Knaus, A., Riedel, Y., Becker, M., Händler, K., Elmzzahi, T., Bassler, K., Reusch, N., Yeghiazarian, L.H., Pecht, T., Saglam, A., Ulas, T., Aschenbrenner, A.C., Kaiser, F., Kubaczka, C., Schultze, J.L. & Schorle, H. (**Accepted for publication**). Induction of Rosette-to-Lumen stage embryoids using reprogramming paradigms in ESCs. Nature Communications

Langkabel, J., Horne, A., Bonaguro, L., Hesse, T., Knaus, A., Riedel, Y., Händler, K., Bassler, K., Reusch, N., Yeghiazarian, L. H., Pecht, T., Aschenbrenner, A.C., Kaiser, F., Kubaczka, C., Schultze, J.L. & Schorle, H. (2021). Induction of peri-implantation stage synthetic embryos using reprogramming paradigms in ESCs. BioRxiv 2021.01.25.428068. DOI: 10.1101/2021.01.25.428068

Kaiser, F., Kubaczka, C., Graf, M., Langer, N., **Langkabel, J.**, Arévalo, L. & Schorle, H. (2020). Choice of factors and medium impinge on success of ESC to TSC conversion. Placenta *90*, 128-137. DOI: 10.1016/j.placenta.2019.12.017

Bonn, 2021 _____

Jan Michael Langkabel

List of Abbreviations

2D	Two-dimensional space
2i	Two inhibitors
3D	Three-dimensional space
5F ESCs	5 Factor ESCs
AP	Anterior posterior
AVE	Anterior visceral endoderm
AUC	Area Under the Curve
Blimp1 (Prdm1)	PR domain containing 1
Bmp2	Bone morphogenetic protein 2
Bmp4	Bone morphogenetic protein 4
Bmp8b	Bone morphogenetic protein 8b
BSA	Bovine serum albumin
Cdx2	Caudal type homeobox 2
Cer1	Cerberus 1
c-Myc /Myc	Cellular Myelocytomatosis Oncogene
DiExE	Distal extraembryonic ectoderm
Dkk1	Dickkopf WNT signaling pathway inhibitor 1
DMEM	Dulbecco's modified Eagle's medium
DNA	Deoxyribonucleic acid
DOX	Doxycycline
Dppa3 (Stella)	Developmental pluripotency-associated 3
DVE	Distal visceral endoderm
E	Embryonic day
E. coli	*Escherichia coli*
EAA	Essential amino acids
EB	Embryoid bodies
Elf5	E74-like factor 5
EmVE	Embryonic visceral endoderm
Eomes	Eomesodermin

EPC	Ectoplacental cone
Epi	Epiblast
EpiSC	Epiblast stem cell
EPS	Expanded potential stem (cell)
ERK	Extracellular signal-regulated kinase
ESC	Embryonic stem cell
ESRRB	Estrogen related receptor beta
et al.	Et alii, aliae, alia; latin: and others
EtOH	Ethanol
Ets2	E26 avian leukemia oncogene 2, 3' domain
ExE	Extraembryonic ectoderm
ExVE	Extraembryonic visceral endoderm
FACS	Fluorescence-activated cell sorting
FCS	Fetal calf serum
Fgf	Fibroblast growth factor
Fgf4	Fibroblast growth factor 4
Fgfr2	Fibroblast growth factor receptor 2
Furin	Furin, paired basic amino acid cleaving enzyme
Gata3	GATA binding factor 3
Gata4	GATA binding factor 4
Gata6	GATA binding factor 6
GFP	Green fluorescent protein
GO	Gene ontology
h	Hour(s)
Hesx1	Homeobox gene expressed in ES cells
Hhex	Hematopoietically expressed homeobox
ICM	Inner cell mass
iGATA6 ESCs	Inducible *Gata6* (transgene) embryonic stem cells
iPSC	Induced pluripotent stem cell
iTSC	Induced trophoblast stem cell
iXEN	Induced extraembryonic endoderm (stem cell)

Kit	KIT proto-oncogene receptor tyrosine kinase
Klf4	Kruppel-like factor 4
Lefty1	Left right determination factor 1
LIF	Leukemia inhibitory factor
MAPK	Mitogen-activated protein kinase
MEF	Mouse embryonic fibroblasts
min	Minute(s)
ml	Milliliter
mm	Millimeter
Nanog	Nanog homeobox
Nanos3	Nanos C2HC-type zinc finger 3
NEAA	Non-essential amino acids
nM	Nano molar
Nodal	Nodal growth differentiation product
o/n	Over night
Oct3/4 (Pou5f1)	Octamer-binding transcription factor 3 / 4 (POU domain, class 5, transcription factor 1
Oct6 (Pou3f1)	Octamer-binding transcription factor 6 (POU domain, class 3, transcription factor 1)
OSKM	Oct4, Sox2, Klf4 and Myc
Otx2	Orthodenticle homeobox 2
P	Passage
Pace4 (Pcsk6)	Proprotein convertase subtilisin/kexin type 6
PBS	Phosphate buffered saline
PC	Proprotein convertase
PE	Parietal endoderm
Pen/Strep	Penicillin/Streptomycin
PFA	Paraformaldehyde
PGC	Primordial germ cell
Prdm14	PR domain containing 14
PrE	Primitive endoderm
PrExE	Proximal extraembryonic ectoderm

PS	Primitive streak
RNA	Ribonucleic acid
rpm	Revolutions per minute
RPMI	Roswell Park Memorial Institute medium
RT	Room temperature
RtL	Rosette-to-Lumen
rtTA	Reverse tetracycline transactivator
s	Second(s)
scRNA-Seq	Single cell RNA sequencing
SFCA	Surfactant-free cellulose acetate
Sox2 (SRY)	Sex determining region Y-box 2
Stat3	Signal transducer and activator of transcription 3
TE	Trophectoderm
tetO	Tet operon
Tfap2c	Transcription factor AP-2 gamma
TSC	Trophoblast stem cell
TX	Defined TSC medium
UMAP	Uniform Manifold Approximation and Projection
v/v	Volume solute per volume of total solution
w/o	Without
w/v	Weight solute per volume of total solution
VE	Visceral endoderm
Wnt	Wingless Int-1
WT	Wildtype
XEN	Extraembryonic endoderm
γMEFs	Mitotically inactivated murine embryonic fibroblasts (gamma irradiated)
µl	Microliter
µM	Micromolar
µm	Micrometer

Table of Contents

List of Figures

List of Tables

Summary

This research project focuses on the generation and characterization of a stem cell-based organoid model system, that can model early murine embryonic development *in vitro* and *ex utero*. Such embryo-like cell culture models allow for deeper insights into early lineage segregation and cellular reprogramming in complex 3D co-culture environments. The recently emerging field of stem cell-based embryo models aims to recreate hallmark events of embryonic development *in vitro*. So far, research in the field was based on the co-culture of the three stem cell lines that can be generated from blastocysts at embryonic day (E) 3.5, embryonic stem cells (ESC), trophoblast stem cells (TSC) and extraembryonic endoderm (XEN) stem cells. These stem cell populations were shown to aggregate and self-organize into structures resembling early murine embryos at ~E5.0. However, the generation of these embryo-like structures relies on complex cell culture requirements for maintenance of each of the three stem cell types. In this study, a new strategy for the generation of embryo-like organoids was developed, based on transcription factor mediated reprogramming of a solely ESC-based starting cell population in a 3D cell culture environment. Therefore, three genetically modified ESC lines were used for the inducible system presented in this thesis: Kermit ESCs, carrying an *Oct3/4* promotor driven GFP expression cassette, 5 Factor ESCs (5F ESCs) carrying doxycycline inducible transgenes of *Cdx2*, *Tfap2c*, *Eomes*, *Gata3* and *Ets2*, and iGATA6 ESCs, carrying doxycycline inducible *Gata6* transgenes. Upon doxycycline mediated induction of transgene expression, 5F ESCs underwent cell fate conversion towards an induced TSC- (iTSC) identity, while iGATA6 ESCs reprogrammed towards an induced XEN (iXEN) cell fate. Reprogramming of the two ES cell lines in co-culture with a third ES cell line (Kermit ESCs) in a 3D cell culture environment resulted in the generation of embryo-like organoids, that acquire early embryo architecture with an epiblast (Epi), extraembryonic ectoderm (ExE) and visceral endoderm (VE) -like compartment. These embryo-like organoids were shown to induce several hallmarks of embryogenesis, such as induction of rosettes and subsequent lumenogenesis, in Epi- and ExE-like compartments. Additionally, the generation of a distal-/anterior- VE cell lineage was detected, indicating patterning events mediated by interaction of all three induced cellular compartments, as observed during murine embryonic development. Furthermore, single cell RNA-Seq (scRNA-Seq) analysis showed individual, highly specific transcriptional profiles for each of the three embryo-like compartments and revealed high similarity to natural murine embryos between E4.5 – E5.5. Together, the system introduced in this study provides an easy-to-use, inexpensive tool to study specific hallmarks of early embryogenesis and cellular reprogramming in 3D co-culture with cellular signaling interactions comparable to those observed during natural embryonic development.

1. Introduction

1.1 Early murine embryonic development

1.1.1 From zygote to blastocyst – preimplantation embryonic development

Embryonic development starts with the fertilized zygote (E0.5) which undergoes multiple cell cleavages, doubling the number of totipotent blastomeres with each cleavage step. At E2.25, the 8 blastomeres start to compact, generating the first asymmetry in the developing embryo, with apical cell domains facing outwards and basolateral domains facing inwards (Figure 1) (reviewed in Rossant and Tam, 2009). At the morula stage around E2.75, cells start to commit to either an inner cell mass (ICM) or trophectoderm (TE) fate, depending on their position within the developing structure. Cells located on the outside of the growing cell aggregate start to adopt a TE identity, marked by the upregulation of caudal type homeobox 2 (*Cdx2*) (Beck et al., 1995).

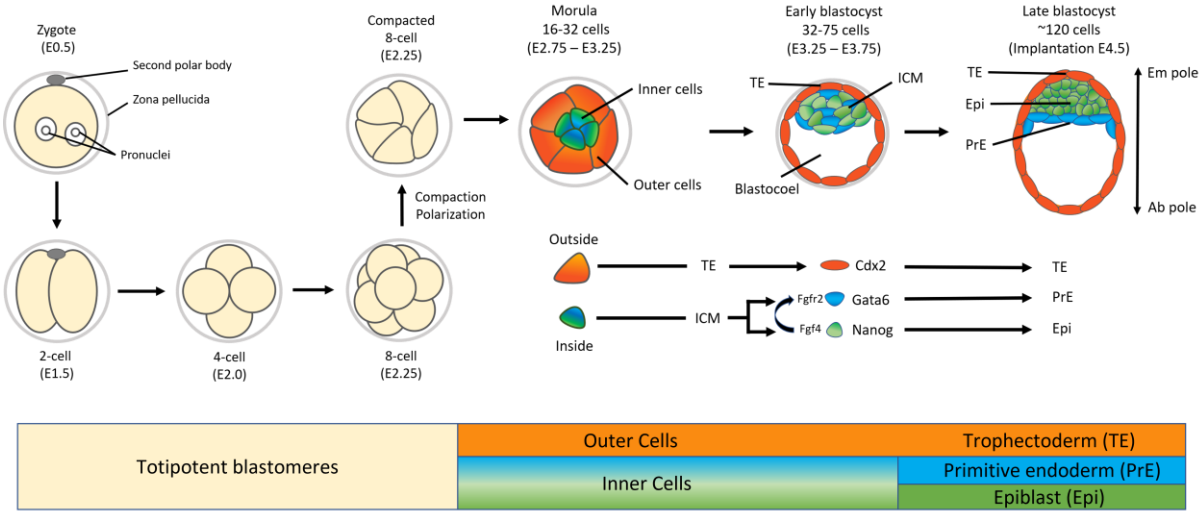

Figure 1 – Development of the mouse preimplantation embryo between E0.5 – E4.5. Schematic summary of cell cleavages and divisions and resulting tissue development during early embryonic development starting with the fertilized zygote at E0.5 to the late blastocyst at implantation stage ~E4.5. TE = Trophectoderm, ICM = Inner Cell Mass, Epi = Epiblast, PrE = Primitive endoderm, Em pole = Embryonic pole, Ab pole = Abembryonic pole. (Adopted and modified from Rossant & Tam 2009).

Cells located on the inside express POU class 5 homeobox 1 (*POU5F1*, also called *Oct3/4*) and SRY-Box transcription factor 2 (*Sox2*) ultimately leading to induction of an ICM fate (Nichols et al., 1998; Keramari et al., 2010). At the early blastocyst stage (~E3.5) TE cells spherically surround the ICM cells and a fluid-filled cavity (blastocoel). At this time, another specification takes place within the ICM, leading to homeobox transcription factor Nanog (*Nanog*)-expressing Epiblast (Epi) progenitor cells and GATA binding factor 6 (*Gata6*)-expressing primitive endoderm (PrE) progenitor cells, organized in a "salt and pepper" distribution in the ICM (Chazaud et al., 2006). The exact mechanism of this lineage specification is still under debate and several models have been proposed. The currently most commonly accepted model is based on the expression of key

lineage-specific transcription factors *Gata6* and *Nanog* in PrE- and Epi-progenitors respectively, and their influence on FGF/ERK signaling pathways (Chazaud et al., 2006). In early blastocysts, *Nanog* and *Gata6* are co-expressed in all cells of the ICM, which is then resolved as cells expressing higher levels of NANOG give rise to Epi progenitors, downregulating expression of *Gata6*, while PrE progenitors display high expression levels of *Gata6* and downregulation of *Nanog* (Chazaud et al., 2006; Bessonnard et al., 2014). This commitment to the respective cell fates is further reinforced by FGF/MAPK signaling, as Epi progenitors secrete Fibroblast growth factor 4 (FGF4), which binds to its receptor Fibroblast growth factor receptor 2 (FGFR2) on PrE progenitor cells (Figure 1) (Bessonnard et al., 2014; Schröter et al., 2015). The random distribution of PrE- and Epi-progenitor cells within the ICM is subsequently resolved with the sequestration of PrE cells to the surface of the ICM, forming an epithelium in contact to the blastocoel at the late blastocyst stage (E4.5) (Xenopoulos et al., 2012). At this developmental timepoint the pre-implantation blastocyst has acquired an embryonic-abembryonic (Em-Ab) axis with the Em pole consisting of the epiblast surrounded by the polar TE and the PrE, while the Ab pole is comprised of the mural TE enclosing the blastocoel (Figure 1) (Chávez et al., 1984; Christodoulou et al., 2019).

1.1.2 From blastocyst to egg cylinder – postimplantation embryonic development

After implantation into the uterus around E4.5, ICM derived epiblast (Epi) cells become polarized, generating a rosette-like structure with a lumen at its center shortly after implantation ~E5.0 – E5.5 (Figure 2) (Bedzhov and Zernicka-Goetz, 2014). At this developmental stage, the polar TE gives rise to the extraembryonic ectoderm (ExE) located at the most proximal part of the embryo, while the PrE-derived visceral endoderm (VE) surrounds the now polarized, epithelial Epi and the ExE. The mural TE differentiates into a layer of primary trophoblast giant cells (primary TGCs), which, together with the PrE-derived parietal endoderm (PE) and the Reichert's membrane in between the two, comprise the outermost layer of the embryo (Figure 2) (Reviewed in Sutherland, 2003 and Hu & Cross 2010). Next, at the egg cylinder stage (~E5.5), the post-implantation embryo undergoes morphological changes, when the epiblast reorganizes into a cup-like shaped epithelium, adjacent to the extraembryonic ectoderm (ExE) (Figure 2 and Figure 3 A). At this time, a second rosette emerges within the extraembryonic ectoderm, which

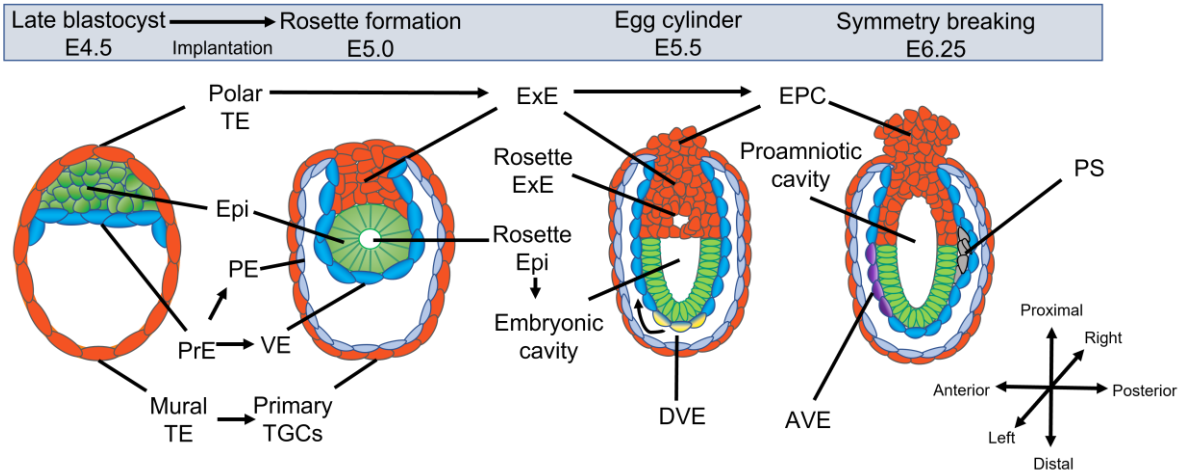

Figure 2 – Development of the mouse postimplantation embryo between E4.5 – E6.25. Schematic summary following development of the three primary tissues comprising the late blastocyst and maturation into their descendant cell lineages. Crossed arrows on the lower right side indicates embryonic axes. TE = Trophectoderm (red); Epi = Epiblast (green); PrE = Primitive endoderm (blue); PE = Parietal endoderm (light blue); VE = Visceral endoderm (blue); TGCs = Trophoblast giant cells (red); ExE = Extraembryonic ectoderm (red); DVE = Distal visceral endoderm (yellow), AVE = Anterior visceral endoderm (purple), EPC = Ectoplacental cone (red); PS = Primitive streak (gray)

subsequently fuses with the embryonic cavity generated from the first rosette formation in the Epi, forming a single, unified lumen, the proamniotic cavity at ~E6.0 (Figure 2 and Figure 3) (Christodoulou et al., 2018). The structural composition of the developing embryo results in multiple, individual signaling sites at the borders of the neighboring embryonic and extraembryonic compartments, that differ in signaling molecule expression profiles and subsequently regulate different signaling pathways. One of those signaling complexes can be found at the border of Epi and ExE, where Epi cells secret trophoblast stem cell (TSC) maintaining factors into the ExE, while TSCs in this resulting stem cell niche within the ExE conversely secret

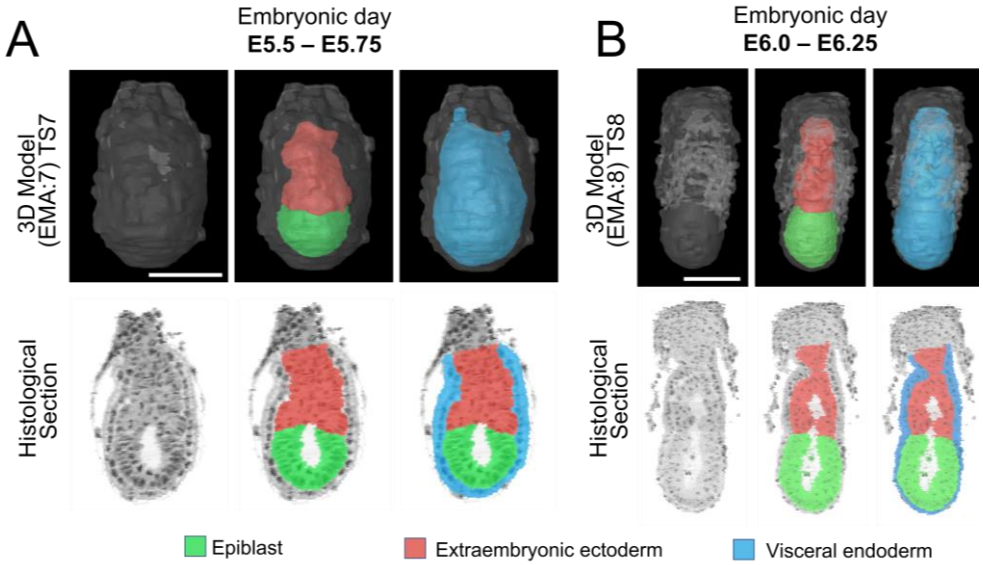

Figure 3 – 3D Models and histological sections of murine embryo between E5.5 – E6.25. 3D Models (upper row) and corresponding scans of histological sections (lower row) (Histological stain: 1% Toluidine Blue; Histological section: 2.00 µm) of mouse embryos at (**A**) E5.5 – E5.75 and (**B**) E6.0 – E6.25 were obtained from the EMAP eMouse Atlas Project (http://www.emouseatlas.org; EMAP Code: (**A**) = EMA:7, (**B**) = EMA:8; (Richardson et al., 2014). Color indicate Epi (Green), ExE (red), and VE (blue); Scale bar = 100 µm.

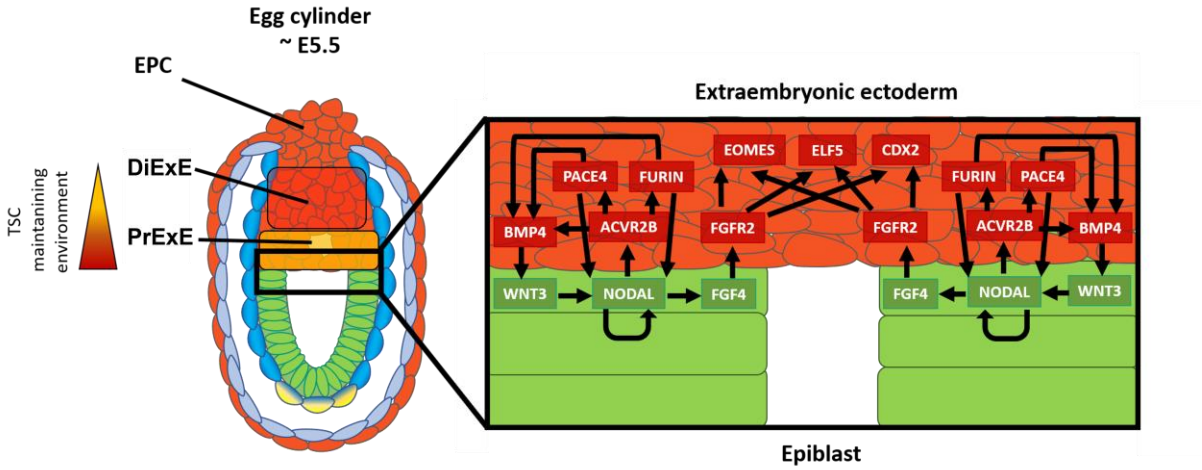

Figure 4 – Schematic representation of signaling feedback loops between Epi and ExE. At the egg cylinder stage ~E5.5, signaling between the two inner compartments maintains a TSC niche at the most proximal part of the ExE (PrExE; orange). ExE cells situated further distally (DiExE; red) are lacking those stem cell enhancing signaling cues, resulting in increased differentiation, which ultimately leads to emergence of the ectoplacental cone (EPC) at the most distal part of the DiExE.

Nodal growth differentiation factor (Nodal) and Wingless Int-1 (Wnt) enhancing signaling molecules to the Epi (Figure 4). In detail, these signaling feedback loops are maintained by NODAL, which is secreted by the Epi and activates activin receptor 2B (ACVR2B) in the ExE (Ben-Haim et al., 2006). ACVR2B then stimulates expression of Bone morphogenetic protein 4 (*Bmp4*) and its convertases proprotein convertase subtilisin/kexin type 6 (*Pcsk6*, also called *PACE4*) and Paired basic amino acid cleaving enzyme (*Furin*) in the ExE, leading to increased levels of secreted BMP4 into the EPI, which in turn enhances expression of Wingless-Type MMTV Integration Site Family Member 3 (*Wnt3*) and *Nodal*, thereby reinforcing the signaling feedback loops between Epi and ExE (Figure 4) (Ben-Haim et al., 2006). Additionally, NODAL in the Epi stimulates expression of *Fgf4*, which is secreted into the ExE, where it binds to and activates its receptor FGFR2, which in turn enhances expression of TSC specific stem cell-fate maintaining factors, like *Cdx2*, E74 Like ETS Transcription Factor 5 (*Elf5*) and Eomesodermin (*Eomes*) (Tanaka et al., 1998). Distally situated ExE cells are lacking the stem cell enhancing signaling cues from the epiblast, resulting in a gradient of differentiation within the ExE compartment, which can therefore be divided into a proximal ExE (PrExE), comprised of the trophoblast stem cell niche, and a more differentiated, distal ExE (DiExE) (Donnison et al., 2015) (Figure 4). Ultimately, the most distal part of the DiExE differentiates into the ectoplacental cone (EPC), consisting predominantly of secondary TGCs that invade the maternal uterine endothelium, hence establishing the maternal-fetal interface (Donnison et al., 2015) (Figure 4). Corresponding to this bipartite character of the ExE, it has been shown that mitogen-activated protein kinase / extracellular signal-regulated kinases (MAPK/ERK) signaling exhibits a specific spatial and temporal pattern of activity within the ExE, that can be visualized by detection of phosphorylated ERK (pERK) (Corson et al., 2003). Initially, pERK can be detected throughout the ExE at E5.5,

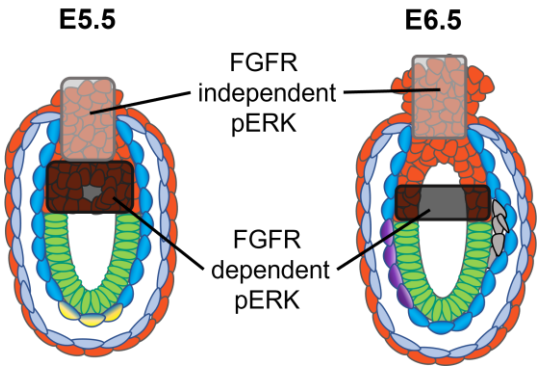

Figure 5 – Schematic representation of ERK signaling patterns in the ExE. At E5.5 pERK can be detected throughout the ExE. At E6.5 pERK can be detected in two domains of the ExE, at the most distal part within the EPC (FGFR independent) and a distinct ring in the PrExE adjacent to the Epi (FGFR dependent).

functioning either FGFR dependent in PrExE cells adjacent to the Epi, or FGFR independent in DiExE cells (Figure 5) (Corson et al., 2003). At E6.5, pERK can be detected in two domains of the ExE, i) FGFR dependent in a band of PrExE cells and ii) FGFR independent in the EPC emerging from the DiExE (Figure 5) (Corson et al., 2003).

1.1.3 Anterior-Posterior axis formation at the egg cylinder stage

At the egg cylinder stages, the VE encloses both inner compartments, the Epi and ExE, albeit differing in its interactive signaling cascades with the respective compartments. Therefore, the VE can be distinguished in either an extraembryonic VE (ExVE) identity for the part of the VE lining the ExE or an embryonic VE (EmVE) identity, for the part of the VE adjacent to the Epi, both of which fulfil individual functions in the developing conceptus (Kwon et al., 2008). In general, the VE is associated with nutrient uptake and transport, as it expresses several specialized proteins, responsible for uptake, digestion, and secretion of nutrients, before a maternal-embryonic circulation is established (Cross et al., 1994; Bielinska et al., 1999). Additionally, the VE also plays a major role as a signaling center mediating the formation of an anterior-posterior (AP) axis within the developing embryo. This process starts with the specification of a distinct subpopulation of EmVE cells located at the distal tip of the VE at ~E5.5 (Figure 6) (Yamamoto et al., 2009). The induction of this subpopulation, referred to as distal visceral endoderm (DVE), relies on exposure to low levels of NODAL signaling, mediated trough interactions between extraembryonic and embryonic tissues (Brennan et al., 2001). At early post-implantation stages, *Nodal* is expressed throughout the epiblast, which subsequently resolves when a proximal-distal gradient of *Nodal* expression is formed within the epiblast (Varlet et al., 1997). The proximal epiblast secrets pro-NODAL, which is converted to NODAL by two members of the proprotein convertase (PC) family, PACE4 and FURIN, in the proximally located ExE (Beck et al., 2002; Ben-Haim et al., 2006). In addition to the proximal-distal gradient of NODAL, the formation of the DVE is also known to be regulated by inhibition through secretion of BMP4 from the ExE, further

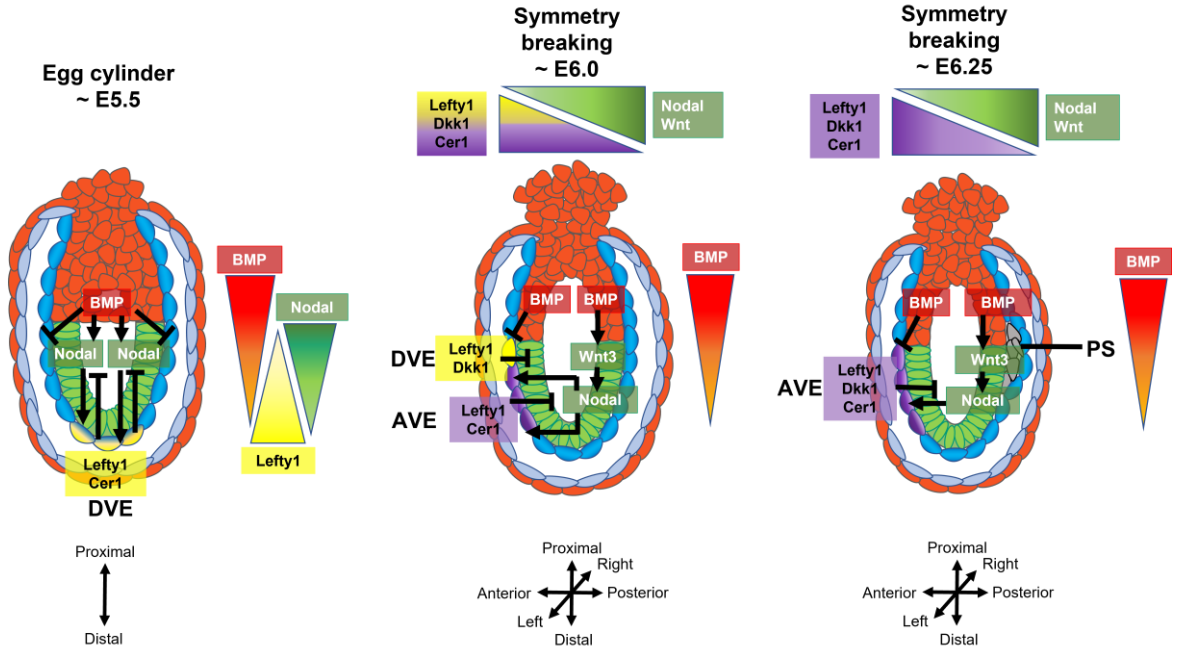

Figure 6 – Schematic representation of DVE/AVE and subsequent AP-axis formation. Schematic representation of signaling events resulting in the formation of an anterior-posterior axis in embryos ~E6.0. Formation of DVE and AVE at E5.5, E6.0 and E6.25 and signaling between DVE (yellow), AVE (purple), Epi (green) and ExE (red). Gradients of BMP, Lefty1 and Nodal concentrations are indicated next to schematics, embryonic axes are displayed at the bottom.

restricting DVE specification to the distal pole of the EmVE (Figure 6) (Yamamoto et al., 2009). The DVE expresses antagonists of Wnt and Nodal signaling pathways, including the DAN Family BMP antagonist Cerberus 1 (*Cer1*) and Left-Right determination factor 1 (*Lefty1*), further strengthening the proximal-distal NODAL gradient (Figure 6) (Yamamoto et al., 2009). The DVE then migrates towards the future anterior side of the embryo, where it localizes next to a second signaling center, the anterior visceral endoderm (AVE), emerging at ~E5.75 (Figure 6) (Takaoka et al., 2011). The complex of DVE/AVE cells continue expressing antagonists of Nodal and Wnt signaling, like *Cer1*, *Lefty1*, Hematopoietically expressed Homeobox (*Hhex*) and Dickkopf WNT signaling pathway inhibitor 1 (*Dkk1*), creating a gradient within the epiblast, restricting activity of Wnt and Nodal to the posterior of the embryo, thereby patterning the epiblast and facilitating the generation of an anterior-posterior axis (Figure 6) (Hoshino et al., 2015; Perea-Gomez et al., 2002; Kemp et al., 2005; Bardot and Hadjantonakis, 2020). When migrating DVE cells have reached the embryonic/extraembryonic junction, they do not cross the junction and instead migrate back in a lateral-distal direction towards the distal tip of the VE, where they adopt an AVE identity and again migrate towards the anterior side, this time fated to become AVE cells (Takaoka et al., 2011). Thereby, the DVE first guides and then drives the formation of the AVE, which ultimately remains the only anterior signaling center secreting Wnt and Nodal antagonist like LEFTY1, DKK1 and CER1 (Figure 6) (Takoaka et al., 2011; Takaoka and Hamada, 2012). However, the exact mechanisms involving DVE/AVE cell migration remain unclear and are subject of active research (reviewed in Bardot and Hadjantonakis, 2020).

1.1.4 Primordial germ cell specification

In mammals, passing on of genetic information across generations relies on germ cells, a specialized set of cells originating from primordial germ cells (PGCs), which are first specialized during early embryonic development between ~E6.25 to ~E13.5 from most proximally situated epiblast cells (Saitou and Yamaji, 2012). The proximal epiblast is subject to signaling from the ExE, which secrets BMP4 and BMP8b to the adjacent region of the epiblast (Figure 7) (Lawson et al., 1999, Ying et al., 2000). Together with BMP2, originating from the VE, these BMP signaling molecules were shown to be crucially important for the initiation of primordial germ specification in cells of the epiblast (Figure 7) (Lawson et al., 1999; Ying et al., 2000; Ying and Zhao, 2001; Ohinata et al., 2009). The main driving factor in this signaling cascade is thought to be BMP4, which alone is sufficient to drive epiblast cells into epiPGCs *in vitro* (Ohinata et al., 2009). BMP8b has been proposed to control AVE development, functioning in PGC specification by restricting AVE-derived inhibitory signals against germ cell specification to appropriate levels (Ohinata et al., 2009). BMP2, which has been shown to be expressed in the VE starting at ~E5.5, induces expression of downstream PGC specification factors B-Lymphocyte-induced maturation protein 1 (*Blimp1*, also known as *PRDM1*) and PR Domain zinc finger protein 14 (*Prdm14*), albeit to a lesser extent than BMP4 (Ying and Zhao, 2001). As BMP4 induces expression of *Blimp1* and *Prdm14* in a dose-dependent manner, BMP2 might serve as a safeguard ensuring sufficient BMP signaling levels for PGC specification (Ohinata et al., 2009). The expression of *Blimp1* and *Prdm14* leads to the expression and regulation of downstream germ cell development–specific genes Transcription factor AP-2 Gamma (*Tfap2c*), Developmental pluripotency-associated 3 (*Dppa3*, also known as *Stella*), Nanos C2HC-type zinc finger 3 (*Nanos3*) and Kit proto-oncogene receptor tyrosine kinase (*Kit*), ultimately resulting in specification of a small subset of epiblast cells to PGCs (Figure 7) (Mintz and Russel, 1957; Saitou et al., 2002; Sato et al., 2002; Payer et al., 2003; Suzuki et al., 2008; Weber et al., 2010).

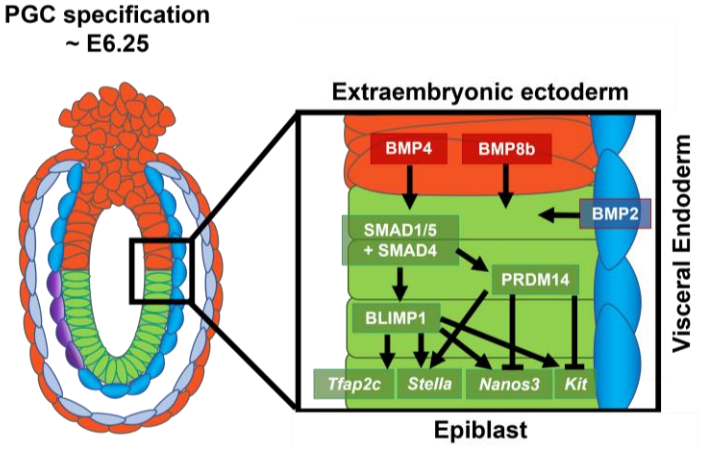

Figure 7 – Schematic representation of signaling pathways resulting in PGC specification. Schematic representation of the molecular signaling cascade initiating specification of a subset of epiblast cells towards primordial germ cells.

1.1.5 Gastrulation and germ layer development

Upon definition of an anterior-posterior (AP) axis, which is firmly established at E6.25, the embryo undergoes gastrulation, a process involving definitive specification of pluripotent epiblast cells into the three germ layers: ectoderm, mesoderm, and endoderm. The process of gastrulation occurs between E6.25 – E9.5 and is initiated by the formation of the primitive streak (PS) at the posterior epiblast at E6.25 – E6.5 when epiblast cells undergo epithelial-to-mesenchymal transition (EMT), migrating and invading into the space between Epi and VE (Figure 2, Figure 6, and Figure 8) (Reviewed in Bardot and Hadjantonakis, 2020). EMT into the

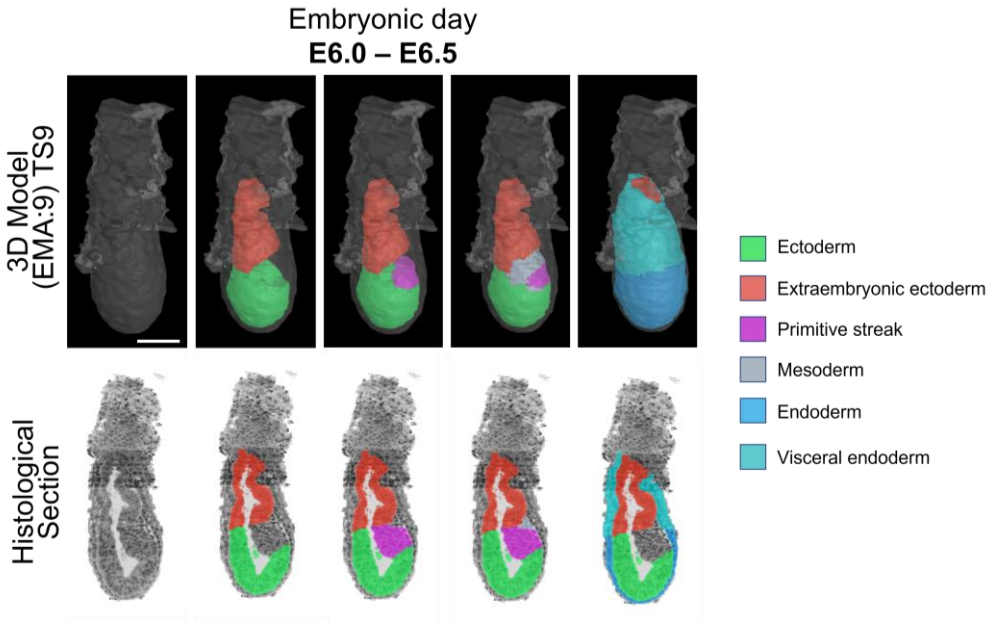

Figure 8 - 3D Model and histological sections of murine embryo at E6.0 – E6.5. 3D Models (upper row) and corresponding scans of histological sections (lower row) (Histological stain: 1% Toluidine Blue; Histological section: 2.00 µm) were obtained from the EMAP eMouse Atlas Project (http://www.emouseatlas.org; EMAP Code: EMA:8; Richardson et al., 2014). Scale bar = 100 µm

primitive streak is coordinated by signaling pathways including Wnt, FGF and BMP, all of which are restricted to the posterior side of the epiblast by the AVE secreting antagonists of Wnt, FGF and BMP, like DKK1 and CER1, as described before (Figure 6) (Ciruna et al., 1997; Ciruna and Rossant, 2001; Huelsken et al., 2000; Winnier et al., 1995). Hence, the position of the PS marks the posterior pole of the embryo, opposite to the location of the AVE. One of the first markers of primitive streak formation is the T-box transcription factor *Brachyury (T)*, that can be detected around E6.0 in the region of the epiblast showing highest expression of *Wnt3* (Rivera-Pérez and Magnuson, 2005). Additionally, expression of *Eomes* and *Snail1* was demonstrated to be necessary for EMT induction, as both repress E-cadherin, thereby preparing the environment of EMT, allowing cells to ingress in the space between Epi and VE (Arnold et al., 2008; Cano et al., 2000; Costello et al., 2011; Bardot and Hadjantonakis, 2020).The epiblast cells that undergo EMT

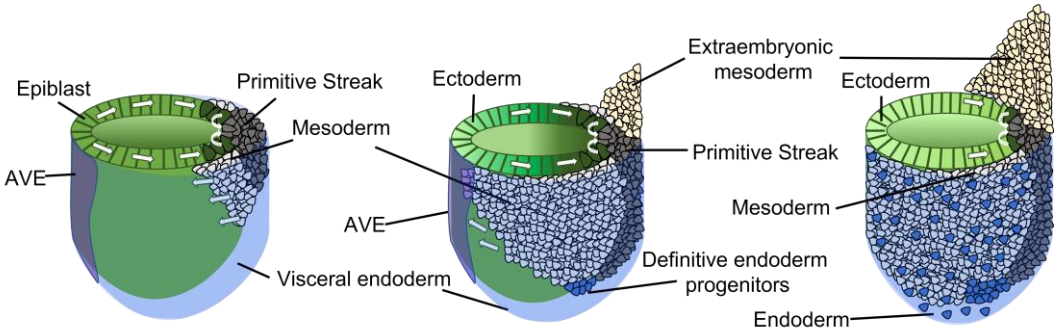

Figure 9 – Schematic representation of EMT at the primitive streak and germ layer formation. Schematics of events leading to the formation of the three germ layers, ectoderm, mesoderm, and endoderm, as well as the extraembryonic mesoderm. **Left**: Epiblast cells (dark green) situated at the posterior epiblast undergo EMT at the primitive streak (dark gray) and build the bilateral wings of the mesoderm (light gray), which moves laterally towards the anterior side (purple) of the embryo in the space between Epi and VE (light blue sheet). **Middle:** Epiblast cells from the anterior keep migrating towards the posterior side, migrating through, and constantly contributing to the PS, developing mesoderm, the definitive endoderm progenitors at the anterior end of the primitive streak and the extraembryonic mesoderm at the posterior end of the PS. **Right:** Remaining epiblast cells cease to undergo EMT at the PS and become replaced by cells originating from the anterior part of the embryo, ultimately leading to the formation of the ectoderm (light green). The mesoderm has surrounded the ectoderm completely and is situated between ectoderm and the endoderm, which has formed by definitive endoderm progenitors that undergo MET and intercalate in the VE layer.

are replaced by cells migrating from the anterior side of the embryo, ultimately leading to a replacement of epiblast cells with cells building the ectoderm (Figure 9). Cells undergoing EMT form the first bilateral wings of the mesoderm, which then migrate laterally in a posterior-to-anterior manner and meet at the anterior side, thereby building a mesenchymal layer between

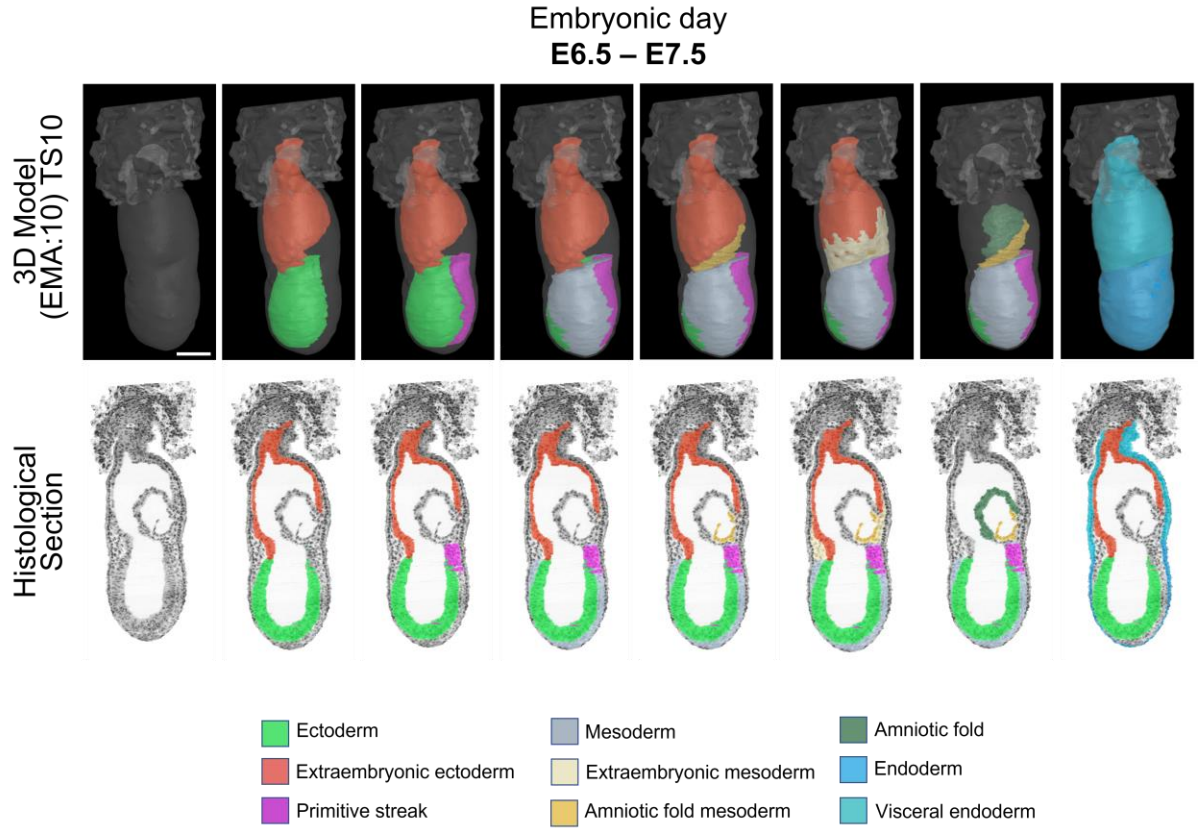

Figure 10 - 3D Model and histological sections of murine embryo at E6.5 – E7.5. 3D Models (upper row) and corresponding scans of histological sections (lower row) (Histological stain: 1% Toluidine Blue; Histological section: 2.00 µm) were obtained from the EMAP eMouse Atlas Project (http://www.emouseatlas.org; EMAP Code: EMA:10; Richardson et al., 2014). Scale bar = 100 µm

the epithelial epiblast and EmVE (Figure 8, Figure 9 and Figure 10) (reviewed in Bardot and Hadjatonakis, 2020). Cells fated to contribute to the endoderm germ layer, the definitive endoderm (DE) progenitors, then undergo mesenchymal-to-epithelial transition (MET) as they intercalate into and subsequently disperse the VE layer, thereby generating the endoderm (Kwon et al., 2008; Viotti et al., 2014; Bardot and Hadjatonakis, 2020) (Figure 9 and Figure 10). At the posterior end of the PS, the extraembryonic mesoderm emerges, surrounding the ExE fated to give rise to the mesoderm of the visceral yolk sac and the allantois, fated to build the umbilical cord of the placenta (Kinder et al., 1999; Downs et al., 2004) (Figure 9 and Figure 10). At around E7.5 the developing embryo consists of the three germ layers, ectoderm, mesoderm and endoderm, and the extraembryonic lineages, building the placental maternal-fetal interface, extraembryonic mesoderm, amniotic fold, and the amniotic fold mesoderm (Figure 10). Ultimately, the ectoderm will give rise to the epidermis and the central and peripheral nervous system, the mesoderm will generate musculoskeletal and circulatory systems and the endoderm is fated to become the epithelial lining of respiratory and digestive tracts and precursors of lungs, liver, and pancreas (reviewed in Rivera-Perez and Hadjantonakis, 2014).

1.2 Blastocyst derived stem cell lines cultured *in vitro*

When cultured *in vitro*, blastocysts can be used to derive three stem cell entities. Depending on cell culture medium conditions pluripotent embryonic stem cells (ESCs) can be derived from the ICM, extraembryonic endoderm (XEN) stem cells can be derived from the PrE, and trophoblast stem cells (TSCs) can be derived from the polar TE (Figure 11) (Evans and Kaufman, 1981; Tanaka et al., 1998; Kunath et al., 2005). The culture of these stem cell lines *in vitro* requires culture medium supplementation tailored specifically to each individual stem cell line to substitute for the signaling cascades that

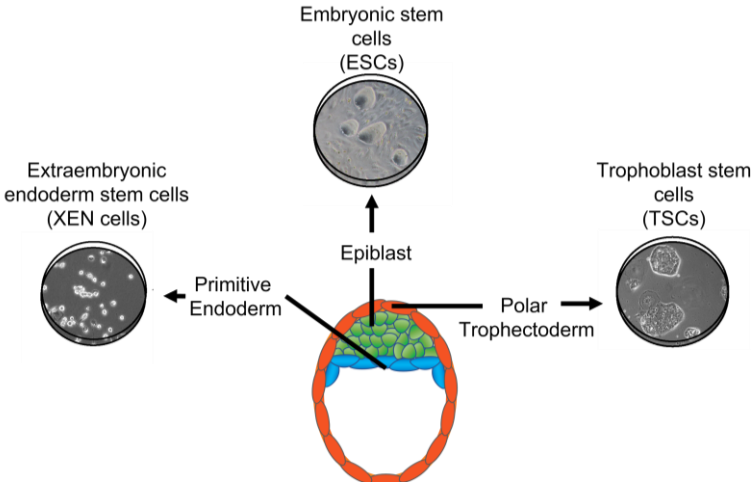

Figure 11 – Schematic representation of blastocyst-derived stem cell lines. Three stem cell lines can be derived from a blastocyst in vitro. Embryonic stem cells (ESCs) can be derived from the epiblast, trophoblast stem cells (TSCs) can be derived from the polar trophectoderm, and extraembryonic endoderm stem cells (XEN cells) can be derived from the primitive endoderm.

would normally be established between the embryonic and extraembryonic tissues stabilizing their respective cellular identity. TSCs for example rely on supplementation with FGF4 to activate the Ras/MAPK signaling pathway stabilizing and maintaining the stem cell characteristics of TSCs (Tanaka et al., 1998). The *in vitro* culture of ESCs on the other hand relies on a multifactorial stimulation of the transcriptional network required for maintenance of an undifferentiated, pluripotent state. Traditionally, this state is achieved by using a combination of cytokine leukemia inhibitory factor (LIF) to activate STAT3 and serum or bone morphogenetic protein (BMP) inducing inhibitor-of-differentiation proteins (Niwa et al., 1998; Ying et al., 2003; Ying et al., 2008). Additionally, ESCs are cultured on a layer of mitotically inactive mouse embryonic fibroblasts ('Feeder' MEFs), that secrete LIF, hence sustaining the propagation of undifferentiated stem cells (Smith, 1991). However, as the culture of ESCs with feeder MEFs in a heterogenous mixed population constrains genetic manipulation and biochemical analysis of the ESCs, over time more advanced techniques were developed. Today, ESCs can be cultured in feeder MEF free conditions using ESC culture medium supplemented with 2 inhibitors (2i) (CHIR-99021 and PD0325901), to inhibit mitogen-activated protein kinase signaling and glycogen synthase kinase-3, in combination with LIF to maintain ground state pluripotency (Silva et al., 2008). The culture of PrE-derived XEN cells is less demanding in terms of culture medium composition and supplementation, as it was demonstrated that XEN cells can be cultured and maintained in feeder-fibroblast conditioned medium without FGF supplementation (Kunath et al., 2005).

1.3 Transcription factor mediated reprogramming of cell fates

Traditionally, cell fate changes have been regarded a unidirectional process generating differentiated cell fates from stem cell fates. Once a cell lineage has been adopted, cells are constricted to their respective cell fate through genetic and epigenetic barriers, that are established and maintained by lineage specific transcriptional circuitries. However, this traditional model has been challenged by the work of Takahashi and Yamanka, who discovered that the combinational expression of *Oct4*, *Sox2*, *Klf4* and *c-Myc* (OSKM) in somatic cells results in reprogramming towards ESC-like cells, known as induced pluripotent stem cells (iPSCs) (Takahashi and Yamanaka, 2006). Similarly, it has been demonstrated that the forced expression of *Gata6* in pluripotent and differentiated cells initiates reprogramming to induced extraembryonic endoderm stem cells (iXEN cells) (Wamaitha et al., 2015) (Figure 12). The expression of TSC fate master regulators *Tfap2c*, *Eomes*, *Gata3* and *Ets2* was shown to facilitate reprograming of murine fibroblasts to induced trophoblast stem cells (iTSCs) (Kubaczka et al., 2015), while the expression of *Cdx2* alone was proven to be sufficient for reprogramming of ESCs

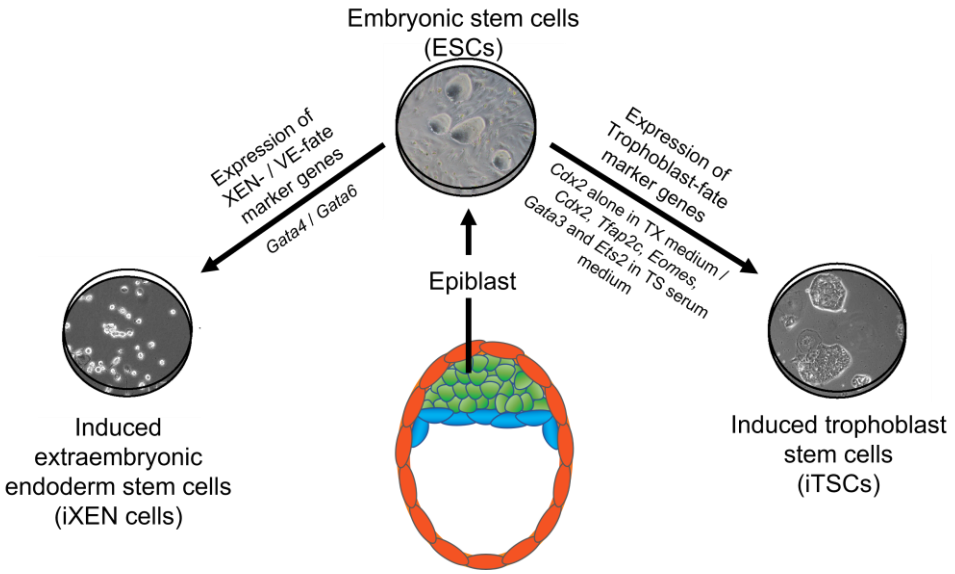

Figure 12 – Schematic representation of transcription factor mediated reprogramming of ESCs. Embryonic stem cells can be reprogrammed to induce an iXEN cell fate by exogenous transgene expression of *Gata4* or *Gata6* or an iTSC fate by expression of *Cdx2* when cultured in defined TX medium, or 5 Factors (*Cdx2*, *Tfap2c*, *Eomes*, *Gata3* and *Ets2*) when cultured in serum TS medium.

to iTSCs in combination with TX Medium, a defined medium for the culture of TSCs (Kubaczka et al., 2014). However, for complete reprogramming of ESCs to iTSCs in standard TS medium supplemented with FGF4 and heparin, a multifactorial approach was proven to be most suitable, based on the expression of five TSC-fate transgenes, *Cdx2*, *Tfap2c*, *Eomes*, *Gata3* and *Ets2* (Kaiser et al., 2020) (Figure 12). These 5 Factor ESCs (5F ESCs) are able to generate iTSCs that show stable expression of TSC marker genes, as well as methylation of the *Oct4* and demethylation of the *Elf5* promoter comparable to bona fide TSCs (Kaiser et al., 2020).

1.4 Organoid culture and *in vitro* generation of embryo-like structures in 3D cell culture

In recent years, the field of organoid culture has gained increasing importance for the *in vitro* study of complex, multicellular tissues. These systems are used to recapitulate certain developmental and functional hallmarks of real organs, based on the self-organization into structured, multicellular architectures and intercellular signaling in a 3D environment. Hence, 3D cell culture systems and organoids can mimic *in vivo* behavior *in vitro* more closely than traditional 2D cell culture systems. Examples of successfully derived organoids include intestinal (Sato et al., 2009), cerebral (Lancaster et al., 2013), gastric (McCracken et al., 2014) and mammary gland organoids (Simian et al., 2001). All these systems are based on the ability of a starting cell population to self-organization into complex, multicellular tissues. Cellular self-organization was previously defined as the capacity of an unordered cellular system to undergo spatial

rearrangement in a system-autonomous manner, facilitated by self-patterning and morphogenetic rearrangements (Sasai, 2013; Rossi et al., 2018). In this context, self-patterning describes the formation of patterns of cellular differentiation within an initially homogenous system, mediated by symmetry-breaking events and intercellular communication (Turner et al., 2016; Rossi et al., 2018). Morphogenetic rearrangement results due to the subsequent process of sorting of the cells undergoing differentiation, facilitated by physical interactions between neighboring cells by differences in cell-cell- adhesion and -signaling (Rossi et al., 2018). Therefore, Rossi et al. defined three prerequisites for the successful derivation of functional organoids: the physical characteristics of the culture environment; the requirement for endogenous and/or exogenous signals, and the starting cell type and system conditions (Rossi et al., 2018).

An interesting example of self-organization by self-patterning and morphogenetic rearrangement offers the recently emerging field of organoids recapitulating early embryonic development. This area of research is rapidly evolving and is currently subject of scientific and ethical importance and actively discussed in the scientific community. Starting with the discovery, that pluripotent stem cells (PSCs), when cultured in suspension, can form cellular aggregates, termed embryoid bodies (EB), that display some degree of cellular and tissue organization, these methods rapidly evolved and are used today to generate a variety of organotypic structures (reviewed in Sahu and Sharan, 2020). Examples of such EB-derived embryonic organoids include 2D micropatterned structures that display specification to germ layer derivatives, amniotic sac structures and gastruloids (Figure 13) (Morgani et. al., 2018, Zheng et al., 2019, Beccari et al., 2018, Rossant and Tam, 2021). However, the ability of these organoids to mimic natural organogenesis is still limited and their use to recreate early organogenesis during embryonic development is subject of debate, as these organoids bypassed earlier phases of embryogenesis from implantation to gastrulation, rendering them inappropriate for studies of embryogenesis and morphogenesis (Rossant and Tam, 2021). Recently, several novel approaches of organoid culture systems have been developed, that can capture and recapitulate early embryogenesis and potentially also early organogenesis in *in vitro* environments more closely, compared to traditional systems based on embryoid bodies. These embryo-like organoid systems can be derived by co-culture of combinations of ES, TS, XEN and expanded potential stem (EPS) cells in a 3D cell culture environment. While ES, TS and XEN cells can represent characteristics of the three blastocyst-tissues they are derived from to some degree, EPS cells (EPSCs) can be derived from 8-cell blastomeres or ESCs/PSCs/iPSCs cells by culture in the presence of a defined chemical cocktail and represent pluripotent stem cells with both, embryonic and extraembryonic developmental potentials (Yang et al., 2017). Rivron et al. have demonstrated that the co-culture of ESCs and

TSCs can give rise to blastocyst-like structures, termed 'blastoids', that resemble murine blastocysts around E3.5 – E4.5 (Rivron et al., 2018a) (Figure 13). These blastoids consist of an ICM-like structure build from ESCs, next to a fluid filled cavity resembling the blastocoel, both surrounded by a TSC-derived trophectoderm-like structure (Rivron et al., 2018a). Similarly, Sozen et al. presented a method to generate extended potential blastoids by co-culture of TSCs and EPSCs, which could provide a more precise model of the *in vivo* blastocyst (Sozen et al., 2019) (Figure 13). The co-culture of all three blastocyst-derived stem cell lineages, ESCs, TSCs and XEN cells in a 3D environment, however, was demonstrated to lead to self-organization into embryo-like structures resembling post-implantation developmental stages around E5.0 – E6.75 (Sozen et al., 2018; Zhang et al., 2019) (Figure 13).

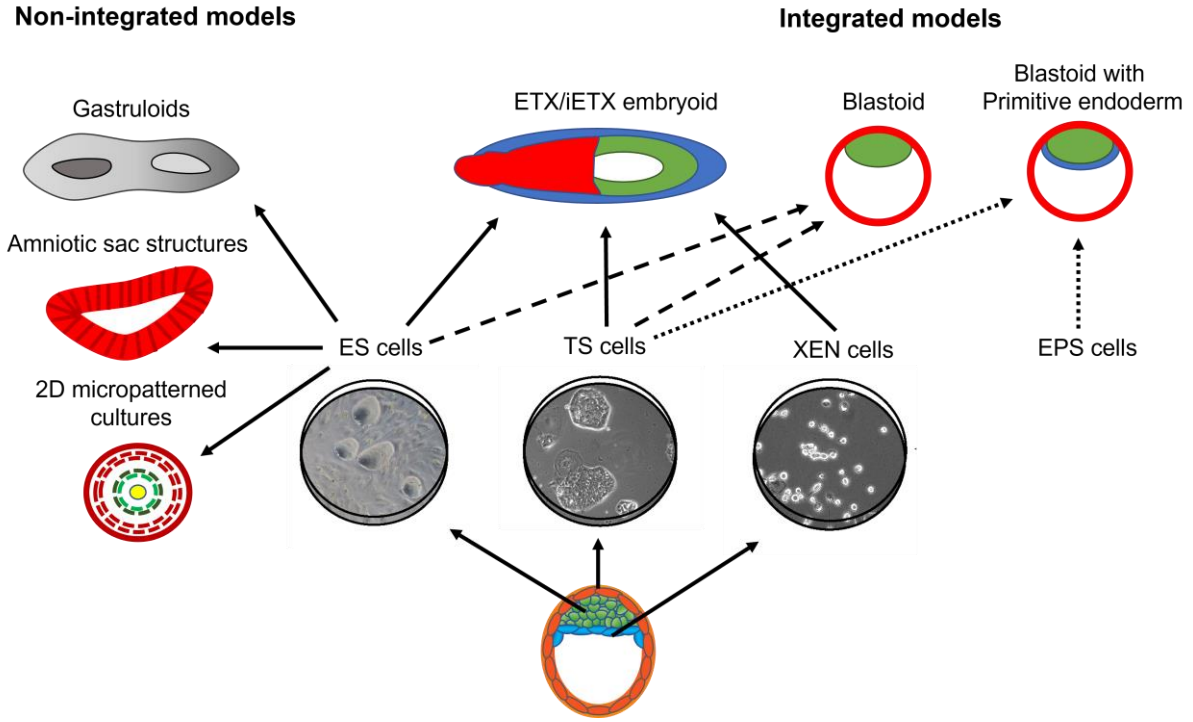

Figure 13 – Overview of non-integrated and integrated stem cell-based embryo models. Non-integrated models include gastruloids, amniotic sac structures and 2D micropatterned cultures that can be derived from ES cell cultures. Integrated models like ETX/iETX embryoids can be generated from ES, TS, and XEN cells, blastoids from ES and TS cells, and blastoids with primitive endoderm can be obtained from co-culture of TS and expanded potential stem (EPS) cells. (Adopted and modified from: Rossant and Tam, 2021).

These embryo-like structures resemble gastrulating natural embryos in morphology, gene expression pattern and have been shown to undergo lumenogenesis, forming a unified cavity stretching from the ExE-like to the Epi-like compartment, comparable to pro-amniotic cavity formation in murine embryos. Furthermore, these embryo-like structures initiate the specification of PGCs as well as cell ingression to form the mesoderm layer (Sozen et al., 2018). Recently, it was demonstrated that such embryo-like structures can be generated by co-culture of ESCs, TSCs and ESCs that can be reprogrammed towards an iXEN cell fate (Amadei et al., 2021). These iETX embryoids, generated in part by cellular reprogramming, were shown to mirror

certain developmental hallmarks more closely compared to ETX embryoids, and reprogrammed cells were demonstrated to be more similar to their natural counterparts regarding transcriptional profiles and marker gene expression (Figure 13) (Amadei et al., 2021). As this field of research is currently rapidly evolving, several propositions regarding terminology were made in order to create a common ground for communication of the scientific community studying embryo-related organoids. Rossant and Tam recently proposed a differentiation between models that mimic the conceptus as a whole (integrated stem cell-based embryo models) and models that represent specific developmental processes or morphogenetic events individually (non-integrated stem cell-based embryo models) (Rossant and Tam, 2021). Therefore, integrated stem cell-based embryo models would include blastoids as well as ETX/iETX embryoids, while gastruloids, amniotic sac structures and 2D micropatterned cultures would represent non-integrated stem cell-based embryo models (Rossant and Tam, 2021) (Figure 13). Very recently, the first human embryo model systems were introduced, that can be generated from naïve human ES cells, human iPSCs or by reprogramming of human fibroblasts. These blastocyst-like structures are termed 'human Blastoids' or in the case of reprogramming 'human iBlastoids', that resemble human blastocysts in terms of morphology, size, cell number and allocation of the different cell lineages and transcriptomic profiles (Yu et al., 2021, Liu et al., 2021). These human embryo model systems can be regarded a first approach to establish model systems that will potentially enhance our understanding and knowledge of early human embryogenesis as well as specific diseases involved in developmental processes.

1.5 Aim of the research project

The aim of this thesis was to answer the question if embryo-like organoids could be generated from a solely ES cell-based starting population by combining 3D cell culture and reprogramming paradigms to induce both extraembryonic cell lineages, ExE and VE. To achieve this goal, I first established an easy-to-use, reproducible 3D culture system that allowed for the generation of large numbers of such embryo-like organoids. Next, I devised a protocol for the induction of embryo-like organoids from three ESC lines, two of which can be reprogrammed towards either an iTSC or iXEN cell fate by controlled induction of transgenes of the respective cell fates, while the third ESC line remained in its pluripotent ES cell fate identity. The structures generated were characterized and analyzed using detection of marker gene and protein expression by immunofluorescent staining and single cell RNA-Seq, which was also used for direct comparison of transcriptional profiles with published datasets obtained from natural murine embryos at

different developmental stages. Furthermore, the structures were analyzed for signs of developmental hallmarks during embryogenesis, such as rosette formation and lumenogenesis, progression from naïve- to primed-pluripotency in cells building the Epi-like compartment, pro-amniotic cavity formation, PGC specification, DVE/AVE formation, and the ability to implant *in utero*.

2. Materials

2.1 Equipment

Adjustable micro pipettes	Research	Eppendorf AG, Hamburg, Germany
Automatic tissue embedding	Tissue-Tek®	Sakura Finetek, Heppenheim, Germany
Autostainer	480 S	Medac, Hamburg, Germany
Bacterial incubator		Memmert, Schwabach, Germany
Cell culture incubator	Heracell 240i CO_2 incubator	Hera Safe
Centrifuges	Multifuge 3 S-R	Kendro, Hanau, Germany
	5417R	Eppendorf AG, Hamburg, Germany
	5415D	Eppendorf AG, Hamburg, Germany
FACS machine	BD Aria III	BD Bioscience Pharmingen, USA
Laminar flow cabinet	Hera Safe	Kendro, Hanau, Germany
Microscopes	DM IRB	Leica, Wetzlar, Germany
	VisiScope confocal	Visitron
MicroTissues 3D Petri Dish micro-mold	MicroTissues® 3D Petri Dish® micro-mold spheroids (256 microwells for 12-Well plates)	MicroTissues Inc.
Orbital shaker and incubator	Innova 4000	New Brunswick Scientific, New Jersey, USA

Thermomixer	Thermoblock compact	Eppendorf AG, Hamburg, Germany
Tissue dispensing console	Tissue-Tek®	Sakura Finetek, Heppenheim, Germany
Vortexer	Vortex-Genie 2	Scientific Industries, New York, USA
Water bath	TW8	Julabo, Seelbach, Germany

2.2 Chemicals

(RS)-N'-(7-chloroquinolin-4-yl)-N,N-diethyl-pentane-1,4-diamine (Chloroquine)	Sigma-Aldrich, St. Louis, MO, USA
Agar	Merck, Darmstadt, Germany
Agarose (cell culture grade)	Sigma-Aldrich, St. Louis, MO, USA
Ampicillin	AppliChem GmbH, Darmstadt, Germany
Bovine Serum Albumine Fraction V	AppliChem GmbH, Darmstadt, Germany
Doxycycline (DOX)	Sigma-Aldrich, St. Louis, MO, USA
Ethanol (EtOH)	Merck, Darmstadt, Germany
Formaldehyde	Merck, Darmstadt, Germany
Hoechst33342	Invitrogen, Carlsbad, Germany
Isopropanol	AppliChem GmbH, Darmstadt, Germany
Paraformaldehyde (PFA)	Merck, Darmstadt, Germany
Poly-L-lysine	Merck, Darmstadt, Germany
Roti-Mount FluorCare DAPI	Carl Roth GmbH, Karlsruhe, Germany
Sodium chloride (NaCl)	AppliChem GmbH, Darmstadt, Germany
Tris (Hydroxymethyl) aminomethane	VWR, Analar Normapur, Radnor, PA, USA
Triton X-100	Merck, Darmstadt, Germany
Tryptone	Merck, Darmstadt, Germany
Tween-20	AppliChem GmbH, Darmstadt, Germany

2.3 Buffers and Solutions

2.3.1 Molecular biology

LB medium (5x)	50 g tryptone; 25 g NaCl; 25 g yeast extract; ad 1 l ddH_2O, autoclaved
LB agar	10 g tryptone; 5 g NaCl; 5 g yeast extract; 16 g agar; ad 1 l ddH_2O, autoclaved

2.3.2 3D Cell Culture system

Saline agarose solution (2%)	1 g agarose (cell culture grade), 0.45 g NaCl, add 50 ml ddH_2O, microwaved until fully molten

2.3.3 Protein biochemistry

Blocking solution for immunofluorescent staining	3 % (w/v) BSA; 0.1 % Triton X-100; PBS
Cell fixation solution	4 % (w/v) PFA; PBS
Cell permeabilization buffer	0.5 % (v/v) Triton X-100; PBS
Wash buffer	0.1 % (v/v) Tween-20; PBS

2.4 Consumables

1.5 ml / 2 ml reaction tubes	Sarstedt, Nuembrecht, Germany
15 ml centrifuge tubes	Greiner, Kremsmuenster, Austria
5 ml reaction tubes	Eppendorf AG, Hamburg, Germany
50 ml centrifuge tubes	Greiner, Kremsmuenster, Austria
5 mL Falcon® Round Bottom Polystyrene Test Tube, with Cell Strainer Snap Cap	Corning Incorporated, Corning, NY, USA
Cellview Cell Culture Dishes	Greiner Bio-One, Solingen, Germany

Cryo tubes	Thermo Fisher Scientific, Waltham, MA, USA
FACS tubes	Sarstedt, Nuembrecht, Germany
Filter tips	Nerbe plus GmbH, Winsen, Germany
Glass slides	Marienfeld GmbH, Lauda-Königshofen, Germany
Multiwell dishes, cell culture grade	TPP, Trasadingen, Switzerland
Paraplast Plus	McCormick Scientific, St. Louis, MO, USA
Pipette tips	Greiner, Kremsmuenster, Austria
Serological pipettes	Corning Incorporated, Corning, NY, USA
Sterile filters, 0.45 µm surfactant-free cellulose acetate membrane (SFCA)	Corning Incorporated, Corning, NY, USA

2.5 Kits

High Sensitivity D5000 ScreenTape	Agilent, Santa Clara, California, USA
NucleoBond® Xtra Maxi Kit	Machery Nagel, Dueren, Germany
Profection® Mammalian Transfection System	Promega, Madison, WI, USA
NextSeq 500/550 High Output Kit v2.5 (75 Cycles)	Illumina, San Diego, California, USA
NextSeq 500/550 Buffer Cartridge v2	Illumina, San Diego, California, USA
NextSeq 500/550 High Output Reagent Cartridge v2	Illumina, San Diego, California, USA
Qubit dsDNA HS Assay Kit	Thermo Fisher Scientific, Waltham, MA, USA

2.6 Mouse strains

Strain name	*Description*
CB6F1	Cross between female BALB/cAnNCrl and male C57BL/6NCrl; Coat color: Agouti

2.7 Cell lines

Cell line name	*Genomic modification*	*Description*
Kermit ESCs	*Oct 3/4* promotor driven GFP expression cassette	Isolated from Oct3/4_GFP transgenic mice (Yoshimizu et al., 1999)
5 Factor ESCs (5F ESCs)	Doxycycline inducible transgene expression cassettes of *Cdx2*, *Tfap2c*, *Eomes*, *Gata3* and *Ets2*	Transgene expression induces iTSC fate (Kaiser et al., 2020). Received from Dr. Caroline Kubaczka.
iGATA6 ESCs	Doxycycline inducible transgene expression cassette of *Gata6*	Transgene expression induces iXEN cell fate (This study and Ngondo et al. 2018)
5 Factor_mCherry ESCs (5F_mCherry ESCs)	5 Factor ESCs transduced with pLV_mCherry	Constitutive mCherry expression allows for live tracking of cells (This study)
iGATA6_mCherry ESCs	iGATA6 ESCs transduced with pLV_mCherry	Constitutive mCherry expression allows for live tracking of cells (This study)
293T	Expression of SV40 large T-Antigen, allowing for amplification of "SV40 origin of replication" plasmids	Human embryonic kidney cell line allowing for episomal replication of transfected plasmids. Received from Dr. Michael Peitz.
KNUT1 ESCs	No genomic modifications	WT ESC line described and characterized in Peitz et al. (Peitz et al., 2007)

2.8 Bacteria

Name	*Genotype*
TOP10	F– mcrA Δ(mrr-hsdRMS-mcrBC) φ80lacZΔM15 ΔlacX74 recA1 araD139 Δ(ara-leu)7697 galU galK λ– rpsL(StrR) endA1 nupG

2.9 Plasmids

psPAX2; HIV-GAG	Addgene (#12260)
pMD2.G; VSV-G	Addgene (#12259)
pCW57.1_Gata6	Addgene (#73537)
pLV_mCherry	Laboratory Stock

2.10 Antibodies

Antibody	*Dilution*	*Manufacturer*
Goat polyclonal anti-CDX2	1:200	Santa Cruz (sc-19478)
Goat polyclonal anti-GATA4	1:400	Santa Cruz (sc-1237)
Goat polyclonal anti-CD40	1:300	R&D Systems (AF440)
Goat polyclonal anti-Lefty1	1:200	R&D Systems (AF746)
Rabbit polyclonal anti-p44/42 MAPK (Erk1/2)	1:100	Cell signaling (#9101)
Mouse polyclonal anti-OCT6	1:10	Absea (060204E04)
Mouse polyclonal anti-ESRRB	1:200	Perseus Proteomics (PP-H6705-00)
Rabbit polyclonal anti-NANOG	1:300	ReproCell (RCAB002P-F)
Rabbit polyclonal anti-EOMES	1:400	Abcam (ab23345)
Goat polyclonal anti-KLF4	1:400	R&D (AF3158)
Rat polyclonal anti-PODXL	1:300	R&D (MAB1556)
Goat polyclonal anti-OTX2	1:400	R&D (AF1979)
Rabbit polyclonal anti-GATA3	1:300	Abcam (ab199428)
Mouse polyclonal anti-OCT4	1:300	Santa Cruz (sc-5279)
Alexa Fluor 488-Phalloidin	5 units/ml	Invitrogen (A12379)
Alexa Fluor 594-Phalloidin	5 units/ml	Invitrogen (A12381)

Donkey polyclonal secondary antibody to Goat IgG-H&L (Alexa Fluor® 594)	1:500	Abcam (ab150132)
Chicken polyclonal secondary antibody to Goat IgG-H&L (Alexa Fluor® 647)	1:500	Invitrogen (A-21469)
Goat polyclonal secondary antibody to Rabbit IgG-H&L (Alexa Fluor® 594)	1:500	Invitrogen (A-11012)
Goat polyclonal secondary antibody to Rat IgG-H&L (Alexa Fluor® 488)	1:500	Invitrogen (A-11006)
Goat polyclonal secondary antibody to Mouse IgG-H&L (Alexa Fluor® 488)	1:500	Invitrogen (A-11001)
Chicken polyclonal secondary antibody to Rat IgG-H&L (Alexa Fluor® 647)	1:500	Invitrogen (A-21472)
Goat polyclonal secondary antibody to Rabbit IgG-H&L (Alexa Fluor® 488)	1:500	Invitrogen (A-11008)

2.11 Cell culture

2.11.1 Cell culture reagents and cytokines

Accutase	eBioscience, San Diego, CA, USA
Advanced DMEM	Gibco®, Life Technologies Inc., Carlsbad, California, USA
β-Mercaptoethanol	Gibco®, Life Technologies Inc., Carlsbad, California, USA
Dimethylsulfoxide (DMSO)	AppliChem GmbH, Darmstadt, Germany
DMEM+GlutaMAX	Gibco®, Life Technologies Inc., Carlsbad, California, USA
Essential amino acids	Gibco®, Life Technologies Inc., Carlsbad, California, USA

Fetal calf serum (FCS)	Gibco®, Life Technologies Inc., Carlsbad, California, USA
Gelatin	Sigma-Aldrich, St. Louis, MO, USA
L-Glutamine, 200 mM	Gibco®, Life Technologies Inc., Carlsbad, California, USA
Non-essential amino acids	Gibco®, Life Technologies Inc., Carlsbad, California, USA
Phosphate-Buffered Saline (PBS)	Gibco®, Life Technologies Inc., Carlsbad, California, USA
Advanced RPMI 1640	Gibco®, Life Technologies Inc., Carlsbad, California, USA
Sodium pyruvate	Gibco®, Life Technologies Inc., Carlsbad, California, USA
TrypLE Express™	Gibco®, Life Technologies Inc., Carlsbad, California, USA
Trypsin-EDTA (0.05%), phenol red solution	Gibco®, Life Technologies Inc., Carlsbad, California, USA

2.11.2 Cell culture media

ESC Medium	DMEM+GlutaMAX; 15% (v/v) FCS; 50 U/ml penicillin/streptomycin; 2 mM L-glutamine; 1x NEAA; 1x EAA; 0.1 mM β-mercaptoethanol; 1000 U/ml LIF; 3 µM CHIR-99021; 1 µM PD0325901
Reconstructed embryo medium (Zhang et al., 2019)	39% (v/v) DMEM; 39% (v/v) Advanced RPMI 1640; 17.5% (v/v) FCS; 50 U/ml penicillin/streptomycin; 2mM L-glutamine; 1x NEAA; 0.1 mM β-Mercaptoethanol; 1 mM sodium pyruvate
TSC medium	RPMI 1640, 20% (v/v) FCS; 50 U/ml penicillin/streptomycin; 2 mM L-glutamine; 1mM sodium pyruvate; 0.1 mM β-mercaptoethanol; 25 ng/ml FGF4; 1 µg/ml Heparin (Final TSC medium consists of 70% feeder-MEF conditioned TSC medium and 30% fresh,

	unconditioned TSC medium.) Culture medium is supplemented with FGF4/Heparin directly before use.
XEN cell medium	RPMI 1640, 15% (v/v) FCS, 2 mM L-glutamine; 50 U/ml penicillin/streptomycin
293T transfection medium	Advanced DMEM; 2% (v/v) FCS; 50 U/ml Penicillin/Streptomycin; 2 mM L-glutamine; 25 µM Chloroquine
293T virus production medium	Advanced DMEM; 5% (v/v) FCS; 50 U/ml Penicillin/Streptomycin; 2 mM L-glutamine
Freezing medium (2x)	FCS; 20% (v/v) DMSO

2.12 Software

Ensembl	Genome database	http://www.ensembl.org
FACS DIVA	Flow cytometry software	BD Bioscience Pharmingen, USA
FlowJo	Analysis of flow cytometry data	https://www.flowjo.com
ImageJ	Image processing software	http://imagej.nih.gov/ij/
Illustrator CS5	Vector graphics software	Adobe, San Jose, CA, USA
Serial Cloner version 2.6.1	Molecular analysis software	http://serialbasics.free.fr/ Serial_Cloner.html
Microsoft 365	Office Software	Microsoft®, Redmond, MA, USA
NCBI	Collection of databases by the National Center for Biotechnology Information (NCBI)	http://www.ncbi.nlm.nih.gov/

3. Methods

3.1 Microbiological methods

3.1.1 Transformation of chemically competent bacteria

For transformation and amplification of plasmids, chemically competent TOP10 *Escherichia coli* (*E. coli*) was used. Cells were slowly thawed on ice, before adding between 0.5 - 2 µl of plasmid solution, depending on concentration of plasmid stock. Cells were incubated on ice for 20 minutes, before performing heat-shock for 45 s at 42°C. The suspension was then cooled on ice for 3 min after which 250 µl of LB medium without (w/o) antibiotics were added. The suspension was then incubated for 1 h at 37°C in an orbital shaker incubator and subsequently spread on LB agar dishes, where the cells could grow overnight at 37 °C.

3.1.2 Plasmid isolation

To isolate large amounts of plasmids the NucleoBond Xtra Kit was used, according to manufacturer's protocol.

3.2 Cell culture

3.2.1 Cell culture conditions

Cells were incubated at 37°C and 7.5% CO_2 under humidified atmosphere. Cell culture maintenance and experiments were performed under sterile conditions in a laminar flow hood.

3.2.2 Passaging of cells

Cells were cultured until reaching approximately 70% confluency before passaging. Therefore, cells were washed twice with PBS and incubated with 0.05% Trypsin-EDTA for 3 - 4 min at 37 °C in the incubator. Trypsin was inactivated by adding growth medium, upon which the cell suspension was transferred to a centrifuge tube and pelleted by centrifugation at 1000 rpm for 3 min. The supernatant was aspirated, and the cell pellet was re-suspended in fresh growth medium before reseeding in appropriate ratios on a fresh cell culture plate.

3.2.3 Embryonic stem cell culture

For the culture of ESCs, cell culture dishes were coated with 0.1% gelatin solution (w/v in PBS) by incubation at 37°C for ~10 min. Prior to seeding of ESCs, gelatin coating solution was aspired, and mitotically inactive murine embryonic fibroblasts (γMEFs) were seeded in ESC medium, forming a layer of feeder cells for the ESCs.

3.2.4 Cryopreservation of cells

Cells were pelleted and re-suspended in culture medium and 2x freezing medium in equal amounts before transfer into cryo tubes. Cells were then first frozen in Styrofoam boxes at -80°C and afterwards transferred into gas phase liquid nitrogen tanks for long-term storage.

3.3 Lentiviral gene delivery

All experiments involving lentiviral vectors were performed according to biosafety laboratory 2 (S2) guidelines.

3.3.1 Lentivirus production

Before lentivirus production plasmids were precipitated and re-suspended in 10 mM Tris buffer (pH 8) and 293T cells were seeded on poly-L-lysine coated cell culture dishes. After 16 h culture medium was changed to 293T transfection medium and 293T cells were transfected using calcium-phosphate precipitation (Table 1).

Table 1: Reaction mixture for DNA transfection by calcium phosphate precipitation

	6-Well plate	10 cm dish
2 M $CaCl_2$	10 µl	61.5 µl
Lentivector-DNA	3 µg	18.5 µg
psPAX2; HIV-GAG	1.5 µg	9.25 µg
pMD2.G; VSV-G	1.5 µg	9.25 µg
ad $_{dd}H_2O$	100 µl	600 µl
2x HBS Buffer	100 µl	600 µl

The transfection mix was prepared and incubated for 15 min at RT and was added dropwise to the 293T cell culture. After 5 – 6 hours the medium was exchanged with 293T virus production medium. Virus containing supernatant was collected 72 h and 96 h after transfection and was filtered through a 0.45 µm SFCA membrane filter. The filtered supernatant was divided into aliquots and stored at -80° C until use.

3.3.2 Lentiviral transduction and selection of transduced cells

To increase transduction efficiencies, ESCs were transduced in the presence of 8 µg/ml polybrene. ESCs were incubated in virus containing and polybrene supplemented ESC medium overnight in

the incubator. The next day, virus-containing medium was replaced with fresh medium and the cells were cultured for another 24 hours in virus-free ESC medium. For the pCW57.1_Gata6 plasmid, carrying a puromycin resistance cassette, selection of positive clones was performed by culture in the presence of 0.8 µg/ml puromycin for 5 days. For pLV_mCherry transduced cells, positive clones were identified by fluorescent signal and isolated by manual colony picking under the microscope.

3.4 Generation of RtL-embryoids

3.4.1 3D cell culture system

For the generation of 3D Petri dishes 3D Petri Dish molds were used. An agarose solution was prepared by mixing 2 g of cell culture-grade agarose with 50 ml DEPC-H_2O and 0.45 g NaCl. The mix was microwaved until the agarose had fully dissolved and was subsequently used for casting of 3D petri dishes from 3D Petri Dish molds. Once the agarose solidified the mold was carefully flexed until the casted agarose 3D Petri dish could be removed, which was then placed in a well of a 12 well cell culture plate filled with 2 ml of reconstructed embryo medium (Zhang et al., 2019). Agarose 3D Petri Dishes were equilibrated in medium for at least 1h at RT.

3.4.2 Preparation of ESC lines for seeding in 3D cell culture system

Prior to seeding in 3D co culture, the individual ESC line cultures where closely monitored for at least 2 weeks, ensuring cell cycle synchronization and proliferative, pluripotent cell states of each ESC line destined for use in 3D cell culture experiments. Cells were passaged when having reached ~85% confluency at low passaging ratios (1:3 to 1:5) for 2 – 3 passages onto gelatin coated culture dishes without γMEFs. This preparation step is performed to stepwise remove γMEFs from the ESC cultures, low passaging numbers were used to ensure survival of ESCs during depletion from γMEFs. Before seeding, ESCs were washed twice with PBS and incubated with 1x Accutase for 8 – 10 min at 37° C to detach cells from the surface of the culture dish. Here, Accutase was used as cell dissociation reagent, as a gentler alternative to Trypsin-EDTA, providing more intact surface molecules on the cells, thereby increasing efficiencies for aggregation in 3D co culture. After incubation, ESC culture medium was added to inactivate Accutase and cells were resuspended into a single cell suspension. Cells were pellet for 3 min at 1000 rpm, the supernatant was aspired, and the cell pellet was resuspended in ESC culture medium.

3.4.3 Seeding of ESCs in 3D co culture

Before adjusting cell counts for seeding, ESC single cell suspensions were transferred on uncoated 24-well plates and incubated at 37° C for 10 – 15 min. Supernatants containing ESCs were then

transferred to another well of the 12-well plate and again incubated at 37° C for 10 – 15 min. These steps were performed to deplete the single cell suspension from remaining γMEFs, which settle and attach to the uncoated culture dish surface faster than ESCs. Transferring the ESC containing supernatant to the next culture well thereby stepwise purifies the ESC suspensions. The supernatant is then transferred to a 5 ml reaction tube and cell counts were determined using a Neubauer Counting Chamber. For seeding in 3D co culture cell counts were adjusted by dilution in fresh ESC culture medium to the target cell count per ml (Table 2).

Table 2: ESC lines and target cell counts for seeding of ESCs in 3D co-culture

ES cell line	*Desired average cell count per microwell*	*Target cell count per ml for seeding*
Kermit ESCs	6 cells/microwell	7.680 cells/ml
5 Factor ESCs	16 cells/microwell	20.480 cells/ml
iGATA6 ESCs	5 cells/microwell	6.400 cells/ml

Next, the ESC starting population was prepared from the diluted ESC single cell suspensions. For seeding in 12 3D Petri Dishes, each placed in a well of a 12-Well plate, a total of 2.4 ml seeding suspension containing all ESC lines in their required target cell count is needed. Therefore, 3 ml of each ESC dilution suspension were pooled in a 15 ml centrifugation tube, resulting in a total of 9 ml. As each ESC suspension is thereby diluted in a 1:3 ratio, the mixed single cell suspension was pelleted at 1000 rpm for 3 min, the supernatant was removed, and the pellet was resuspended in 3 ml fresh, complete ESC culture medium to achieve target cell count per ml again. Before seeding of the starting cell population, all reconstructed embryo medium was carefully aspirated from the 12-Well plate wells and the seeding chamber of the 3D Petri Dishes. 200 µl of the mixed single cell suspension was transferred into the seeding chamber of each 3D Petri Dish and cells were incubated at 37° C and 7.5% CO_2 for 2 h to allow for the cells to settle into the microwells. Once all cells had settled to the bottom of the microwells, 2 ml ESC culture medium were added to the side of the 12-Well plate well and the cells were incubated for 24 h in the incubator.

3.4.4 Initiation of transgene expression, reprogramming and self-organization

Transgene expression in 5 Factor- and iGATA6 ESCs was induced 24 h after seeding of the starting cell population by changing the culture medium to reconstructed embryo medium supplemented with 2 µg/ml doxycycline. Therefore, ESC culture medium was carefully aspirated from the side

of the 12-Well plate well, leaving medium inside the seeding chamber untouched. 2 ml of reconstructed embryo medium, supplemented with 2 µg/ml doxycycline, was added to the side of the well. Cell aggregates were cultured at 37° C and 7.5% CO_2 in presence of DOX for 72 h and culture medium was exchanged daily during this period, as described above. After 72h of culture in DOX supplementation, the medium was changed to reconstructed embryo medium without DOX. Aggregates were cultured for another 24h w/o DOX before analysis.

3.4.5 Harvesting of RtL-embryoids

To harvest the aggregates a new 12-Well plate was prepared with 2 ml PBS per well. The 3D Petri Dishes containing the aggregates were carefully lifted from their culture wells using sterile forceps and placed upside down into the PBS containing wells of the new 12-Well plate. The 12-Well plate was then centrifuged at 500 rpm for 3 min to force the aggregates out of their microwells, which accumulate at the bottom of the wells. The aggregates were collected using 1000 µl pipette tips, from which the very tip was removed with sterile scissors at ~ 1 mm to widen the intake of the pipette tips, decreasing shear forces acting on the structures during handling.

3.5 Immunofluorescent staining of aggregates

Aggregates were generated as described before and collected and pooled in a 5 ml round bottom test tube for immunofluorescent (IF) staining. All resuspension steps during IF staining were performed using 1000 µl pipette tips with widened intakes. Aggregates were centrifuged at 300 rpm for 2 min, forcing the aggregates to the bottom of the tube. PBS was removed and aggregates were fixed in 1 ml 4 % (w/v) PFA at 4° C for 20 min. Aggregates were centrifuged at 300 rpm for 2 min, PFA was removed, and aggregates were washed three times using wash buffer and centrifugation steps at 300 rpm for 2 min in between. Permeabilization of the aggregates was performed by incubation in 0.5 % (v/v) Triton X-100 solution for 30 min at RT. Aggregates were then incubated in blocking buffer (3 % [w/v] BSA, 0.3 % [v/v] Triton X-100 in PBS) with primary antibodies at 4°C overnight. Unbound primary antibody was removed by washing the aggregates three times, before incubation with Alexa-Fluor conjugated secondary antibody in blocking buffer, at 4° C overnight and protected from light. Aggregates were washed again three times, resuspended in Roti®-Mount FluorCare DAPI and were then transferred onto Cellview Cell Culture Dishes, which were closed using 6-Well plate glass slides. Fluorescent microphotographs were taken with either a Leica DM IRB or VisiScope confocal microscope.

3.6 Immunofluorescent staining of fixed cells

For IF staining of cells cultured on cell culture plates, the culture medium was aspired, and cells were washed three times with PBS. Cells were fixed for 10 min with 4% PFA and washed twice with PBS before permeabilization with 0.5 % Triton X-100. Blocking was performed in blocking buffer (2 % [w/v] BSA and 0.1 % [v/v] Triton X-100 in PBS) for 1 h at RT. Primary antibody incubation was performed in blocking buffer overnight at 4° C. Cells were washed three times before incubation with secondary antibody in blocking buffer for 2 h at RT and protected from light. Cells were washed three times and nuclei were stained with Hoechst33342 for 10 min, followed by three washing steps. Imaging was performed using a Leica DM IRB microscope.

3.7 FACS sorting for scRNA-Seq

Aggregates were generated as described before, but iGATA6 ESCs were substituted for iGATA6_mCherry ESCs, which allowed for identification of correctly assembled and compartmented structures. These presented as elongated structures, composed of a mCherry+ sphere-like compartment surrounding GFP+ Kermit ESCs adjacent to non-fluorescent cells originating from 5 Factor ESCs. More than 600 correctly structured aggregates were picked under the microscope, using 1000 µl pipette tips with widened intakes, and pooled in an 8 ml round bottom tube. Aggregates were pelleted by centrifugation at 300 rpm for 2 min and a single cell suspension was generated by incubation in 500 µl Accutase cell dissociation reagent for 15 minutes. 1 ml FACS buffer (2% FCS in PBS) was added, and the aggregates were further dissociated by pipetting up and down and passing through a 40 µm cell strainer. Single cells were pelleted by centrifugation at 500 rpm for 3 minutes, the supernatant was removed, and the cell pellet was resuspended in 1 ml FACS buffer with primary antibody against CD40. After incubation on ice for 30 minutes, the single cell suspension was centrifuged at 500 rpm for 3 minutes, the supernatant was removed, and cells were washed three times with FACS buffer. Cells were resuspended in FACS buffer with Chicken polyclonal secondary antibody to Goat IgG-H&L (Alexa Fluor® 647) and incubated for another 30 min on ice, after which cells were washed three times and the LIVE/DEAD Fixable Yellow Dead Cell Stain Kit was applied according to manufacturer's protocol. Flow cytometry and sorting was performed using the BD Aria III.

3.8 Cellular reprogramming in 2D monoculture

For the comparison of reprogramming outcomes between 2D monoculture and 3D co-culture, iGATA6 ESCs and 5F ESCs were seeded on gelatin coated cell culture dishes in ESC culture medium. 24 h after seeding the culture medium was changed to cell culture media that support

proliferation of the induced stem cell fates. Cellular reprogramming of 5F ESCs towards iTSCs was performed in serum containing TSC medium, consisting of 70% feeder-MEF conditioned medium (CM) and 30% fresh, unconditioned TSC medium, supplemented with FGF4 and Heparin, as published by Tanaka et al. (Tanaka et al. 1998). Cellular reprogramming of iGATA6_mCherry ESCs to iXEN_mCherry cells was performed in serum containing XEN cell medium following the protocol published by Niakan et al. (Niakan et al., 2013). Transgene expression and subsequent cellular reprogramming was initiated by culture medium supplementation with 2 µg/ml doxycycline for 3 days. Identical to the reprogramming approach in 3D co-culture, the 2D mono-cultured cells were kept in their respective culture medium for another 24 h without DOX supplementation before FACS sorting and sequencing. Kermit ESCs were cultured in 2i/LIF supplemented ESC medium until FACS and subsequent sequencing. For sorting of 5F ESCs, the 2D mono-cultured cells were incubated in Accutase for 8 minutes at 37°C before staining against CD40 as described before. Cell sorting by FACS was performed as described before, yielding a CD40+/GFP-/mCherry- iTSC population, a CD40-/GFP+/mCherry- ESC population and a CD40-/GFP-/mCherry+ iXEN cell population.

3.9 *In vivo* transplantation experiments

All experiments involving animals were conducted according to the German law of animal protection and in agreement with the approval of the local institutional animal care committees (Landesamt für Natur, Umwelt und Verbraucherschutz, North Rhine-Westphalia. Approval ID: 81-02.04.2019.A075)

3.9.1 Animal care

Mice were housed in a controlled environment (Humidity and temperature, 12h light and 12 darkness cycles) in plastic cages with bedding. Animals received dry food and water ad libitum. Mice were sacrificed by cervical dislocation.

3.9.2 Transplantation assay

Pseudo-pregnant mice were generated by mating of CB6F1 females with vasectomized males. Plug-positive females were isolated and used for uterine transfer with RtL-embryoids at 2.5 days post coitum (d.p.c.). Correctly assembled RtL-embryoids were generated and identified as described before, using Kermit ESCs, 5 Factor ESCs and iGATA6_mCherry ESCs. 7 days after transplantation the mice were sacrificed and analyzed for possible implantation sites. Angela Egert and Andrea Jäger performed transplantation of RtL-embryoids into uteri.

3.10 Derivation of stem cells from RtL-embryoids

ESC-like and ExE-like stem cells were derived from RtL-embryoids by outgrowth culture performed in 2i/LIF supplemented ESC medium or FGF4/Heparin supplemented TSC medium respectively. Therefore, RtL-embryoids were generated as described before and seeded onto gelatin-coated cell culture plates, in either ES or TS medium, where they were allowed to settle and attach. Aggregates were cultured in these conditions, until cellular outgrowth formed, at which point the cells were dissociated by incubation in TrypLE express and passaged onto a new, gelatin-coated culture plate. Once colonies had formed, they were picked manually using a microscope and a 100 µl pipette. The isolated colonies were cultured in individual monocultures and passaged as described above before characterization by IF staining for ES and TS marker.

3.11 Analysis of the scRNA-Seq dataset

Detailed information about the bioinformatic analysis of the RtL-embryoid scRNA-Seq dataset describing all codes and parameters was published in Langkabel et al. (Langkabel et al., 2021; Langkabel et al., accepted manuscript). Analysis of the scRNA-Seq dataset was performed in cooperation with Arik Horne (AG Schultze - Genomics and Immunoregulation; LIMES Institute; University of Bonn). The data and Seurat objects generated in this study are deposited via FASTGenomics (http://beta.fastgenomics.org/d/200474) and the code (Written by Arik Horne: Langkabel_Horne_2021_Rosette-to-Lumen_stage_embryoids) can be accessed via FASTGenomics (fastgenomics.org). Raw sequencing data of mouse Smart-seq2 generated in this study have been deposited in the Gene Expression Omnibus (GEO) database under accession code GSE188394.

3.12 Data presentation and statistical analysis

All data are presented as mean values ± standard derivation (SD) unless otherwise stated. Graphs were generated with Graphpad Prism and Microsoft Excel. Figures were generated using the R packages Seurat and the ggplot2 package (version 3.3.2, (Wickham, 2016)) and assembled with Adobe Illustrator. Schematics were created using Microsoft PowerPoint. P-values > 0.05 were not considered statistically significant.

4. Results

4.1 ES cell lines for the generation of the *in vitro* embryo model

To create embryo-like structures that are comprised of the three main tissues that make up a blastocyst or general early embryonic architecture, three ESC lines were chosen to induce either an ICM/Epi-like, a PrE/VE-like and a TE/ExE-like cellular identity. For the ICM/Epi-like cell population, Kermit ESCs were chosen, that were derived from blastocysts of transgenic mice carrying an *Oct3/4* promotor driven GFP expression cassette (Figure 14) (Yoshimizu et al., 1999).

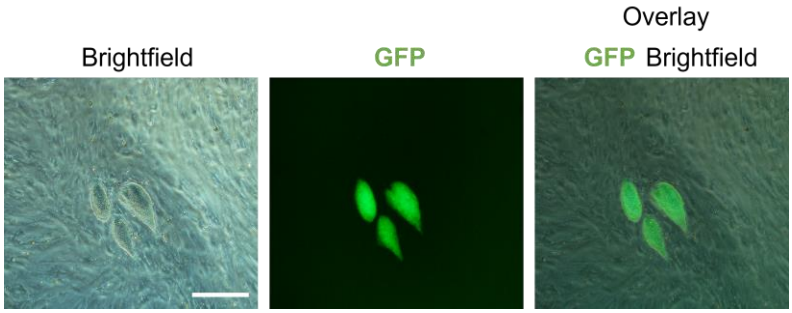

Figure 14 – Kermit ESCs displaying *Oct3/4* promoter driven GFP expression. Photomicrographs of Kermit ESCs carrying an *Oct3/4* promotor driven GFP expression cassette. Detection of GFP is indicative of *Oct3/4* expression and thereby a pluripotent cellular state. Scale bar = 100 µm

The *Oct3/4*-GFP transgene allows for visualization of pluripotent cells that can be used to live track Kermit ESCs within an aggregate in co-culture with other cells. Since the protocol established in this study relies on cellular reprogramming of ESCs to iTSCs or iXEN cells, the culture conditions would not allow for 2i/LIF supplementation of the culture medium to maintain a state of pluripotency in the ICM/Epi-like tissue. Therefore, detection of GFP expressing Kermit ESCs in an ICM/Epi-like tissue would also indicate that a pluripotent cell fate is maintained and stabilized by the cellular crosstalk and microenvironment of the organoid system itself.

The generation of a TE/ExE-like tissue required an ESC line that can be reprogrammed towards trophoblast cell fate-lineages. Here 5 Factor ESCs carrying five doxycycline inducible, trophoblast stem cell-fate related transcription factors: *Cdx2*, *Tfap2c*, *Eomes*, *Gata3* and *Ets2* was chosen, as we were able to demonstrate high efficiency of cell lineage conversion of 5 Factor ESCs to iTSCs, even in serum based, hence undefined, TSC culture medium conditions (Kaiser et al., 2020). This was regarded pre-requisite for the protocol presented in this study, as the culture medium for an embryo-like organoid would have to be suitable to allow for proliferation and maintenance of all three embryo-like tissues and the cell lineages they are comprised of. Expression of the five TSC transgenes in 5 Factor ESCs was validated on protein level by immunofluorescent staining against

the respective proteins, after culture in ES medium supplemented with 2 µg/ml DOX for 3 days (Figure 15) (Kaiser et al., 2020).

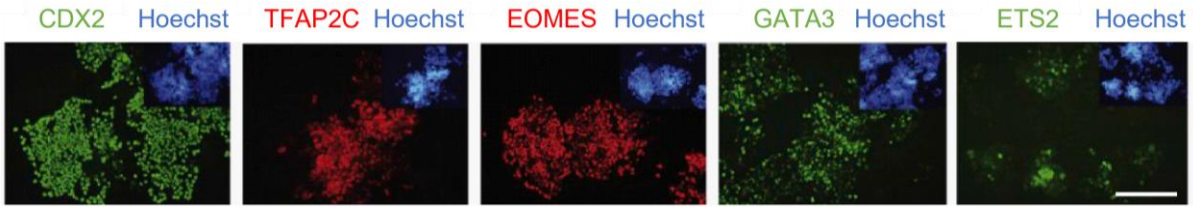

Figure 15 - Detection of TSC marker expression on protein level in 5 Factor ESCs. Photomicrographs of 5 Factor ESCs after IF against CDX2, TFAP2C, EOMES, GATA3 and ETS2 after 3 days of doxycycline mediated transgene induction in ES medium. Inlay images display Hoechst staining indicating nuclei. Scale bar: 250 µm. (Modified from Kaiser et al. 2020)

For the generation of a PrE/VE-like tissue, a third ES cell line was generated by lentiviral transduction of WT ESCs (KNUT1 ESCs) with the pCW57.1_Gata6 plasmid, encoding for a tetracycline (Tet-On) controlled *Gata6* transgene expression cassette (Ngondo et al., 2018). Expression of *Gata6* in ESCs has been shown to be sufficient to initiate reprogramming towards induced extraembryonic endoderm stem cells (iXEN cells) (Wamaitha et al., 2015; Ngondo et al., 2018). After selection for clones that had integrated the construct, by culture in presence of 0.8 µg/ml puromycin for 5 days, surviving colonies were picked and expanded for analysis by IF staining against GATA4. GATA4, a transcription factor involved in the extraembryonic endoderm lineage identity and a downstream target of the induced GATA6 was detected by IF staining after 3 days of culture in ES medium supplemented with 2 µg/ml DOX (Figure 16) (Soudais et al., 1995).

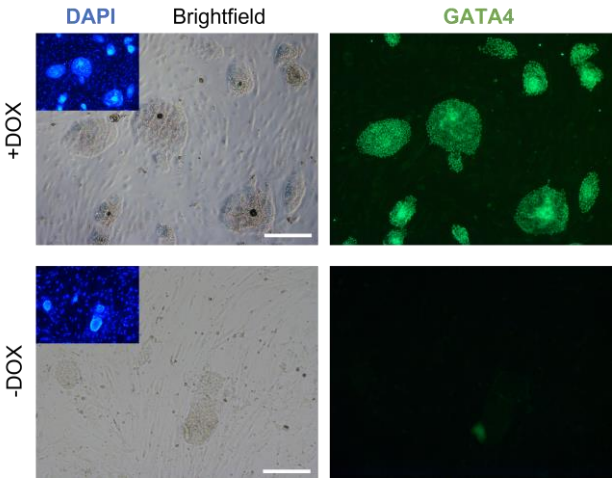

Figure 16 – Detection of XEN cell marker expression on protein level in iGATA6 ESCs. Photomicrographs of iGATA6 ESCS after IF staining against GATA4 after 3 days of culture in ES medium supplemented with 2µg/ml DOX (Upper Panel) or without DOX (lower panel). Inlay images display DAPI staining indicating nuclei. Scale bars = 100 µm.

4.2 Establishing a 3D cell culture environment

Correct assembly and subsequent embryo-like development requires co-culture of the three ES cell lines in a 3D environment. For this study agarose 3D Petri Dishes were used, as they provide an inexpensive, reproducible 3D cell culture system, that can be casted from silicon micromolds using molten, saline 2% agarose solution. These 3D Petri Dishes offer a total of 256 microwells for 3D culture of cells, situated in a framed seeding chamber, holding a volume of 200 µl

(Figure 17). The 3D Petri Dishes can be placed in a well of a 12-well cell culture plate, that can be filled with 2 ml of culture medium after the cells have settled into the microwells. This allows for fast and easy exchange of medium from the side of the well of the 12-well cell culture plate, without disturbing or loosing aggregates, which are located at the bottom of the circular 3D culture recesses (diameter: 400 µm x depth: 800 µm). The defined amount of microwells and volume of the seeding chamber system allows for seeding of single cell suspensions in average-based cell ratios per microwell. As for cell culture medium used for reprogramming in 3D co-culture, reconstructed embryo medium was chosen, as it was already demonstrated to provide a suitable growth environment for embryo-like structures generated from blastocyst-derived stem cell lineages (Zhang et al., 2019). This simple, basal medium consists of 39% advanced RPMI 1640, 39% DMEM, 17.5% FCS, 2 mM GlutaMAX, 1% penicillin-streptomycin, 0.1 mM β-mercaptoethanol, 0.1 mM MEM non-essential amino acids and 1 mM sodium pyruvate (Zhang et al., 2019). It represents a basic growth medium, without cytokines or other signaling pathways enhancing or stabilizing factors, hence allowing for undisturbed signaling between the cell lineages comprising the aggregates.

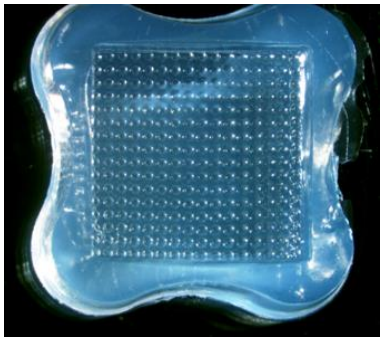

Figure 17 – Agarose 3D Petri Dish. Photomicrograph of a 3D Petri Dish with 256 microwells located in a seeding chamber, casted from micromolds using saline 2 % agarose solution.

Previous research performed by our group indicated that 3D co-culture of Kermit ESCs and a second ESC line, that can be reprogrammed towards an iTSC-fate by DOX controlled expression of *Cdx2* and *Gata3,* resulted in the formation of blastocyst-like structures (iBLAST) (Bachelor thesis Alexej Knaus, 2011) (Buhl et al., 2009). These experiments were performed using hanging drop culture to provide a 3D cell culture environment and reprogramming was initiated by culture in DOX supplemented ES culture medium (w/o 2i/LIF). To evaluate the functionality of the technically potentially more advanced 3D culture system used for this thesis, first experiments were performed to recreate the generation of iBLASTs by co-culture of Kermit ESCs and 5 Factor ESCs in 3D Petri Dishes. Therefore, an average of 4 Kermit ES cells and 4 5 Factor ES cells per microwell were seeded in ESC culture medium supplemented with 2i/LIF and allowed to build cell-cell adhesions and aggregates for 24h, before the culture medium was changed to reconstructed embryo medium supplemented with 2 µg/ml DOX to initiate reprogramming in 5 Factor ESCs. Aggregates were cultured in the presence of DOX for 120 hours, at which point the structures were harvested and analyzed by IF staining against CDX2 to visualize cells undergoing reprogramming towards iTSC-fate, and by FACS for the proportions of GFP positive, hence *Oct3/4* expressing Kermit ESCs (Figure 18). For aggregates cultured without DOX, a random distribution

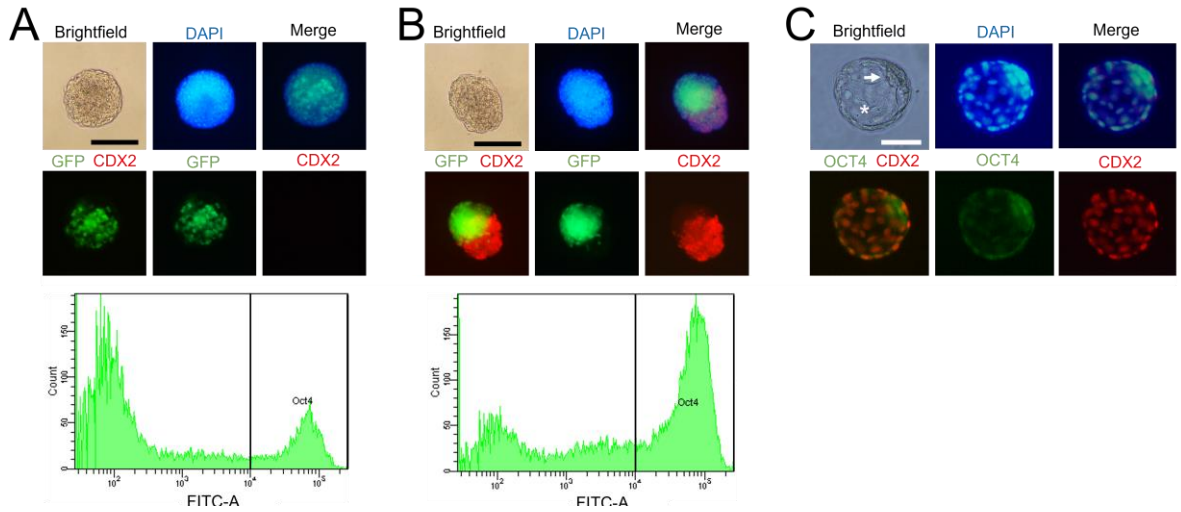

Figure 18 – Characterization of aggregates composed of Kermit ESCs and 5 Factor ESCs. Photomicrographs of aggregates cultured without DOX (**A**) or in presence of 2 µg/ml DOX (**B**) for 120h, analyzed by IF staining against CDX2 (Upper rows) and FACS profiles displaying *Oct3/4*-driven GFP expression in Kermit ESCs (Lower rows), from aggregates pooled and dissociated into single cell suspensions. Scale bars = 100 µm. **C**) Photomicrographs of a blastocyst (~E4.0) analyzed by IF staining against CDX2 and OCT4. Asterisk indicate blastocoel; arrow points towards ICM. DAPI staining indicates nuclei. Scale bar = 50 µm.

of Kermit and 5 Factor ESCs was observed and the majority of cells comprising the aggregate was found to be GFP-negative (Figure 18 A). Aggregates cultured in presence of DOX however, displayed an elongated morphology, with two distinct, organized cellular compartments comprised of Kermit ESCs or 5 Factor ESCs (Figure 18 B). FACS revealed a shift in the profile of GFP expressing cells, indicative of *Oct3/4* expression and a cellular state of pluripotency in those self-organized structures (Figure 18 B). This result indicates that the induced iTSCs originating from 5 Factor ESCs are able to support and sustain pluripotency in co-cultured Kermit ESCs. However, the structures did not resemble natural blastocysts at E3.5 or iBLASTs, with a CDX2+ trophectoderm-like structure surrounding an OCT4+ ICM-like structure next to a fluid filled cavity, but instead showed resemblance to the two inner compartments, Epi and ExE, of early murine embryos at the egg cylinder stage around E5.5 (Figure 2, Figure 3, and Figure 18 B and C). Of note, embryo-like structures presented by Sozen et al and Zhang et al., displayed similar results, when blastocyst-derived TSCs and ESCs were co-cultured in 3D cell culture environments, resulting in the generation of ETS embryoids (Sozen et al., 2018; Zhang et al., 2019). Having confirmed, that the 3D cell culture system provides a suitable cell culture environment for the aggregation, reprogramming and self-organization of cell of the starting population, it was next assessed how a triple ESC line approach would perform, using Kermit ESCs, 5 Factor ESCs and iGATA6 ESCs. Therefore, the starting cell population was prepared in ratios resulting in an average of 4 x Kermit ESCs, 4 x 5F ESCs and 4 x iGATA6 ESCs per microwell of the 3D Petri Dish. Again, cells were allowed to aggregate for 24 h, before changing the culture medium to reconstructed embryo medium supplemented with 2µg/ml DOX to initiate reprogramming of 5 Factor ESCs towards an iTSC fate and iGATA6 ESCs towards an iXEN cell identity. Aggregates were

cultured in presence of DOX for 3 days, after which the culture medium was changed to reconstructed embryo medium w/o DOX for another 24 h before analysis of the generated structures by IF staining against trophoblast-marker CDX2 or XEN cell-/VE- marker GATA4. CDX2 expressing cells were again found to aggregate in a cellular cluster neighboring GFP+ Kermit ESCs, thereby again, resembling the two inner compartments Epi and ExE found murine embryos at the egg cylinder stage (Figure 19). An additional, third tissue was detected, surrounding the two inner compartments, that was comprised of cells that were negative for both, GFP and CDX2 signals. (Figure 19). IF staining against GATA4 revealed that this sphere-like tissue consisted of cells expressing the XEN cell- / VE- marker (Figure 20). Together, these results demonstrate, that co-culture of Kermit ESCs, 5F ESCs and iGATA6 ESCs in a 3D cell culture environment and subsequent reprogramming of 5F ESCs towards an iTSC-fate and iGATA6 ESCs towards an iXEN cell-fate, results in self-organization into structures showing murine embryonic architecture ~E5.5. These structures displayed highly organized cellular compartments, with a GATA4+, spherelike structure, resembling the VE and a GFP+, pluripotent, Epiblast-like compartment, next to a CDX2+ compartment resembling the ExE. However, efficiencies of formation of such organized structures in these preliminary experiments using a 4 + 4 + 4 cell seeding approach were low (~4 %) and the majority of structures displayed incomplete self-organization of the three compartments (Figure 21).

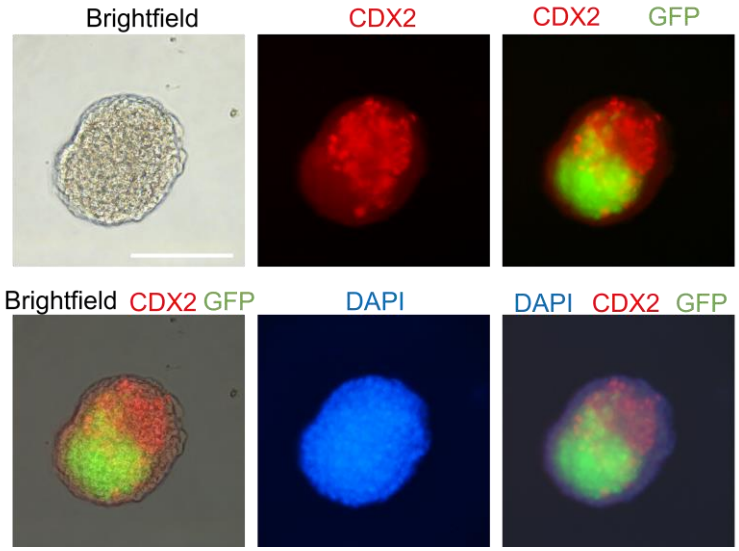

Figure 19 – Detection of TSC marker CDX2 in self organized aggregates. Photomicrographs after IF staining against CDX2 in aggregates composed of Kermit ESCs, 5 Factor ESCs and iGATA6 ESCs after transgene expression by DOX supplementation for 3d and a total of 120 h in 3D co-culture. DAPI staining indicates nuclei. Scale bars = 100 µm

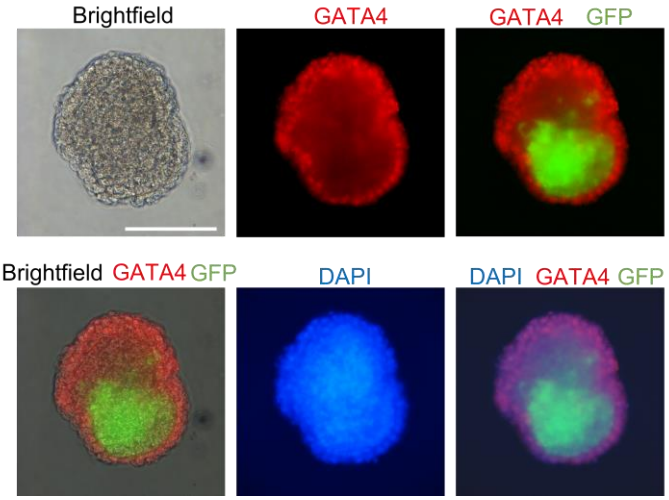

Figure 20 – Detection of XEN cell marker GATA4 in self organized aggregates. Photomicrographs after IF staining against GATA4 in aggregates composed of Kermit ESCs, 5 Factor ESCs and iGATA6 ESCs after reprogramming by DOX exposure for 3d and a total of 120h culture. DAPI staining indicates nuclei. Scale bars = 100 µm

Therefore, different ratios of cells of the three ESC lines were tested to assess whether efficiencies could be further improved, allowing for more detailed studies of correctly self-organized embryo-like structures. In initial experiments Kermit (K), 5 Factor (5F) and iGATA6 (iG6) ESCs were seeded in either equal (4+4+4, 6+6+6 and 8+8+8) or unequal (15+5+5, 5+15+5, 5+5+15) ratios and the number of correctly assembled and compartmented structures was determined (Figure 21). Highest efficiencies were observed for the combination of 5 Kermit-, 15 5F- and 5 iGATA6 ESCs, which resulted in ~16 % of the aggregates displaying correct architecture resembling murine embryos ~E5.5 (Figure 21). Next, this improved ratio of the three ES cell lines was further narrowed down by assessing the self-organization capabilities of starting cell ratios, slightly varying in the range of 5 x Kermit- + 15 x 5F- + 5 x iGATA6- ESCs (Figure 22). Highest efficiency (24.42 %) of self-organization into the three embryo-like tissue was achieved when seeding an average of 6 x Kermit ESCs, 16 x 5F ESCs and 5 x iGATA6 ESCs per microwell of the 3D Petri dish (Figure 22). Next, the percentage of correctly self-organized structures on both, day 4 into the protocol, meaning at the timepoint of omitting DOX supplementation and day 5, 24 h after omission of DOX was assessed (Figure

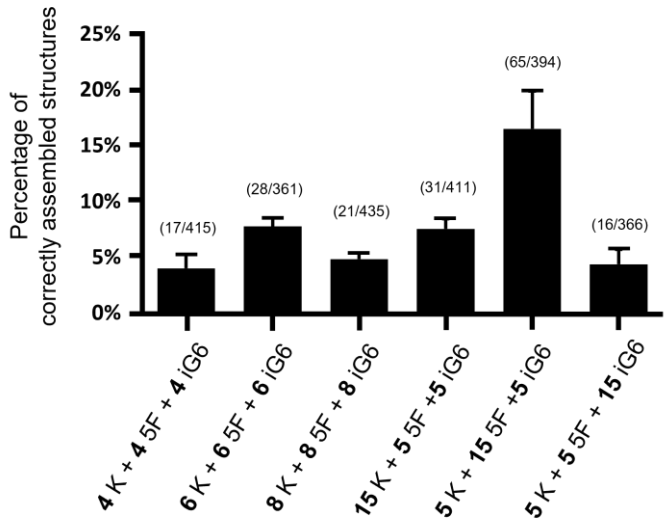

Figure 21 – Efficiency of self-organization within aggregates using varying starting cell ratios. Percentages of correctly assembled and self-organized embryo-like structures after 120h in 3D co-culture (24h aggregation, 72h +DOX, 24h -DOX). K = Kermit ESCs, 5F = 5 Factor ESCs, iG6 = iGATA6 ESCs. Numbers in brackets indicate n of correctly assembled structures versus total n (n / n total). Bar plots represent mean values ± SD of three technical replicates.

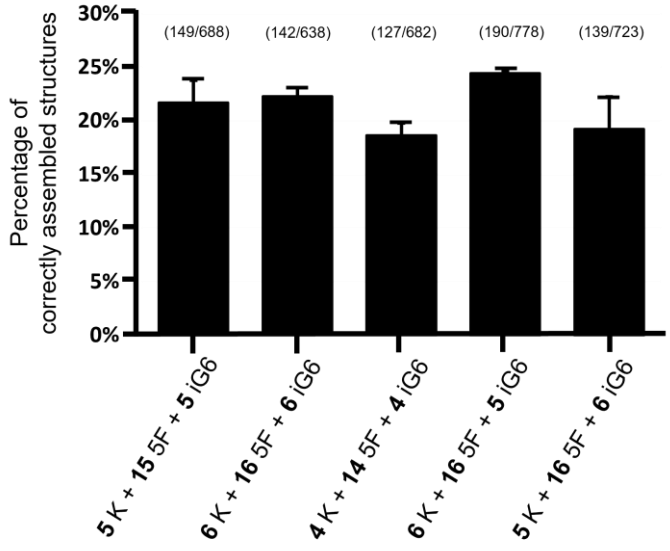

Figure 22 – Efficiency of self-organization using starting cell ratios in range of 5+15+5. Percentages of correctly assembled and self-organized embryo-like structures after 120h in 3D co-culture (24h aggregation, 72h +DOX, 24h -DOX). Numbers in brackets indicate n of correctly assembled structures versus total n (n / n total). Bar plots represent mean values ± SD of three biological replicates.

23). At day 4 about 15 % of the aggregates displayed correct assembly and self-organization, which increased to about 24 % at day 5, most likely due to the additional time for sorting and

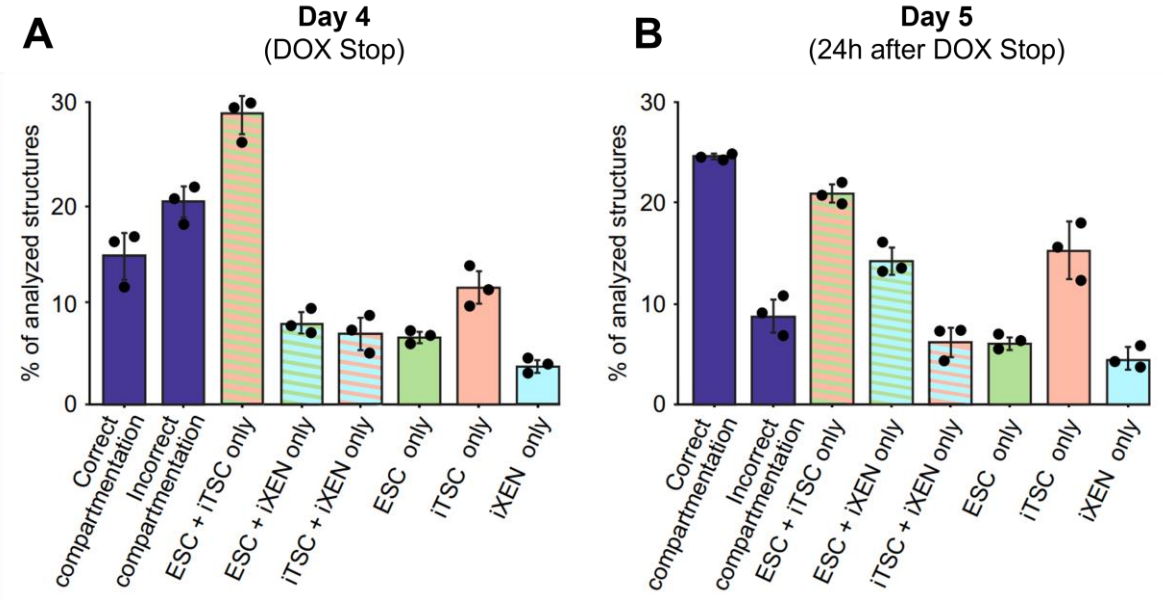

Figure 23 – Efficiency of self-organization of 6 Kermit, 16 5F and 5 iGATA6 starting ES cells. Bar plots represent mean values ± SD of three biological replicates. Total n = 1167 (**A**; Day 4) and 778 (**B**; Day 5). (Modified from Langkabel et al., accepted manuscript).

positioning of cells within the aggregates (Figure 23). Next, it was tested, if the duration and timing of DOX supplementation would have an additional effect on the efficiency of formation of embryo-like structures showing correct embryo-like architecture (Figure 24). Therefore, aggregates were generated from an average of 6 x Kermit-, 16 x 5F- and 5 x iGATA6 ESCs per microwell, as this ratio has been demonstrated to yield highest efficiencies (Figure 22 and Figure 23). Three conditions were tested to assess the effect of varying DOX conditions. Aggregates seeded directly into reconstructed embryo medium supplemented with DOX, cultured under these conditions for 72 h, before a period w/o DOX of 48h and subsequent analysis, resulted in ~13 % of correctly assembled embryo-like structures (Figure 24). When using the same experimental procedure as described before for evaluation of optimal seeding ratios, meaning seeding of the starting cell population in ES medium (2i/LIF) and 24 h to aggregate before switching to reconstructed embryo medium +DOX for 72h and -DOX for another 24 h, about 20% of the aggregates displayed embryo-like architecture (Figure 24).

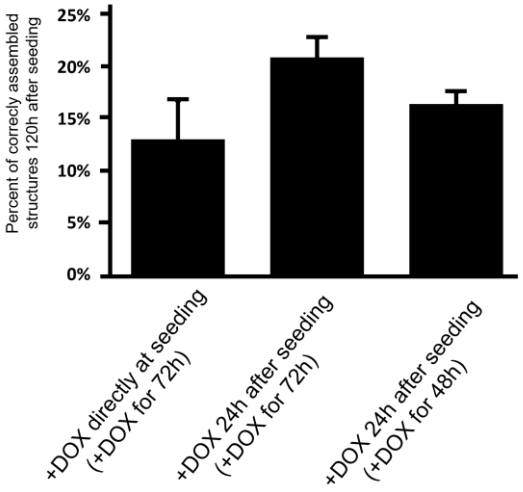

Figure 24 – Efficiency of self-organization using varying DOX conditions. Bar plots represent mean values ± SD of three technical replicates. Analysis of correctly assembled structures was performed 120 h after seeding.

Lastly, aggregates were seeded in ES medium (2i/LIF), given 24 h to aggregate and were then cultured in DOX supplemented reconstructed embryo medium for only 48 h before a period of another 48 h in -DOX conditions, to test the effect of a shortened period of DOX supplementation. In this condition, 16,44% of the aggregates displayed complete self-organization into the three embryo-like tissues (Figure 24). Based on all observations made, regarding average ratios of the three ES cell lines, timing, and duration of DOX administration and timepoint of analysis, a protocol for the generation and analysis of embryo-like structures was devised (Figure 25). On Day 0, the three ES cell lines are seeded in ES medium (2i/LIF) in an average ratio of 6 x Kermit ESCs, 16 x 5F ESCs, and 5 x iGATA6 ESCs per microwell of the 3D Petri Dish. 24 h later the cells have aggregated and formed small embryoid bodies, at which point the culture medium is replaced with reconstructed embryo medium supplemented with 2 µg/ml DOX to induce transgene expression. Aggregates are kept under in +DOX conditions for a total of 72 h, after which the culture medium is replaced with reconstructed embryo medium w/o DOX. 24 h later the aggregates are harvested from their microwells and used for further analysis. All following results presented in this study were generated from analysis of embryo-like structures that were created according to this protocol.

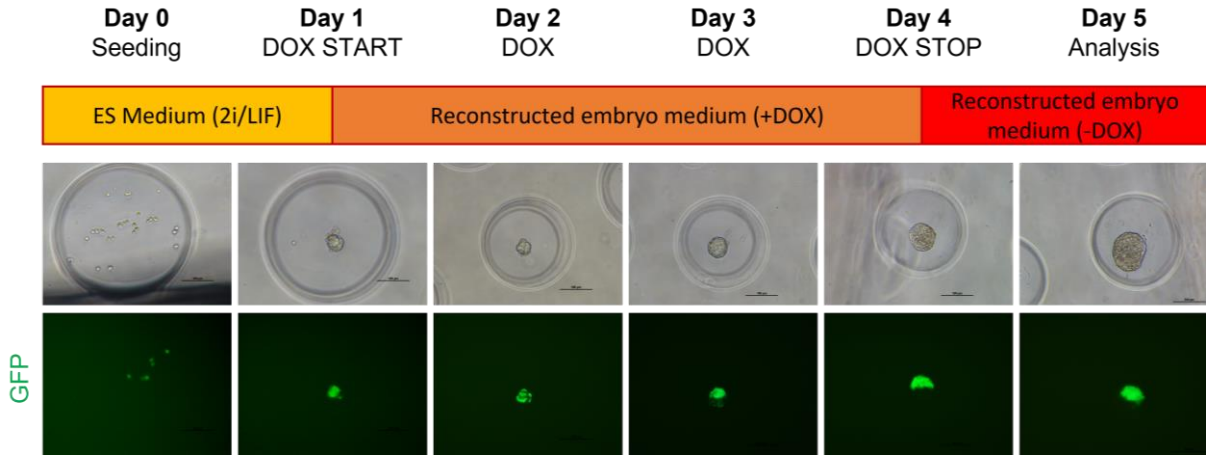

Figure 25 – Overview of the protocol for the induction of embryo-like structures. Upper row**:** Overview of steps during the protocol for the induction of embryo-like structures over the course of 5 days. Lower rows: Representative photomicrographs of the Brightfield and GFP channels at each day of the protocol, following the development of the embryo-like organoid and the self-organization of GFP+ Kermit ESCs into an Epi-like compartment. Scale bars = 100 µm

4.3 Live tracking of ESCs during self-organization

To assess the self-organizing capabilities of the aggregates and follow the spatial-temporal rearrangement of the stem cell lines during the protocol more closely, fluorescent versions of 5F- and iGATA6 ESCs were generated. Therefore, 5F ESCs and iGATA6 ESCs were transduced with a lentiviral construct constitutively expressing mCherry, creating the two daughter cell lines 5Factor_mCherry ESCs and iGATA6_mCherry ESCs (Figure 26). Together with *Oct3/4* driven GFP expression in Kermit ESCs, this allowed for live tracking of two of the three ES cell types during reprogramming and self-organization. To study self-organization of 5F ESCs and their reprogrammed derivates, embryo-like structures were generated from Kermit ESCs, 5 Factor_mCherry ESCs, and iGATA6 ESCs, using the protocol previously established. Detection of GFP and mCherry expressing cells over the course of the protocol allowed for visualization of self-assembly of the two inner, Epi- and ExE-like compartments, surrounded by the non-fluorescent VE-like compartment (Figure 27). Segregation of Kermit ESCs and 5 Factor_mCherry ESCs into

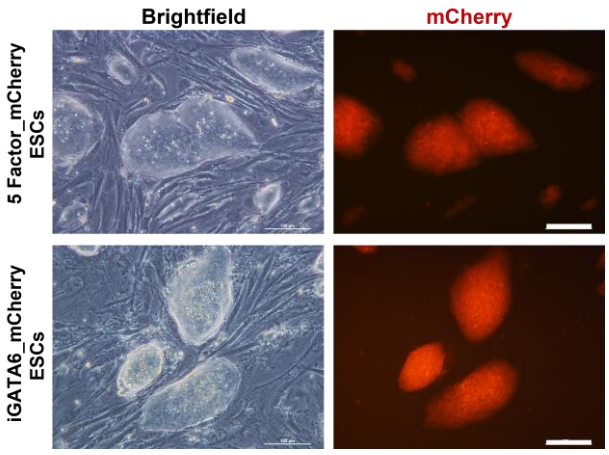

Figure 26 – Generation of mCherry expressing 5F- and iGATA6- ESC lines. Photomicrographs of 5 Factor_mCherry (Upper panel) and iGATA6_mCherry (Lower panel) ESC clones, transduced with a constitutive mCherry expression cassette. Scale bars = 100 µm

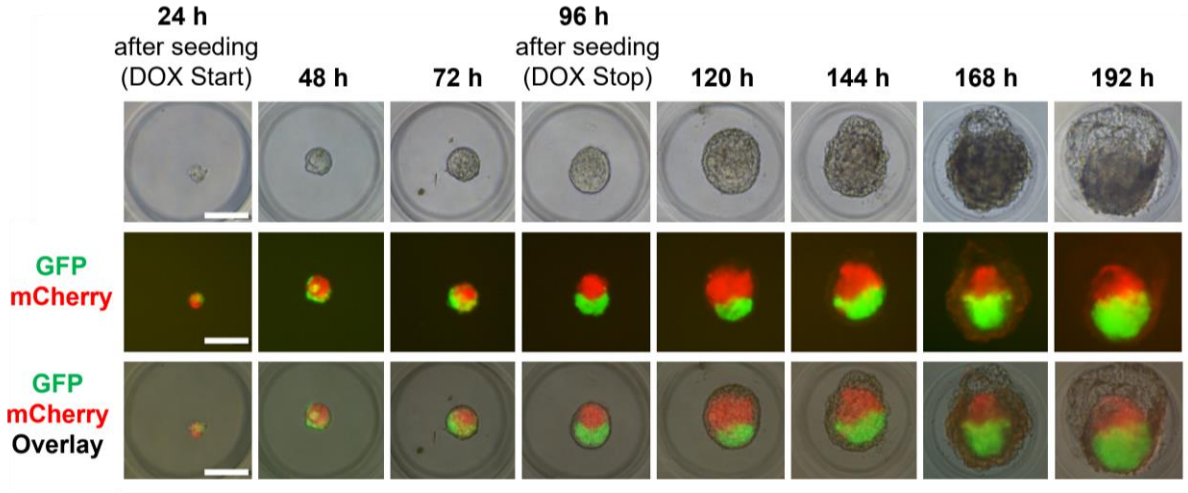

Figure 27 – Self-organization within aggregates over time following Kermit and 5 Factor ESCs. Photomicrographs of development of embryo-like structures build from Kermit ESCs, 5 Factor_mCherry ESCs and iGATA6 ESCs. Detection of GFP and mCherry allows for live tracking of assembly in an Epi-like (GFP+) and ExE-like (mCherry+) compartment. Scale bars = 100 µm (This figure has been published in Langkabel et al., 2021).

two clearly distinguishable compartments was observed earliest at 96h into the protocol, indicating, that complete reprogramming of 5F ESCs towards an iTS/iExE cell-fate requires the full duration of 3 days of doxycycline mediated transgene expression, to allow for the generation of an ExE-like compartment (Figure 27). Similar observations were made, when analyzing the ESC-to-iTSC conversion of 5F ESCs in standard, serum-based TS medium, which likewise required DOX mediated transgene expression for a total of 72h (Kaiser et al., 2020). Completely segregated Epi-and ExE-like compartments remained in their positions throughout *in vitro* culture for a total of 192 hours (Figure 27).

To visualize the self-organization of iGATA6 ESC descendent cells into a VE-like compartment, embryo-like structures were generated from Kermit-, 5F- and iGATA6_mCherry ESCs and mCherry and GFP expression was again followed for a total of 192 h (Figure 28). Again, the GFP+, Epi-like compartment was found completely compacted, as soon as 96 h into the protocol, neighboring the non-fluorescent ExE-like compartment. Following segregation of mCherry+ cells reprogrammed from iGATA6 ESCs revealed self-assembly into a sphere-like structure surrounding the two other cell types as soon as 24 h after start of DOX supplementation (Figure 28).

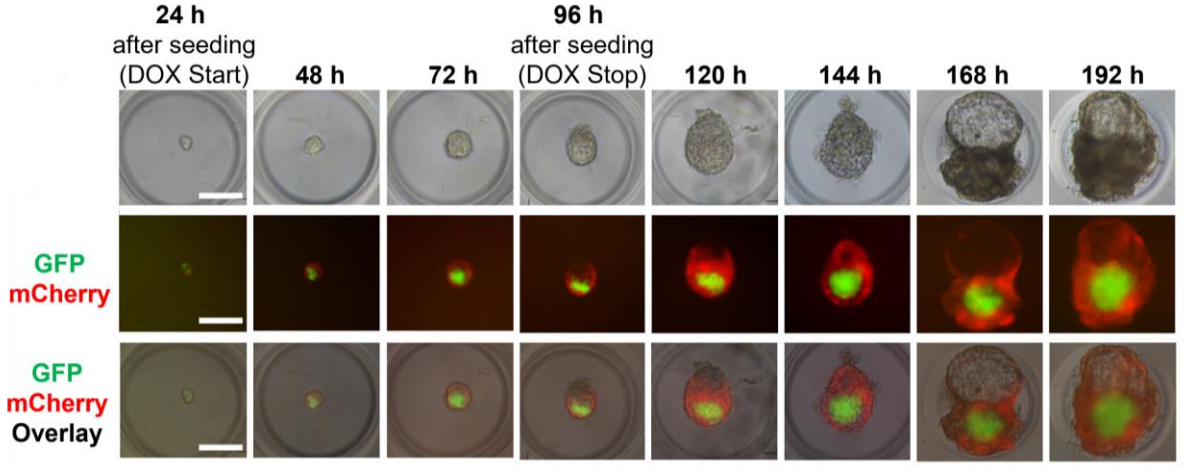

Figure 28 – Self-organization within aggregates over time following Kermit and iGATA6 ESCs. Photomicrographs of development of embryo-like structures build from Kermit ESCs, 5 Factor ESCs and iGATA6_mCherry ESCs. Detection of GFP and mCherry allows for live tracking of assembly in an Epi-like (GFP+) and VE-like (mCherry+) compartment. Scale bars = 100 µm. (This figure has been published in Langkabel et al., 2021)

The mCherry+ sphere was found to continuously surround the two inner-compartments and the structures adopted an elongated VE-like shape, as soon as 96 h into the protocol, hence the end of DOX supplementation and corresponding with the timepoint the two inner compartments were demonstrated to be completely organized (Figure 27 and Figure 28). Starting at around 144 h into *in vitro* culture the VE-like compartment started to show drastic morphological changes on the proximal site, neighboring the ExE-like compartment. This part of the VE-like compartment consistently displayed a structural outgrowth, that was limited to the proximal part of the

structures, indicating differential signaling pathways between parts of the VE-like compartment neighboring either the Epi- or ExE-like compartments (Figure 28).

4.4 Assessment of embryonic architecture by confocal microscopy

To allow for studies of the structural details of the embryo-like model, confocal microscopy was applied. Considering previous observations made regarding the timepoint of complete self-organization into embryo-like architecture at 120 h into the protocol, this timepoint was determined to be most suitable for more detailed studies of the structures generated. Immunofluorescent staining against trophoblast-/ExE- marker CDX2 further highlighted the previously observed segregation of Epi- and ExE-like cellular compartments, as CDX2 positive cells were clearly restricted to the ExE-like compartment build from cells originating from 5F ESCs (Figure 29). GFP+ Kermit ESCs were again detected to be compacted into an Epi-like

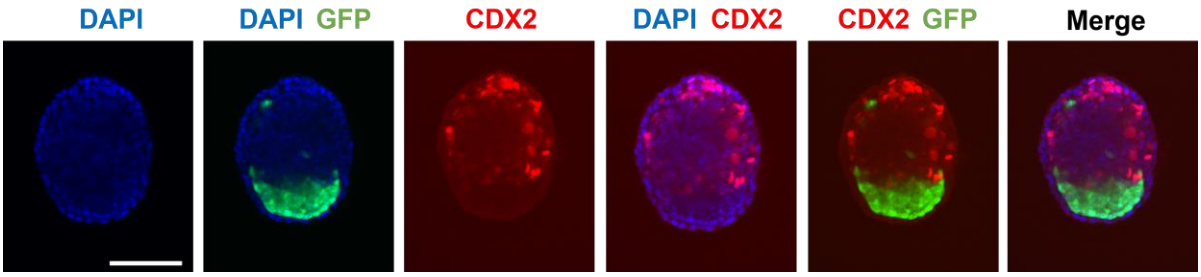

Figure 29 – Confocal microscopy images of embryo-like organoid after IF staining against CDX2. Photomicrographs after IF staining against CDX2 performed on embryo-like organoids generated from Kermit-, 5F- and iGATA6- ESCs according to the previously established protocol. DAPI staining indicates nuclei. Scale bar = 100 µm. (Modified from Langkabel et al., 2021)

compartment, that was found to be absent of CDX2+ cells. The two inner compartments were again demonstrated to be fully surrounded by a VE-like tissue comprised of GATA4+ cells as previously detected by IF staining against the XEN-/VE- cell fate marker protein (Figure 30). Confocal microscopy imaging furthermore confirmed that this VE-like structure is comprised of a monolayer of cells (Figure 30). Having established a functional, reproducible protocol for the induction of embryo-like structures using reprogramming paradigms in ESCs, Kermit ESCs were

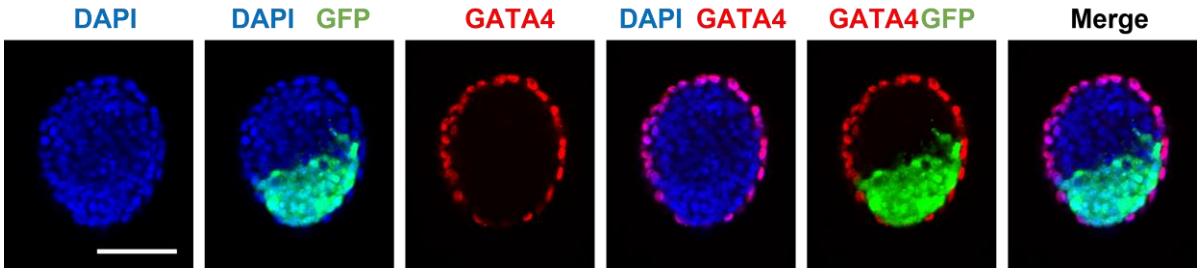

Figure 30 – Confocal microscopy images of embryo-like organoid after IF staining against GATA4. IF staining against GATA4 performed on embryo-like organoids generated from Kermit-, 5F- and iGATA6- ESCs according to the previously established protocol. DAPI staining indicates nuclei. Scale bar = 100 µm. (Modified from Langkabel et al., 2021)

then substituted for with KNUT1 ESCs, a wildtype ESC line derived by our group (Peitz et al., 2007). This allowed for a variety of fluorophore combinations during immunofluorescent staining for the presence or absence of marker proteins. Embryo-like structures generated from KNUT1-, 5F- and iGATA6-ESCs displayed similar organizational capacities, generating an OCT4+ Epi-like compartment, next to a GATA3+ ExE-like compartment, both of which are surrounded by a GATA4+ VE-like compartment (Figure 31). Considering that the embryo-like organoids resemble murine embryo architecture ~E5.5 and this timepoint corresponds with the transformation of epiblast cells into a cup-shaped epithelium, the aggregates were next analyzed for possible signs of rosette formation and lumenogenesis within the Epi- and ExE-like compartments. Rosette formation is initiated by compaction of actin fibers, which can be detected

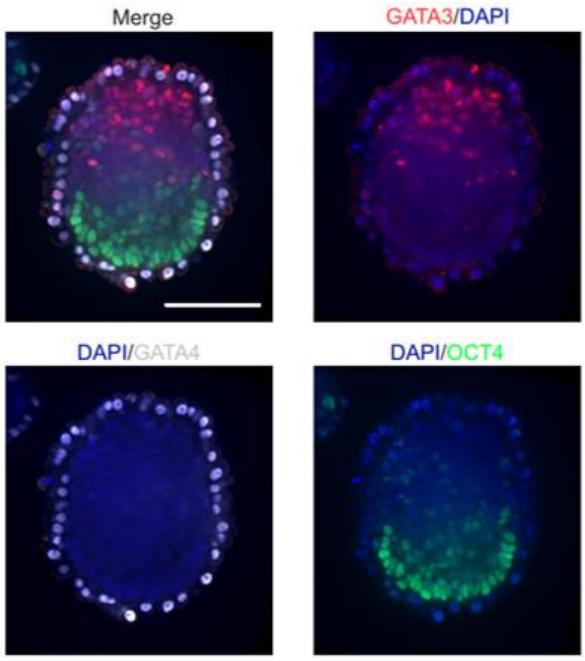

Figure 31 – IF staining in embryo-like organoids generated from KNUT1-, 5 F- and iGATA6- ESCs. Photomicrographs of embryo-like organoids stained using antibodies for GATA3 (red), GATA4 (Grey) and OCT4 (Green). DAPI staining indicates nuclei. Scale bar = 100 µm. (Modified from Langkabel et al., accepted manuscript)

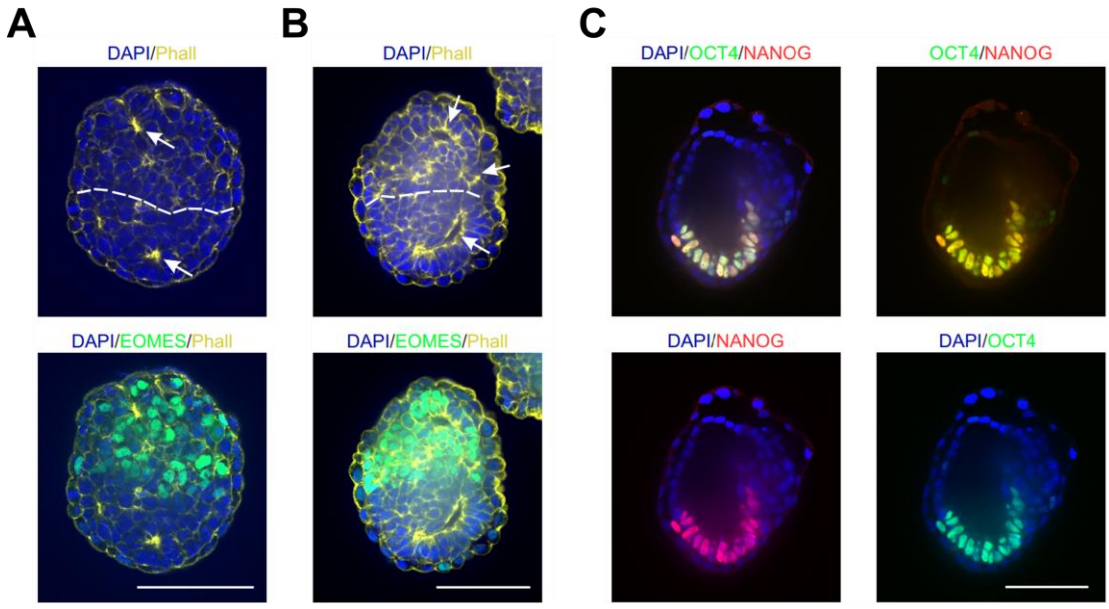

Figure 32 – Rosette formation and lumenogenesis in embryo-like organoids. Photomicrographs of embryo-like organoids stained against actin (Phalloidin/Phall; yellow) and EOMES (ExE marker) showing rosette formation (**A**) and lumenogenesis (**B**) in Epi- and ExE-like compartments (White arrows highlight location of rosettes and lumen; dotted lines indicate border of Epi- and ExE-like compartments). Fusion of the lumen in Epi-like (indicated by IF staining against OCT4 and NANOG) and ExE-like compartment to a pro-amniotic cavity-like structure was rarely observed (**C**). DAPI staining indicates nuclei. Scale bars = 100 µm. (Modified from Langkabel et al., accepted manuscript)

using staining with phalloidin, a peptide binding to actin filaments, conjugated to a fluorescent dye. Embryo-like structures displayed rosette formation and subsequent lumenogenesis in both, Epi- and ExE-like compartments (Figure 32 A and B) and in rare cases fusion of the two lumen into a structure resembling the pro-amniotic cavity was observed (Figure 8 and Figure 32 C). Structures that exhibited a complete fusion of the lumina into a pro-amniotic cavity could not be analyzed in more detail, due to their rare occurrence, however, they do highlight the developmental potential of the embryo-like structures presented here. Together, self-organization of the three stem cell lineages into embryo-like architecture comprised of Epi-, ExE- and VE-like tissues, as well as rosette formation and lumenogenesis indicate, that the embryo-like model presented in this study is able to mimic aspects of embryonic developmental stages between E5.0 – E5.5 (Figure 33). In order to give the structures an acronym that properly describes the stem cell-based embryo model and the developmental stages it can reflect *in vitro*, we therefore opted for the term Rosette-to-Lumen embryoids (RtL-embryoids). The stem cell-based embryo model presented in this study will be referred to as RtL-embryoids in the following chapters.

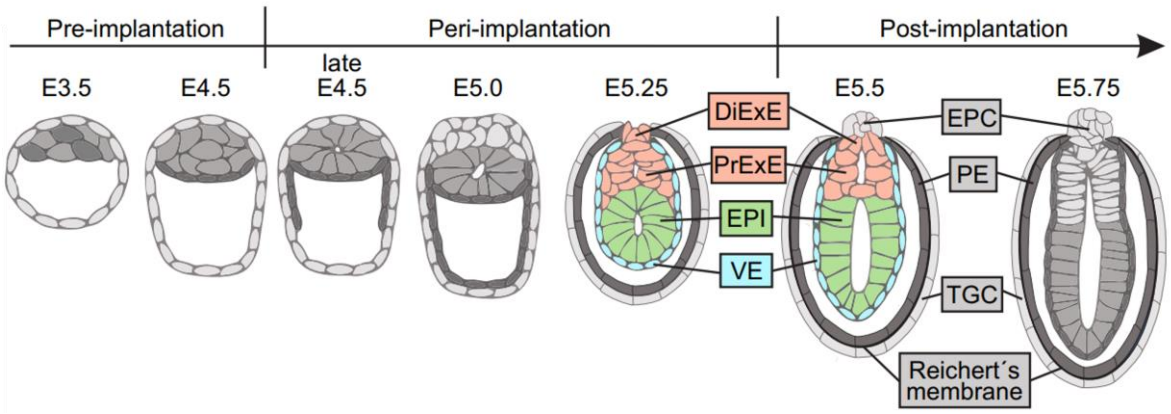

Figure 33 – Overview of (extra-)embryonic tissues that are present or absent in RtL-embryoids. Starting with the blastocyst during pre-implantation stages, the conceptus matures towards the egg cylinder stage at the late peri-implantation and early post-implantation stages. Structures and tissues that are represented in the stem cell-based embryo model presented in this study are highlighted in color, while tissues that are missing are shaded in gray. (Modified from Langkabel et al., accepted manuscript)

4.5 Characterization of RtL-embryoid compartments using scRNA-Seq

Morphological analysis by IF staining revealed high capacity for self-organization into three compartments resembling murine embryonic architecture around the egg cylinder stage between E5.0 – E5.5. This indicated that intercellular signaling between the three tissues potentially also mirrored signaling pathways present in murine embryos. To investigate such hypothesized

signaling pathways and in general global transcriptional changes in cells of the induced cell fates a comprehensive single cell RNA-Sequencing (scRNA-Seq) analysis was performed. The scRNA-Seq and bioinformatic analysis described in the following chapters were performed in close collaboration with Arik Horne and Prof. Dr. Joachim L. Schultze, Genomics and Immunoregulation, Life and Medical Sciences (LIMES) Institute, University of Bonn, Bonn, Germany.

For cell sorting by FACS and subsequent RNA-Seq, RtL-embryoids were generated from Kermit ESCs, 5F ESCs and iGATA6_mCherry ESCs, allowing for live tracking of Kermit ESCs by detection of GFP and iGATA6_mCherry ESCs, constitutively expressing mCherry. This enabled identification of correctly assembled and compartmented structures, which presented as mCherry+ VE-like spheres, surrounding a GFP+ Epi-like compartment, next to an unstained ExE-like compartment

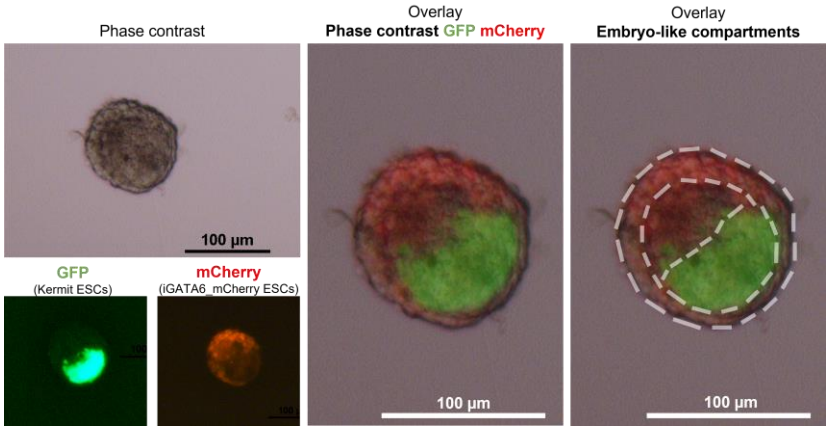

Figure 34 - Identification of correctly assembled RtL-embryoids. RtL-embryoids were generated from Kermit ESCs, 5 Factor ESCs and iGATA6_mCherry ESCs to allow for identification of correctly assembled and structured aggregates. Descendants of iGATA6_mCherry ESCs can be seen organized into a mCherry+ VE-like compartment, surrounding a GFP+ Epi-like compartment build from Kermit ESCs, adjacent to an unstained ExE-like compartment. Scale bar = 100 µm.

(Figure 28 and Figure 34). More than 600 of such correctly assembled structures were handpicked, pooled, and dissociated into a single cell suspension, which was then stained against CD40, a TS cell surface marker, that can be used to isolate TS/ExE- cells from single cell suspensions generated from murine embryos (Rugg-Gunn et al., 2012). This allowed for fluorescence activated cell sorting (FACS) and isolation of GFP+ Kermit ESCs from the Epi-like compartment, mCherry+ descendants of iGATA6 ESCs building the VE-like compartment, and

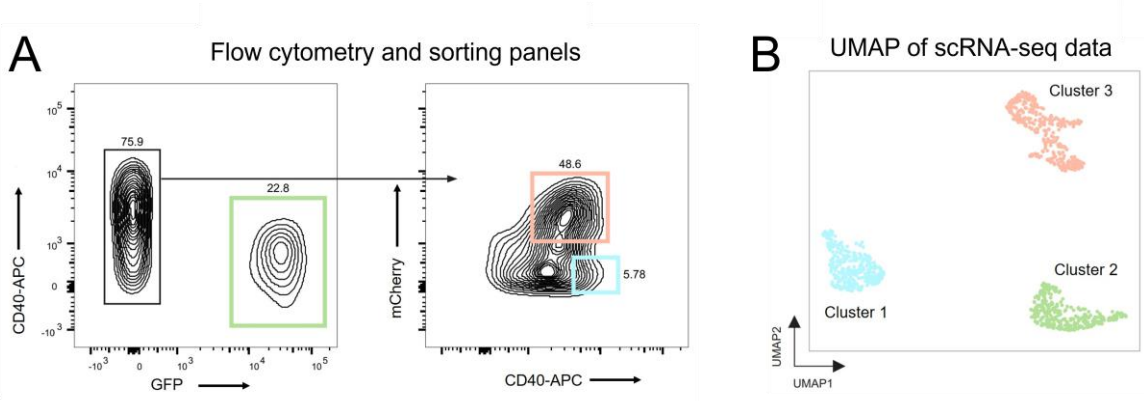

Figure 35 - Flow cytometry sorting panels and clustering of cells in bioinformatic analysis. A) Identification and sorting of GFP+ cell population (Left) and mCherry+ or CD40(APC)+ populations (right). **B**) Uniform Manifold Approximation and Projection (UMAP) of sorted cells revealed three distinct transcriptional cluster. (This figure has been published in Langkabel et al., 2021)

CD40+ cells of the ExE-like compartment originating from 5F ESCs (Figure 35 A). The sorted cells were shown to cluster in three distinct transcriptional cell clusters after performing Uniform Manifold Approximation and Projection (UMAP) (Figure 35 B). To characterize and identify the three transcriptional cell clusters, the expression of marker genes for VE (*Amn*, *Dkk1*, *Gata4*, *Sox17*), Epi (*Pou5f1* [*Oct3/4*], *Nanog*, *Gdf3*, *Tdgf1*) and ExE (*Cdx2*, *Elf5*, *Eomes*, *Tfap2c*) was analyzed. VE-marker genes were found to be expressed in Cluster 1, while Cluster 2 showed highest expression of Epi-marker genes and Cluster 3 displayed highest expression of ExE-marker genes (Figure 36 A). Therefore, the three transcriptional clusters will be referred to as VE-like, Epi-like and ExE-like cluster in the following.

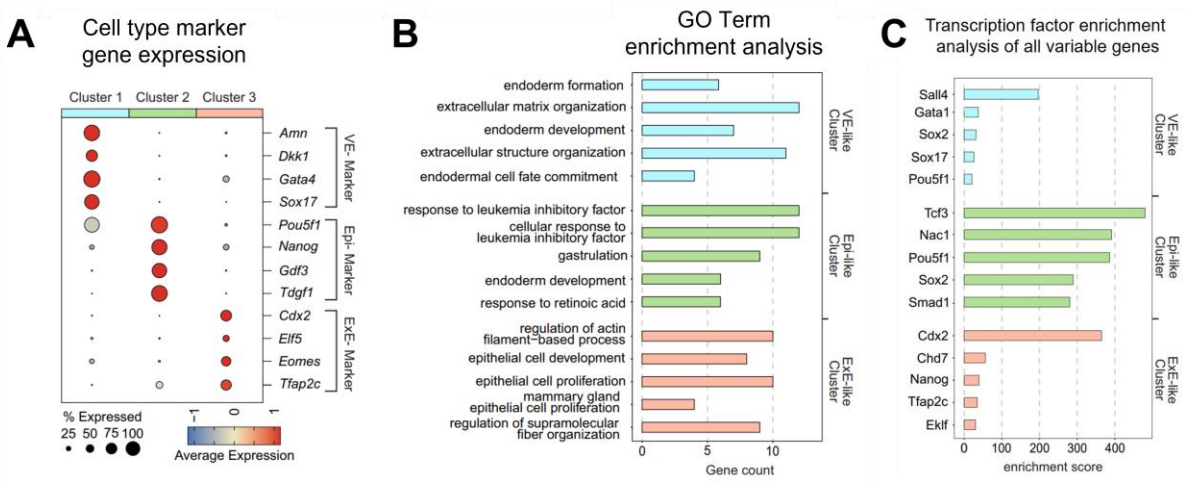

Figure 36 – Characterization of the three transcriptional clusters isolated from RtL-embryoids. A) Dot Plots showing VE-, Epi- and ExE- Marker gene expression in the three cell clusters. Diameter of dots represents number of cells expressing the marker gene within the respective cluster (in percent). **B**) GO Term enrichment analysis based on top 100 most variable genes for each cluster. **C**) Transcription factor enrichment analysis of all variable genes for all three clusters. (Modified from Langkabel et al., 2021)

Assessment of potential biological functions by GO Term enrichment analysis and analysis of transcription factor enrichment revealed an enrichment in endoderm-related gene sets and the transcription factor *Sall4* for cells of the VE-like cluster (Figure 36 B and C). *Sall4* has previously been identified as the key regulator of several VE-lineage associated genes like *Gata4*, *Gata6*, *Sox7* and *Sox17*, all which were also found among the top 30 differentially expressed genes (DEGs) characterizing the VE-like cells (Figure 37) (Lim et al., 2008). In addition, expression of *Cubn* was detected within the VE-like cluster, an important multiligand receptor for vitamin, iron, and protein uptake, involved in histiotrophic nutrition, the initial transfer of nutrition from maternal to embryo during peri-implantation development (Figure 37) (Assémat et al., 2005). The epiblast-like cluster was characterized by highest enrichment in leukemia inhibitory factor- and gastrulation-related gene sets in GO Term enrichment analysis and enrichment in transcription factors *Tcf3*, *Nac1* and *Pou5f1* (*Oct3/4*) (Figure 36 B and C). *Tcf3* and *Nac1* are known key regulators of epiblast-lineage specification in gastrulating mouse embryos (Hoffman et al., 2013;

Malleshaiah et al., 2016). Furthermore, *Tdgf1* (*Cripto*) was found among the top 30 DEGs in the Epi-like cell cluster, known as one of the earliest epiblast markers and regulator sustaining mESC self-renewal by modulation Wnt/β-catenin and maintaining pluripotency in epiblast stem cells (EpiSCs) through Nodal/Smad2 signaling (Figure 37) (Fiorenzano et al., 2016).

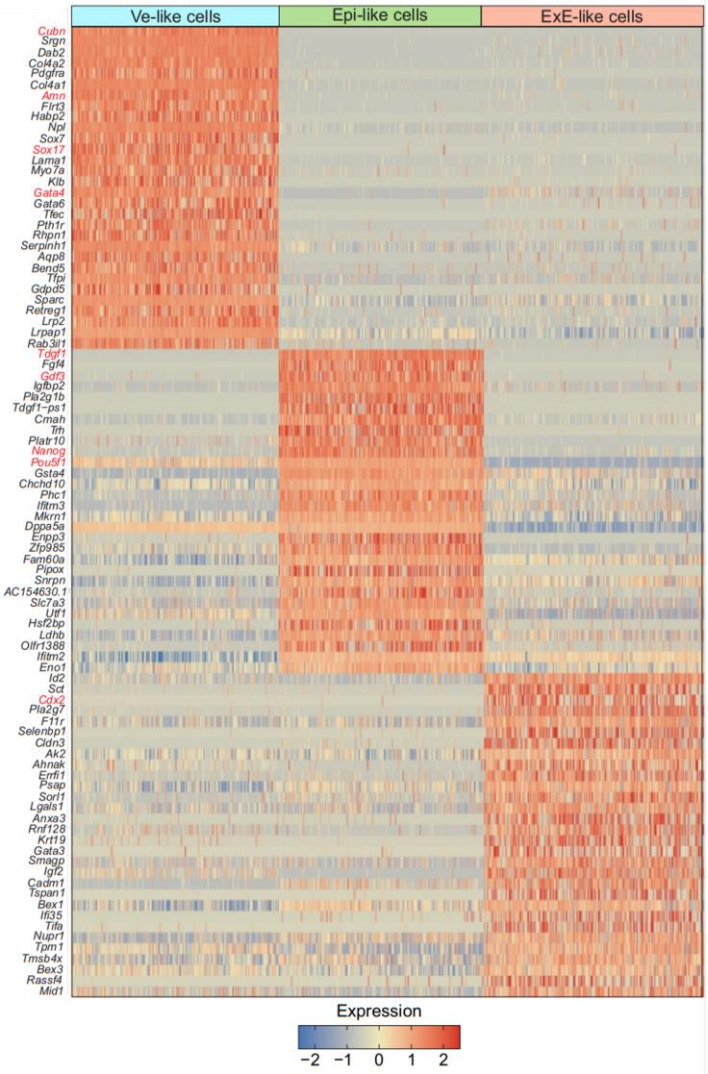

Figure 37 – Heatmap displaying expression of top 30 DEGs for VE-, Epi- and ExE- like cluster. Genes in rows; cells (and clusters) in columns. Marker genes for the respective embryonic compartments are highlighted in red. (This figure has been published in Langkabel et al., 2021)

The ExE-like cell cluster was characterized by an enrichment in epithelial cell-related GO terms like 'epithelial cell development', 'epithelial cell proliferation' and 'mammary gland epithelial proliferation' (Figure 36 B). The ExE-like cluster also displayed high enrichment of transcription factor *Cdx2*, as previously described, a marker of trophectoderm-derived lineages and lineage specific transcriptional repressor of pluripotency networks during the first developmental cell fate segregations (Figure 36 C) (Huang et al., 2017). Among the top 30 DEGs of the ExE-like cluster were *Id2*, an important regulator of placental differentiation, *Sct*, a placental hormone expressed in the murine placenta during pregnancy, and *Krt19*, a cytokeratin involved in mouse placental development (Selesniemi et al., 2016; Knox et al., 2011; Tamai et al., 2000) (Figure 37). After a basic characterization of the three cell clusters by detection of marker gene expression for the respective embryonic tissues, the assumptive cluster identities were

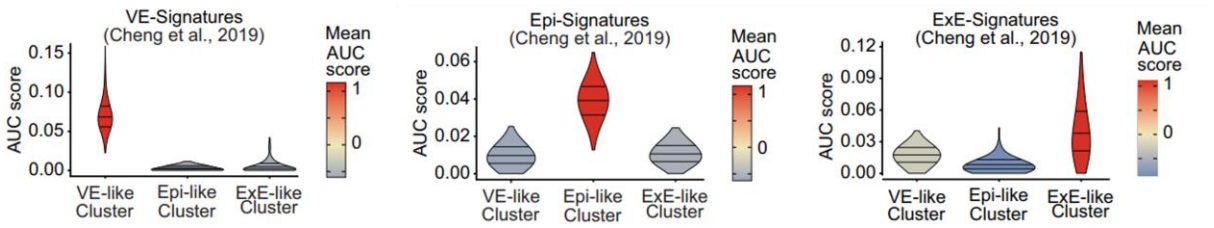

Figure 38 – Comparison of gene expression signatures from RtL-embryoids and murine embryos. Violin plots showing enrichment in gene signatures of VE, Epi and ExE of murine embryos obtained from Cheng et al. 2019. Highest similarity is indicated by highest Area Under the Curve (AUC) scores. Expression levels of the genes included in the respective signatures are indicated by color. (This figure has been published in Langkabel et al., 2021)

confirmed by comparison to scRNA-Seq gene signatures derived from mouse embryos (Cheng et al., 2019) (Figure 38). Again, the induced embryo-like compartments displayed highest similarity to their respective natural counterparts, indicated by "Area Under the Curve" (AUC) scores, that calculate whether a critical subset of the input gene signature is enriched within the expressed genes for each cell (Figure 38). Together, these results suggest successful lineage conversion of the reprogrammed cell lines and adaptation of transcriptional profiles resembling those of

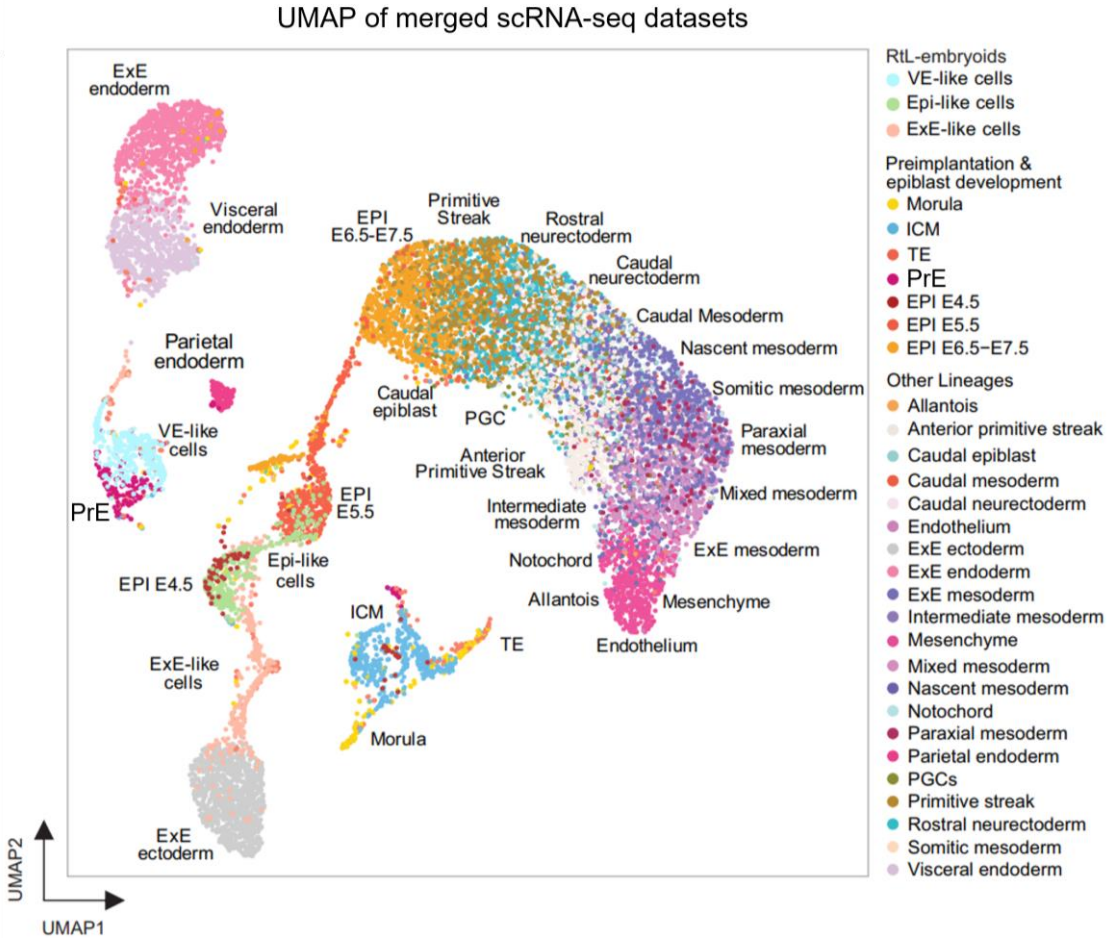

Figure 39 – UMAP representation of merged scRNA-Seq datasets. Merged UMAP representation of scRNA-Seq datasets obtained from mouse embryos between E3.5 – E7.5. VE-like cells of RtL-embryoids clustered closest with PrE cells, while Epi-like cells clustered with E4.5 and E5.5 EPI cells. ExE-like cells from RtL-embryoids display more broad clustering, with some cells clustering with ExE ectoderm cells, while other ExE-like cells clustered closer to EPI E4.5 cells. Datasets were obtained from: Chen et al., 2016; Mohammed et al., 2017; Posfai et al., 2017; Pijuan-Sala et al., 2019. (Modified from Langkabel et al., accepted manuscript).

murine VE, Epi and ExE. Having characterized the three induced embryo-like tissues comprising RtL-embryoids by marker gene expression, transcription factor enrichment and comparison to published VE-, Epi- and ExE-signatures, a more detailed scRNA-Seq signature comparison was performed by merging the scRNA-Seq dataset of RtL-embryoids with a variety of scRNA-seq datasets obtained from murine embryos, covering developmental stages from E3.5 – E7.5 (Figure 39) (Chen et al., 2016; Mohammed et al., 2017; Posfai et al., 2017; Pijuan-Sala et al., 2019). Supporting the observations of rosette formation and lumenogenesis, the UMAP representation revealed that Epi-like cells of RtL-embryoids clustered closest to EPI cells of mouse embryos at E4.5 and E5.5, confirming the previously observed developmental stage of the Epi-like compartment in RtL-embryoids (Figure 39 and Figure 40). VE-like cells of RtL-embryoids clustered mainly with primitive endoderm (PrE) cells of murine embryos, indicating that the cells characterized as VE-like cells could be at the onset of developmental progression from the PrE towards VE cells, which occurs between E4.5 and E5.0 in mouse embryos (Figure 2, Figure 38, and Figure 39). Of note, approximately 20% of VE-like cells did show higher transcriptional similarity with TE cells, indicating, that conversion from ESC-to-iXEN cell fate by overexpression of *Gata6* in a 3D environment could result in a certain degree of plasticity regarding the outcome of cellular reprogramming (Figure 40). Cells of the ExE-like compartment of RtL-embryoids showed highest similarity with cells of TE and ExE ectoderm, as expected, however, a part of the ExE-like cells was found to cluster with EPI cells (~28%) or VE cells (~6%), indicating that these cells did not have fully converted towards a true ExE-like identity (Figure 39 and Figure 40). Considering the previous characterization of the ExE-like compartment by IF staining, GO term enrichment analysis, transcription factor enrichment analysis and gene signature comparison, it can be assumed, that this subpopulation does induce a general ExE-like identity, with some cells retaining a residual ESC transcriptomic character. Supporting this observation, we were able to demonstrate that reprogramming of ESC-to-iTSC using 5F ESCs in serum-based standard TS medium results in incomplete demethylation of the *Oct4* promotor, which could be interpretated as a possible cause for the residual ESC transcriptomic 'footprint' within cells of this ExE-like subpopulation (Kaiser et al., 2020).

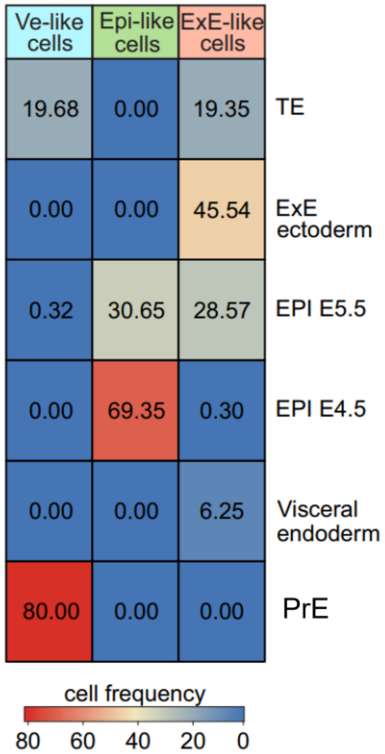

Figure 40 – Quantification of transcriptional overlapping cell populations. Quantification of VE-, Epi-, and ExE-like cells clustering with natural TE-,ExE-, Epi 4.5, Epi 5.5, VE, and PrE cells. Color-code indicates cell frequency, ranging from red (highest) to blue (lowest). Datasets were obtained from: Chen et al., 2016; Mohammed et al., 2017; Posfai et al., 2017; Pijuan-Sala et al., 2019. (Modified from Langkabel et al., accepted manuscript)

To test, if the cell fate conversion and culture in a 3D co-culture system results in different reprogramming outcomes compared to traditional cellular reprogramming in 2D monoculture, an additional scRNA-Seq dataset was generated. Therefore, Kermit ESCs cultured in 2i/LIF supplemented ESC medium, iXEN cells obtained from iGATA6_mCherry ESCs reprogrammed and cultured in standard XEN cell medium and iTSCs obtained from 5 Factor ESCs reprogrammed and cultured in FGF4/Heparin supplemented standard TS medium were subjected to the identical reprogramming, sorting and scRNA-sequencing procedures as described before. The two datasets are referred to as 2D monoculture induced and 3D co-culture induced cells in the following. 3D co-culture induced VE-like cells were detected to cluster close, but not overlapping with 2D monoculture induced iXEN cells in UMAP representation and gene signature enrichment analysis revealed highest enrichment in signatures of PrE/VE for 3D co-culture induced cells compared to 2D monoculture induced iXEN cells (Figure 41 A and B). 2D monoculture induced iXEN cells displayed a more homogenous character with a decreased enrichment in the PrE signature and strong enrichment in the VE signature (Figure 41 B). The comparison of 3D co-

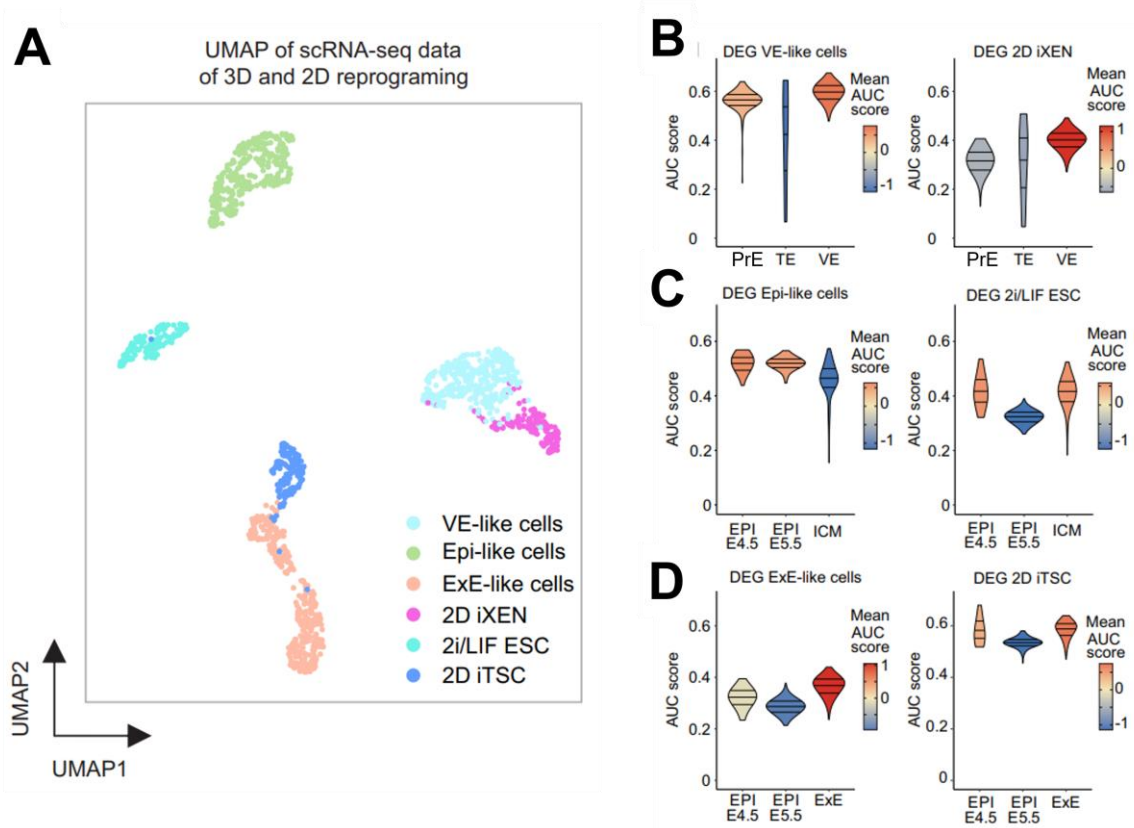

Figure 41 – Comparison of 2D mono- and 3D co- culture cellular reprogramming. A) UMAP of scRNA-seq datasets obtained from 2i/LIF cultured ESCs, 2D mono-culture reprogrammed iTSCs and iXEN cells and their 3D co-culture induced equivalents. **B**) Violin plots comparing 3D co-culture induced VE-like cells and iXEN induced in 2D monoculture with PE, TE and VE gene signatures. **C**) Violin plots comparing 3D co-cultured Epi-like cells and ESCs cultured in 2i/LIF 2D monoculture with ICM, and E4.5 and E5.5 EPI gene signatures. **D**) Violin plots comparing 3D co-culture induced ExE-like cells and 2D monoculture induced iTSCs with gene signatures of E4.5 and E5.5 EPI cells, as well as ExE cells. (Highest AUC score indicates highest enrichment in gene signature; width of violin plots indicate amount of cells at the respective AUC score; Color code indicates mean expression of genes included in the compared signatures). (Modified from Langkabel et al., accepted manuscript).

cultured Epi-like cells and ESCs cultured in 2i/LIF supplemented 2D monoculture revealed distant transcriptional clustering in UMAP representation (Figure 41 A). Supporting this observation, 3D co-cultured ESCs showed highest enrichment in gene signatures of E4.5 and E5.5 EPI cells and lowest enrichment in the gene signature of ICM cells. As expected for 2i/LIF supplemented 2D mono cultured ESCs, highest enrichment was observed for gene signatures of ICM and E4.5 EPI cells and lowest enrichment was observed for EPI E5.5 cells (Figure 41 C). Together these results further support the previously observed developmental progression from E4.5 to E5.5 of cells comprising the EPI-like compartment. For cells of the ExE-like cluster we observed close clustering of FGF4/Heparin supplemented 2D monoculture induced iTSCs with a subpopulation of 3D co-culture induced ExE-like cells, indicating a bipartite transcriptional character of cells comprising the ExE-like cluster (Figure 41 A). Gene signature comparison revealed an enrichment in the gene signature of E4.5 EPI cells for both, 2D monoculture- and 3D co-culture- induced iTS-/ExE- cells. However, iTSCs reprogrammed in 2D monoculture displayed a strong enrichment for both ExE and E4.5 EPI signatures, while ExE-like cells obtained from 3D co-culture were less enriched in the residual E4.5 EPI transcriptomic signature (Figure 41 D). This observation further strengthens the hypothesis, that a part of the ExE-like cells retains a residual ESC identity due to incomplete reprogramming, as previously observed for 5 Factor ESCs during ES-to-iTSC reprogramming in serum-based TS medium (Kaiser et al., 2020). However, this residual ESC character seems to be less prominent in 3D co-culture reprogramming compared to traditional 2D monoculture reprogramming. Together, these results are indicative of differences in reprogramming outcomes of induced cell identities, applying 2D monoculture compared to 3D co-culture reprogramming protocols. Next, the scRNA-Seq datasets of the three embryo-like compartments were subjected to more in-depth analysis individually to evaluate if RtL-embryoids undergo key molecular hallmarks of embryonic development.

4.6 The VE-like compartment initiates VE-lineage specification and DVE/AVE induction

In natural murine embryos the VE consists of the EmVE, covering the epiblast and the ExVE, surrounding the extraembryonic ectoderm. Interestingly, the VE-like cell cluster of RtL-embryoids also displayed two transcriptionally diverging subpopulations in UMAP representation, termed VE-like subclusters 1 & 2 (Figure 42 A). To assess if the VE-like

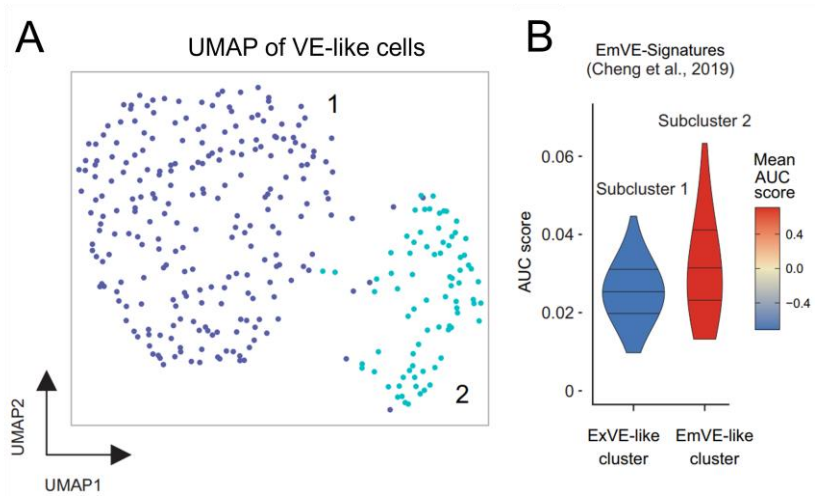

Figure 42 - The VE-like cluster consists of two transcriptionally diverging subpopulations. A) UMAP representation of the VE-like cluster, showing two diverging subclusters. **B**) Violin plots showing ExVE and EmVE marker gene signature enrichment among cells of the two VE-like subpopulations (Cheng et al., 2019). Bars indicate median of cell numbers. (This figure has been published in Langkabel et al., 2021).

subpopulations could be linked to the bipartite VE lineages present in murine embryos, the expression of published EmVE marker genes within cells of the VE-like subpopulations was analyzed, revealing highest similarity of the EmVE gene signature to VE-like subcluster 2 (Figure 42 B) (Cheng et al., 2019). Apart from its role in nutrient uptake and transport before a maternal-embryonic circulation is established (Cross et al., 1994; Bielinska et al., 1999), the VE functions as a signaling center, secreting instructive signaling cues from the EmVE to the epiblast, ultimately resulting in patterning events and the formation of an anterior-posterior (AP) axis within the developing embryo. The main mechanism by which this axis formation is induced is the formation of the distal- and subsequently anterior- visceral endoderm (DVE/AVE), a small subpopulation of VE cells within the EmVE, secreting antagonists of Nodal and Wnt signaling (Figure 6 and Figure 43 A). In RtL-embryoids, the expression of AVE marker genes was detected predominantly within cells of the EmVE-like cluster, all of which displayed high average expression of the respective marker genes compared to cells of the ExVE-like cluster (Figure 43 B). All key determinants of DVE/AVE specification and AP axis formation within the EmVE cluster, like *Lefty1*, *Dkk1*, *Sfrp1* and *Sfrp5* were found to be highly expressed in varying percentages of cells of the EmVE-like cluster (Figure 43 B) (Takaoka et al., 2011; Mukhopadhyay et al., 2001; Satoh et al., 2006; Finley et al., 2003). Apart from Nodal and Wnt antagonists, the expression of

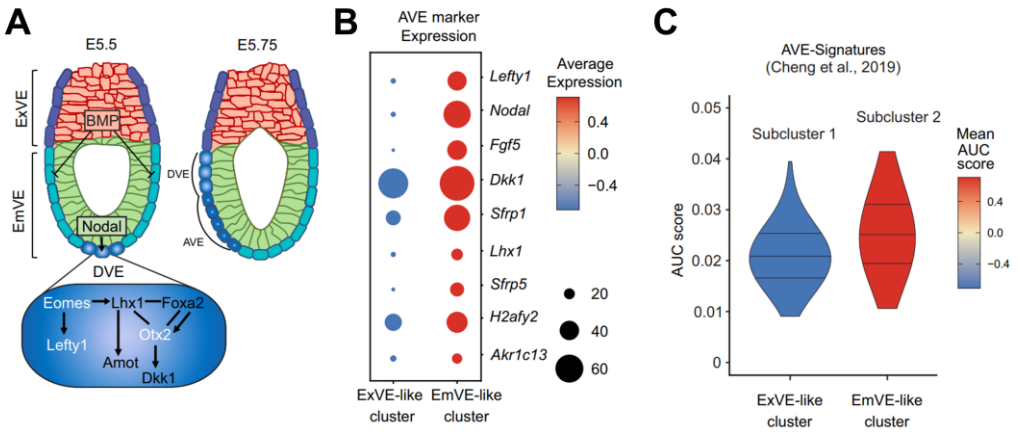

Figure 43 – DVE/AVE induction in RtL-embryoids. A) Schematic representation of DVE/AVE induction between E5.5 and E5.75 **B)** Dot plots showing AVE marker gene expression within cells of the ExVE- and EmVE-like clusters. Size of circles represent percent of cells expressing marker gene and color code indicates average expression of the respective AVE marker gene. **C)** Violin plots displaying enrichment in AVE signatures obtained from murine embryos (Cheng et al., 2019) in gene sets obtained from ExVE- and EmVE-like cells. (Modified from Langkabel et al., accepted manuscript)

Nodal itself was also detected at high levels in EmVE-like cells, which was previously reported to be necessary for maintenance of appropriate Nodal levels in the epiblast and AVE migration in the VE of early murine embryos (Kumar et al., 2015). A direct comparison of gene signatures from cells of the ExVE- and EmVE-like clusters with an AVE signature obtained from murine embryos showed high expression of the genes included in the AVE signature within cells of the EmVE-like cluster, further supporting the presumed AVE-like cell identity within cells of the EmVE-like cluster (Figure 43 C) (Cheng et al., 2019). As the induction and migration of a DVE/AVE signaling center within the EmVE occurs in a spatially confined manner, additional IF staining against DVE/AVE markers was performed to ensure proper localization of the presumed DVE/AVE-like cells within the EmVE-like compartment. IF staining using antibodies against EOMES and OTX2 detected expression of the markers in their respective compartments (EOMES+ ExE-like compartment and OTX2+ Epi-like compartment) (Figure 44). Additionally, a small subset of cells located within the hypothesized EmVE-like compartment displayed distinctive co-expression of EOMES and OTX2, indicative of DVE specification in these cells (Figure 43 A and Figure 44) (Nowotschin et al., 2013; Perea-Gomez et al., 2001; Kimura-Yoshida et al., 2005). Having

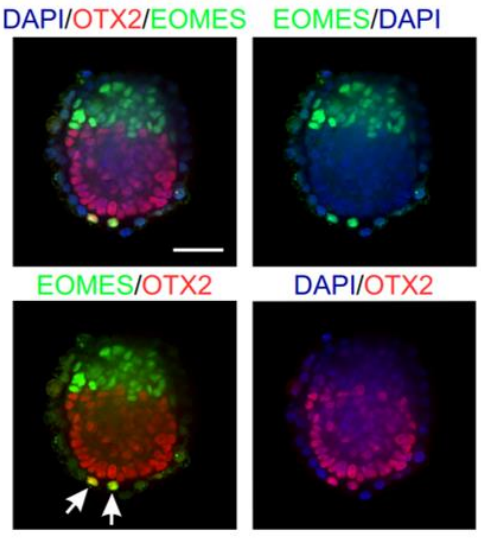

Figure 44 – IF staining against DVE/AVE markers OTX2 and EOMES. Photomicrographs of RtL-embryoids stained against EOMES and OTX2. EOMES expression was detected in the ExE-like compartment, while OTX2 expression was restricted to cells comprising the Epi-like compartment. A small subpopulation of EmVE-like cells (white arrows) was detected to co-express both, EOMES and OTX2, indicative of DVE/AVE specification. DAPI staining indicates nuclei. Scale bar = 50 µm. (Modified from Langkabel et al., accepted manuscript)

detected co-expression of DVE/AVE key determinants EOMES and OTX in this EmVE-like subpopulation, an additional IF staining against LEFTY1 was performed, to evaluate if EOMES downstream factors were induced in this DVE/AVE-like cell population as well (Figure 45). LEFTY1+/EOMES+ double-positive cells were detected to be spatially confined in an asymmetrical manner within the EmVE-like compartment (Figure 45 A). As expected regarding

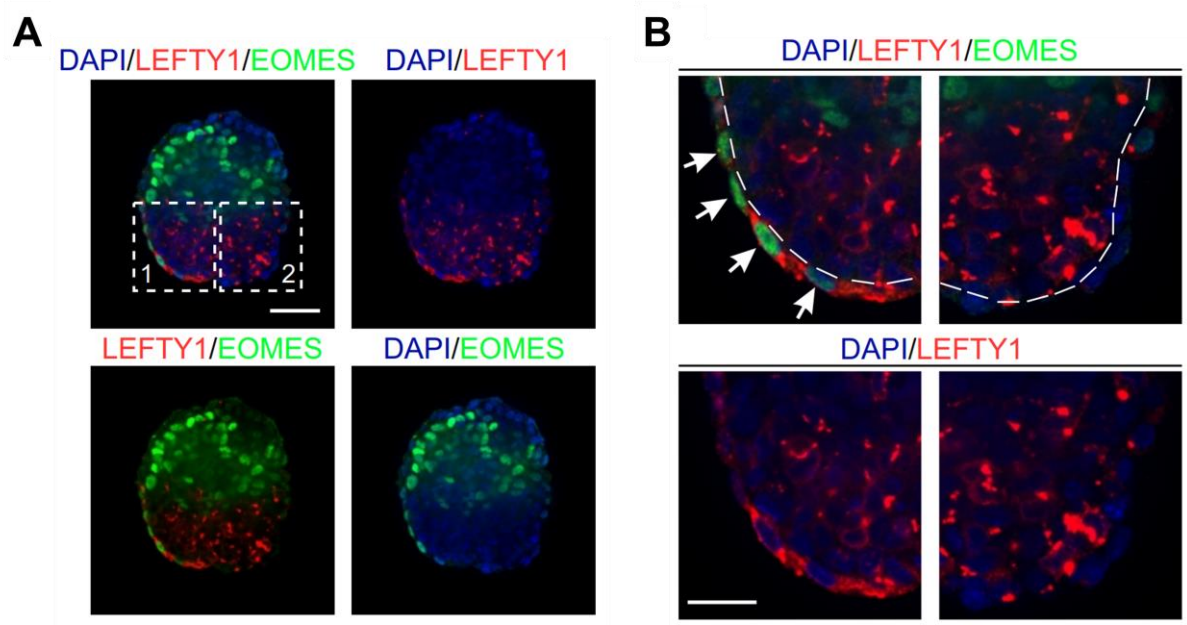

Figure 45 – IF staining against DVE/AVE markers LEFTY1 and EOMES. Photomicrographs of RtL-embryoids after IF staining against EOMES and LEFTY1. **A**) IF staining of RtL-embryoid using antibodies against DVE/AVE markers EOMES and LEFTY1 showing asymmetrical, spatially confined LEFTY1+/EOMES+ cells within the EmVE-like compartment. **B**) Digitally enlarged sections of the indicated areas (dotted squares) in Image A. Arrows indicate EOMES+/LEFTY1+ positive cells. DAPI staining indicates nuclei. Scale bars = 25 µm. (Modified from Langkabel et al., accepted manuscript)

its involvement in induction and maintenance of the transcriptional program responsible for DVE/AVE- cellular identity the expression of EOMES was detected in nuclear localization within the EOMES+/LEFTY1+ DVE/AVE-like cells (Figure 45 B). Conversely, LEFTY1 was detected within the cytoplasm of EOMES+/LEFTY1+ EmVE-like cells, as would be the case during DVE/AVE-mediated signaling to the epiblast by secretion of LEFTY1 (Figure 6 and Figure 45 B). To evaluate, if DVE/AVE formation in RtL-embryoids mirrors DVE/AVE migration from distal to anterior positioning during embryonic development, the localization of LEFTY1+ cells in relation to the Epi-like compartment was analyzed (Figure 46). Therefore, three localizations were defined and the number of RtL-embryoids displaying LEFTY1+ cells in the respective localizations was counted. LEFTY1+ cells at the most distal tip respective to the Epi-like compartment were designated as distal positioned (Distal) (Figure 46 A). LEFTY1+ cells asymmetrically spanning from the most distal tip towards a one lateral side but not reaching the border of Epi- and ExE-like compartment were counted to be positioned in transition (Transition). LEFTY1+ cells localized asymmetrically and spanning from the most distal tip to the border of Epi- and ExE-like compartments were counted to be in an anterior position (Anterior)

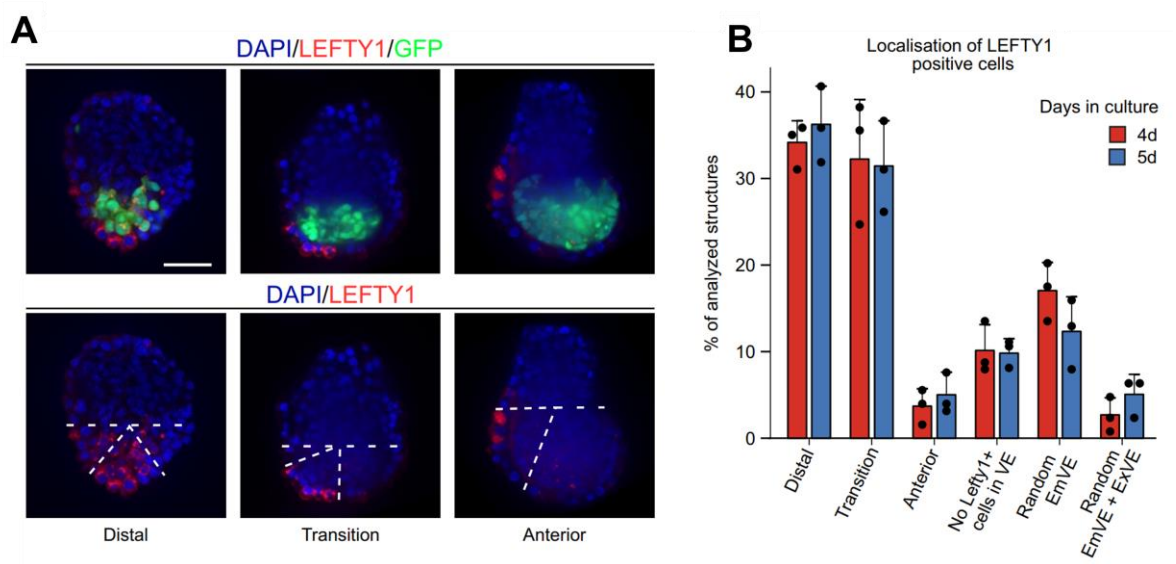

Figure 46 – Localization and quantification of LEFTY1+ DVE/AVE-like cells. A) Photomicrographs of RtL-embryoids build from Kermit-, 5F- and iGATA6- ESCs analyzed for LEFTY1 expression by IF staining. Lower Panel indicates examples of LEFTY1+ cells in distal-, transition- or anterior- position within the EmVE covering the GFP+ Epi-like compartment. DAPI staining indicates nuclei. Scale bar = 50 µm. **B)** Quantification of LEFTY1+ cells in the localizations indicated on the Y-axis, 4d (red) or 5d (blue) into the protocol. Experiments were performed in technical triplicates, total n = 375 for both 4d and 5d. (Modified from Langkabel et al., accepted manuscript)

(Figure 46 A). Additionally, as we occasionally observed a total lack of or miss-localization of LEFTY1+ cells within either just the EmVE- or both EmVE- and ExVE-like compartments, we defined additional criteria for missing or miss-located LEFTY1+ cells (No Lefty1+ cells in VE; Random localization in EmVE; Random localization in both EmVE + ExVE). The localization of LEFTY1+ cells according to these criteria was analyzed at both 4 days, as well as 5 day into the protocol, in order to evaluate a possible migratory character of the DVE-/AVE-like cell population. The number of aggregates showing LEFTY1+ in either of the defined positions did not differ significantly between days 4 and 5 of the protocol, indicating limited migratory potential of the DVE/AVE-like cell population (Figure 46 B). In general, the majority of RtL-embryoids displayed LEFTY1+ cells in either a distal (34,13% at 4d; 36,27% at 5d) or transitioning position (32,27% at 4d; 31,47% at 5d) and few RtL-embryoids showed LEFTY1+ cells spanning in a complete distal-to-anterior-manner (3,73% at 4d; 5,06% at 5d) (Figure 46 B). Of note, RtL-embryoids with weak contribution of cells to the ExE-like compartment displayed LEFTY1 expressing cells among the EmVE-like compartment as a whole, most likely due to missing inhibitory signaling from the ExE-like compartment, as BMP signaling from the ExE is known to function in restriction of DVE/AVE

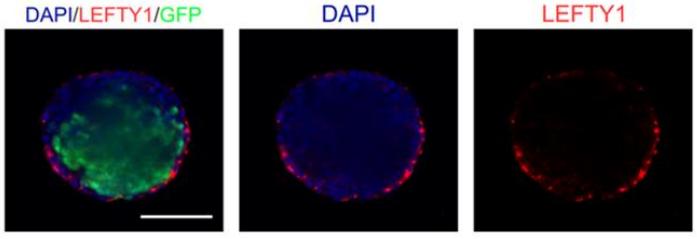

Figure 47 – Example of failure of LEFTY1 restriction to the distal tip of the EmVE. Photomicrograph of IF staining against LEFTY1 in RtL-embryoids build from Kermit-, 5F- and iGATA6- ESCs, that display weak contribution of cells comprising the ExE-like compartment. LEFTY1 expression is not restricted to the most distal VE-like cells, but still limited to the EmVE-like compartment. DAPI staining indicates nuclei. Scale bar = 100 µm. (Modified from Langkabel et al., accepted manuscript)

specification to the most distal tip of the EmVE in furthest proximity to the ExE (Figure 43 A and Figure 47) (Yamamoto et al., 2009). Together, gene signature enrichment and marker expression in a spatially confined manner as detected by IF staining strongly support the notion, that RtL-embryoids induce specification of a DVE/AVE-like subpopulation within EmVE-like cells, however, the migratory potential of this DVE/AVE-like population seems to be limited.

4.7 Progression from naïve- to primed-pluripotency in the Epi-like compartment

The Epi-like cluster of RtL-embryoids displayed a tripartite character of transcriptionally diverging subpopulations (Figure 48). As analysis of the VE-like cluster indicated the induction of a DVE/AVE-like signaling center the Epi-like cluster was analyzed for a possible response to DVE/AVE signaling cues from the VE-like compartment. Therefore, the transcriptional signature of the Epi-like cell cluster was compared to anterior-, transition-, and posterior- epiblast signatures obtained from early murine embryos (Cheng et al., 2019). The highest enrichment was found in comparison to the signature of anterior epiblast cells (Figure 49). In contrast, significant enrichment in transition- or posterior- epiblast signatures was not detected (Figure 49). Supporting these observations, assessment of expression levels of specific marker genes revealed proportionally highest expression of anterior epiblast marker genes *Aire, Fam25c, Inpp5d, Dppa2, Spp1* in cells of the Epi-like cluster (Figure 50) (Cheng et al., 2019). Of transition epiblast marker genes only *Trh* was found to be expressed on high level in ~60 % of the cells, while posterior epiblast marker genes were almost absent in the dataset (Figure 50). Together, these results indicate, that genes involved in anterior epiblast cell fates are upregulated in the Epi-like compartment in response to DVE/AVE induction and signaling from within the VE-like compartment of RtL-embryoids. Considering the observed

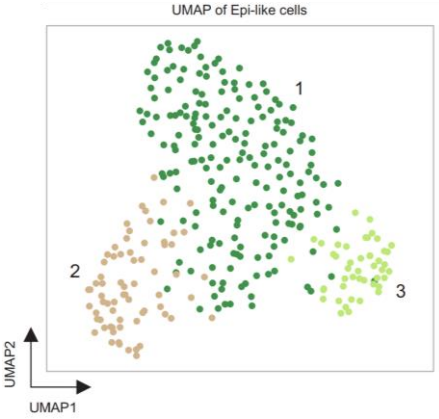

Figure 48 – UMAP representation of the Epi-like cluster. Epi-like cells clustered in three transcriptionally diverging subpopulations. (Modified from Langkabel et al., accepted manuscript)

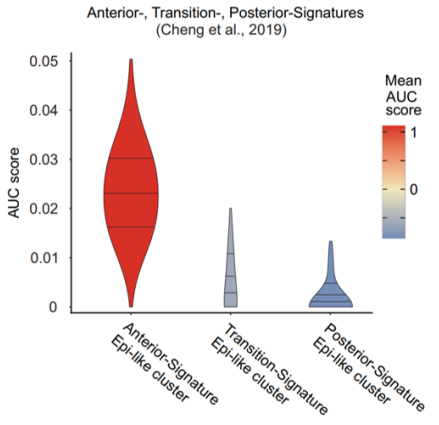

Figure 49 – Signature enrichment analysis of the Epi-like cluster. Violin plots showing AUC enrichment scores of transcriptional signatures of Anterior-, Transition-, and Posterior- Epiblast signatures obtained from early murine embryos (Cheng et al., 2019). (This figure has been published in Langkabel et al., 2021)

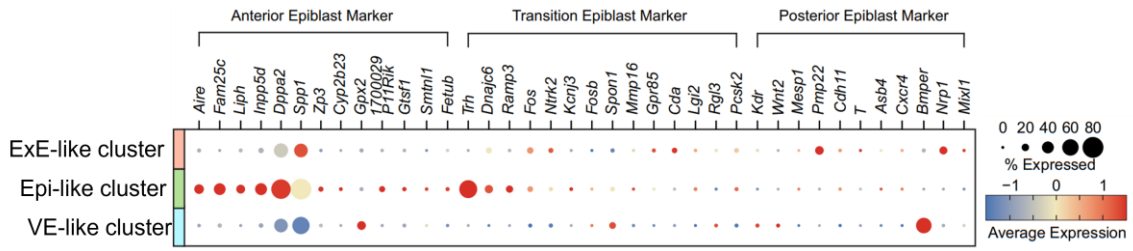

Figure 50 – Detection of anterior-, transition- and posterior- epiblast marker gene expression. Dot plots displaying expression of marker genes for anterior-, transition- and posterior-epiblast in the three cell clusters. Size of dots represent percentage of cells expressing the respective gene, color code indicates expression levels. (Cheng et al., 2019). (This figure has been published in Langkabel et al., 2021)

limited migratory potential of the DVE/AVE-like subpopulation in the VE-like compartment it can be assumed, that the missing enrichment in transition- or posterior-epiblast signatures could be the result of missing or weak patterning cues from the DVE/AVE-like subpopulation. As the formation of rosettes and progression to lumenogenesis was detectable and scRNA-Seq revealed highest similarity to E4.5 – E5.5 epiblast cells of natural murine embryos (Figure 39), it was next assessed, if Epi-like cells of RtL-embryoids progress from naïve- to primed-pluripotency as described during mouse embryogenesis (Neagu et al. 2020). This progression is accompanied and mediated by a switch of transcription factors regulating the respective pluripotency states. During rosette to lumen formation, the progression from naïve- (KLF4+, NANOG+, ESRRB+, OTX2+, OCT6-) to primed- (KLF4-, NANOG-, ESRRB-, OTX2+, OCT6+) pluripotency can be analyzed by detection of presence or absence of the respective pluripotency transcription factors (Neagu et al., 2020). In addition to the switch of transcription factor mediated pluripotency states, the progression from naïve- to primed- pluripotency is accompanied by pulses of pERK in single cells of the epiblast, that increases in frequency during rosette to lumen maturation (Neagu et al., 2020). In RtL-embryoids a similar transition of the transcription factor circuitry was observed, as naïve-pluripotency markers KLF4 and ESRRB were detected to be weakly expressed in Epi-like

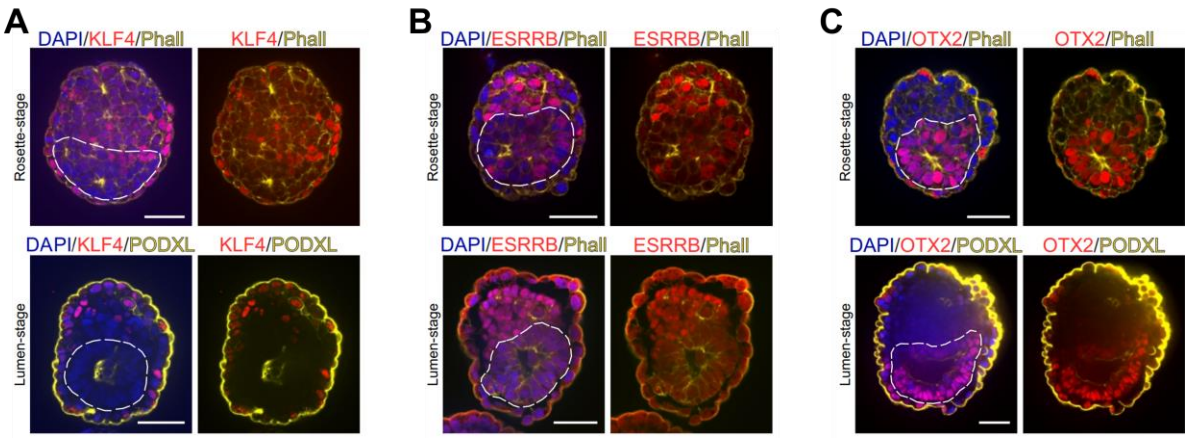

Figure 51 – Transition of transcriptions factors during rosette to lumen progression. Photomicrographs of RtL-embryoids after IF staining against **(A)** KLF4, **(B)** ESRRB and **(C)** OTX2 in RtL-embryoids at rosette- (**upper rows**) or lumen- (**lower rows**) stages. Phalloidin (Phall) was used to stain actin filaments. PODXL staining was used to detect polarized epithelial cell layers. DAPI staining indicates nuclei. Scale bars = 50 µm. (Modified from Langkabel et al., accepted manuscript)

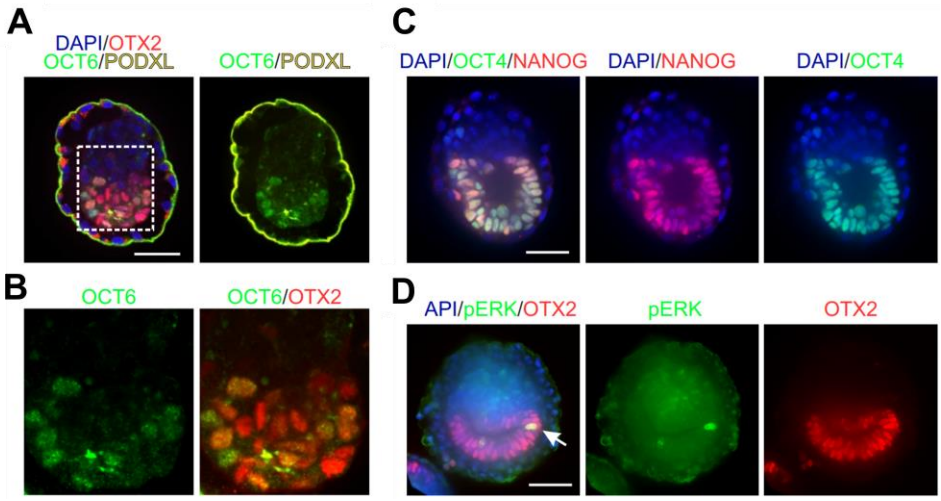

Figure 52 – Progression of naïve- to primed- pluripotency. Photomicrographs of RtL-embryoids after IF staining against pluripotency associated markers on protein level. **A**) IF staining against OCT6 revealed weak expression of the primed-pluripotency factor in RtL-embryoids at lumen stage. **B**) Magnification of the area indicated with dotted square in A, showing co-expression of OTX2 and OCT6 in Epi-like cells. **C**) IF staining against core-pluripotency factor OCT4 and naïve-pluripotency factor NANOG reveals failure in downregulation of NANOG during pluripotency progression. **D**) IF staining against pERK showing single pERK+ cells within the Epi-like compartment at lumen-stage. DAPI staining indicates nuclei. Scale bars = 50 µm. (Modified from Langkabel et al., accepted manuscript)

cells at rosette stage and completely downregulated in RtL-embryoids that had progressed towards lumen stage (Figure 51 A and B). The expression of OTX2 was detected at both stages, similar to observations made in murine embryos (Figure 51 C) (Neagu et al., 2020). Furthermore, the expression of the primed pluripotency factor OCT6 was detected in OTX2+ Epi-like cells at lumen stage, indicating that progression from naive- to primed-pluripotency is present and accompanied by Rosette-to-Lumen progression in RtL-embryoids. Assessment of naïve pluripotency factor NANOG did however reveal a steady expression throughout the culture period, indicating either a delay or failure to complete the switch of the pluripotency associated transcription factor circuitry from naïve- to primed-pluripotency (Figure 52 C). Supporting a presumed delay in progression of pluripotency states, single pERK+ Epi-like cells were detectable, but restricted to RtL-embryoids at lumen-stage, while pERK pulses can be readily detected in the epiblast of murine embryos at rosette stage and their appearance increases as the embryo progresses to lumen-stage (Neagu et al., 2020) (Figure 52 D). Considering the low expression of OCT6, steady expression of naïve-pluripotency marker NANOG and the delayed appearance of pERK+ cells at

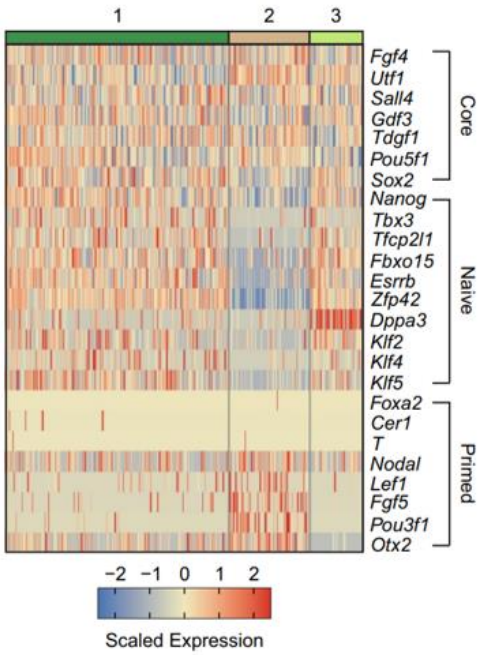

Figure 53 – Expression of pluripotency marker genes in Epi-like subclusters. Heatmap displaying the expression of core-, naïve- and primed- pluripotency marker genes across cells of the three Epi-like subclusters. Epi-like subclusters are designated as 1, 2 and 3 as in Figure 48. (Modified from Langkabel et al., accepted manuscript)

lumen-stage, it can be assumed that cells of the Epi-like compartment undergo naïve- to primed-pluripotency progression in a delayed manner compared natural murine embryos. To further validate the observed delayed progression in pluripotency states, the gene expression of core-, naïve- and primed- pluripotency markers across the three Epi-like subclusters was evaluated (Figure 48 and Figure 53). The expression of core-pluripotency marker genes *Fgf4*, *Utf1*, *Sall4*, *Gdf3*, *Tdgf1* and *Oct4* (*Pou5f1*) was detectable throughout cells of the three Epi-like subclusters (Figure 53). Epi-like subcluster 1 was characterized by high expression levels of naïve-pluripotency marker genes *Nanog*, *Tbx3*, *Tfcp2l1*, *Fbxo15*, *Esrrb*, *Zfp42*, *Klf2*, and *Klf4*, and low to absent levels of primed-pluripotency marker genes (Figure 53). Epi-like subcluster 2 showed a clear reduction of naive-pluripotency marker gene expression, and an increased expression of primed-pluripotency marker genes *Nodal*, *Lef1*, *Fgf5*, *Oct6* (*Pou3f1*) and *Otx2*, compared to Epi-like subcluster 1. Epi-like subcluster 3 displayed a similar gene expression pattern as Epi-like subcluster 1, except for expression of *Stella* (*Dppa3*), which was detected highly upregulated in Epi-like subcluster 3, compared to the other Epi-like subclusters (Figure 53). Supporting the observation of a delay or failure in progression from naïve- to complete primed- pluripotency, the expression of primed-pluripotency factors *Foxa2*, *Cer1* and *T* was not detected across all Epi-like subclusters, except for single cells (Figure 53).

Considering that two of the main stem cell lineages present in RtL-embryoids are derived by reprogramming from an ESC fate, the expression of pluripotency marker genes was additionally assessed throughout the whole dataset, revealing that both, VE-like and ExE-like cells predominantly downregulated the expression of pluripotency factors (Figure 54). Specific transcription factors for the respective cell fates were detected in the corresponding cellular compartment, such as previously discussed *Sall4*, a key regulator of the VE stem cell identity,

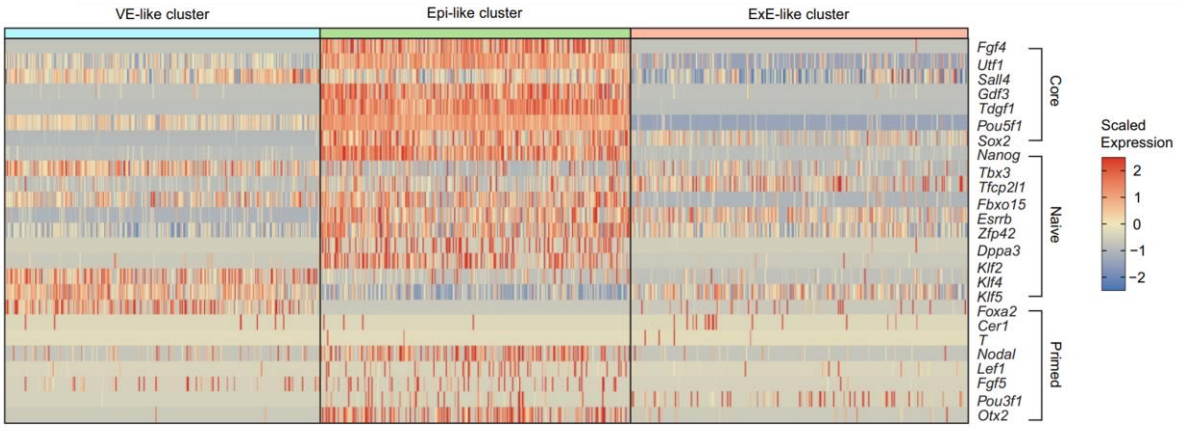

Figure 54 – Expression of pluripotency marker genes in all cellular clusters of RtL-embryoids. Heatmap depicting the expression of core-, naïve- and primed- pluripotency marker genes across the whole scRNA-Seq dataset of RtL-embryoids showing downregulation of most pluripotency marker genes in both of the induced VE- and ExE-like tissues. (Modified from Langkabel et al., accepted manuscript)

which was found to be expressed in cells of the VE-like cluster, as expected (Lim et al., 2008) (Figure 54).

4.8 Initiation of PGC specification in an Epi-like subcluster

Having identified *Stella* (*Dppa3*), a marker gene of primordial germ cell (PGC) specification, as the most highly upregulated pluripotency marker gene characterizing Epi-like subcluster 3, the scRNA-Seq dataset was analyzed for a possible PGC-like population (Figure 7). PGC specification in mice is initiated in Epi cells lining the ExE, by instructive BMP signaling secreted from both, ExE and VE. In RtL-embryoids, the expression of *Bmp2* was detected in single cells of the VE-like cluster, while expression of *Bmp4* and *Bmp8b* was found to be predominantly restricted to a

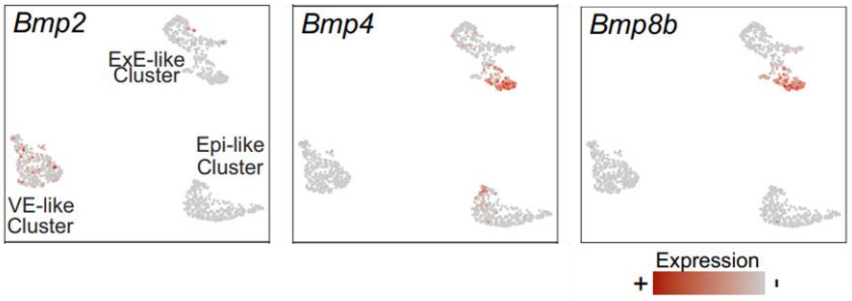

Figure 55 – FeaturePlots of *Bmp* expression mapped on RtL-embryoid UMAP representation. Expression levels are indicated by color intensity, with red highlighting cells that display the highest expression levels. (This figure has been published in Langkabel et al., 2021)

subpopulation of cells within the ExE-like cluster (Figure 55). As such, BMP-signaling in RtL-embryoids mirrors the situation described in murine embryos between E4.5 – E6.5, with BMP2 secretion from the VE and BMP4 and BMP8B secretion from ExE cells lining the Epi (Lawson et al., 1999; Lee et al., 2007; Ying et al., 2000; Ying et al, 2001). BMP signaling from the ExE and VE induces PGC specification in these Epi cells, resulting in expression of PGC marker genes, like *Nanos*, *Kit*, *Stella* (*Dppa3*) and *Tfap2c* (Figure 7). In RtL-embryoids a similar response to the instructive BMP signaling could be observed, as expression of the four PGC marker genes was detected to be predominantly restricted to Epi-like subcluster 3 of the three previously

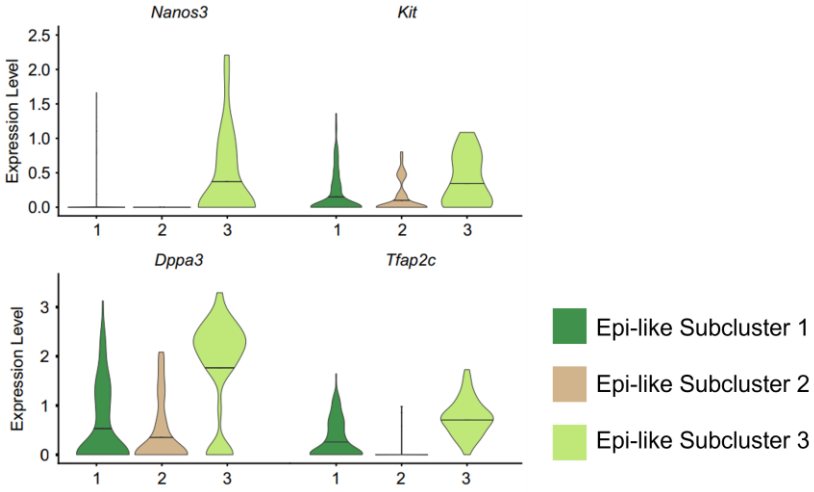

Figure 56 – Violin plots displaying the expression of PGC marker genes in Epi-like subclusters. Expression levels are indicated on the Y-axis, Epi-like subclusters are indicated by 1,2 or 3 on the X-Axis and by color code. Bar in Violin plots highlights mean of number of cells. (Modified from Langkabel et al., accepted manuscript)

introduced Epi-like subclusters (Figure 48, Figure 53, and Figure 56). Of note, the expression of *Nanos3* was found to be highly restricted to Epi-like subcluster 3 and the PGC marker gene *Stella* (*Dppa3*) showed highest expression levels in the majority of cells of this Epi-like subcluster (Figure 53 and Figure 56). Together, BMP signaling from the respective embryo-like compartments and expression of downstream PGC marker genes in a subpopulation of Epi-like cells supports the notion, that RtL-embryoids induce PGC specification and that Epi-like subcluster 3 identifies as a PGC-like population.

4.9 The ExE-like compartment displays bipartite composition of cell subclusters

Having identified a possible bipartite transcriptional character of the ExE-like cluster by analysis of *Bmp4* and *Bmp8b* expression it was next assessed if such a diverging character of ExE-like cells could be further characterized and correlated with the situation found in murine embryos (Figure 4 and 55). UMAP representation of the ExE-like cluster supported the observed bipartite character, as ExE-like cells were found transcriptionally diverging into two ExE-like subpopulations, hereafter termed ExE-like subcluster 1 and 2 (Figure 57 A). Supporting the observation of a bipartite character of the ExE-like cluster, the expression of ubiquitous ExE- / TSC- marker genes like *Id2*, *Igf2*, *Tfap2c* and *Gata3* was detected in cells of both ExE-like subclusters, while expression of more specific TSC marker genes *Eomes*, *Bmp4*, *Bmp8b*, *Hand1*, *Plet1* and *Elf5* was found to be highly restricted to cells of ExE-like subcluster 1 (Figure 57 B). To assess if this bipartite character of the ExE-like cluster can be correlated with a possible

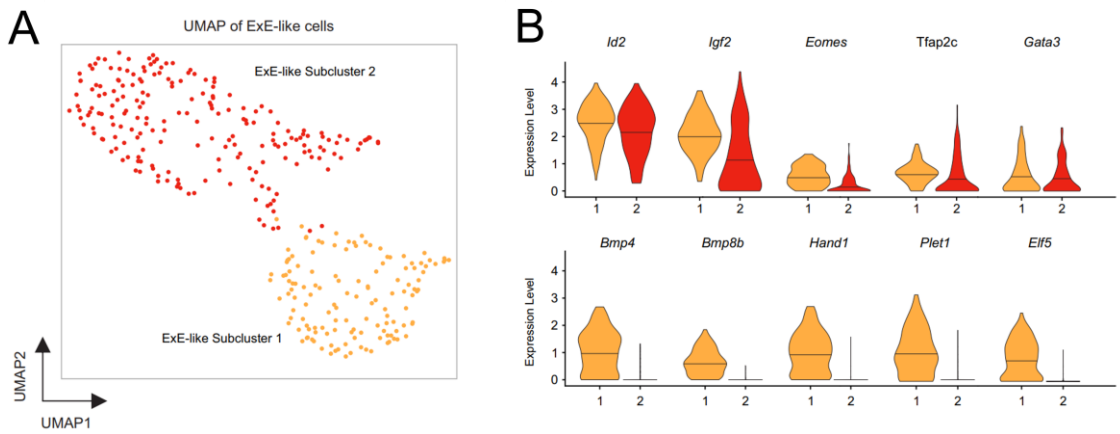

Figure 57 – Bipartite transcriptional character of the ExE-like cell population. A) UMAP representation of ExE-like cells showing two transcriptionally diverging cell populations, termed ExE-like subcluster 1 and 2. **B**) Violin plots displaying expression of trophoblast marker genes in the two ExE-like subclusters, indicated by either 1 or 2 on the X-Axis and color code (orange = ExE-like subcluster 1; red = ExE-like subcluster 2). Expression levels are indicated on the Y-Axis and ExE-like subclusters 1 and 2 are labeled on X-Axis. Bar inside violin plots shows mean of number of cells. (This figure has been published in Langkabel et al., 2021)

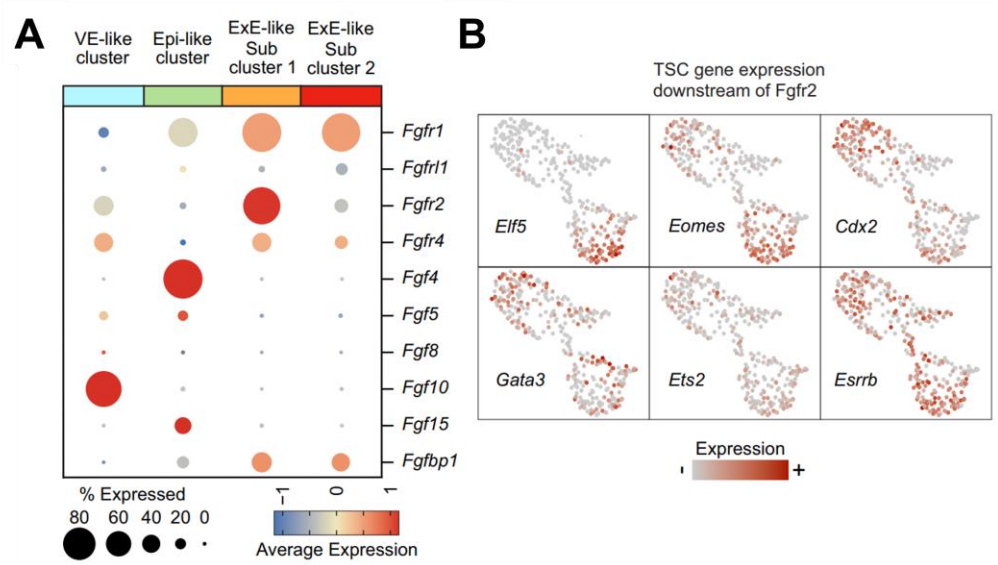

Figure 58 – Expression of FGF ligands and receptors and TSC marker genes downstream of FGFR2. A) Dot plots displaying the expression of FGF ligands and receptors across (Sub-) clusters of RtL-embryoids. Diameter of dots represent percentage of cells within the corresponding cluster expressing the respective gene. Color code indicates expression levels, as indicated below. **B)** FeaturePlots showing expression of TSC marker genes downstream of FGFR2 mapped on UMAP representation of the ExE-like cluster. Expression levels are indicated by color code, with red highlighting cells that show high expression of the respective marker gene. (This figure has been published in Langkabel et al., 2021)

segregation of a PrExE and DiExE cell population as described for murine embryos, the expression of FGF ligands and receptors was analyzed (Figure 4 and Figure 58 A). The expression of *Fgf4* was detected to be restricted to the Epi-like cell cluster, while its receptor *Fgfr2* was found to be highly expressed in the majority of cells of ExE-like subcluster 1 (Figure 58 A). *Fgfr2* expression within cells of ExE-like subcluster 2 was detected only in few cells, that displayed significantly lower average expression levels of the FGF4 receptor (Figure 58 A). Next, TSC marker genes that are situated downstream of FGFR2 in the transcriptional network regulating TSC-fate in ExE cells, were analyzed. The expression of *Elf5* and *Eomes* was predominantly restricted to ExE-like subcluster 1, similar to the situation described for murine embryogenesis, in which the expression of *Elf5* and *Eomes* can be detected in the cells of the PrExE, lining the epiblast (Figure 58 B) (Donnison et al., 2015). Supporting this observation, highest expression of *Ets2* was detected in cells of ExE-like subcluster 2, again showing similarity to mouse embryos, in which Elf5 and Ets2 maintain the ExE in a dosage dependent synergistic manner, thereby defining PrExE (Elf5^{high}/Ets2^{low}) and DiExE (Elf5^{low}/Ets2^{high}) (Figure 58 B) (Donnison et al., 2015). Further highlighting the bipartite

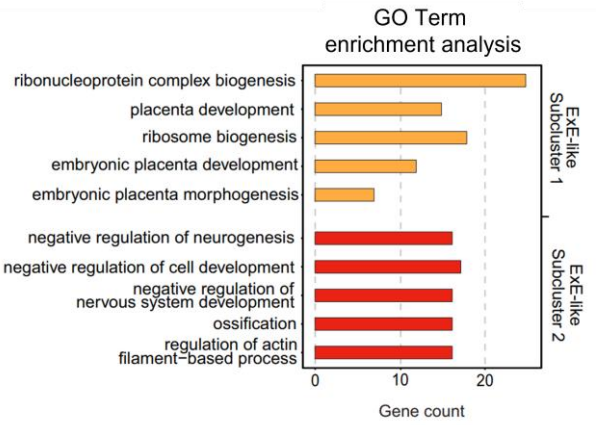

Figure 59 – GO term enrichment analysis performed on the two ExE-like subclusters. GO terms enrichment created from DEGs of ExE-like subcluster 1 and 2, indicates diverging biological functions of the two subclusters. (This figure has been published in Langkabel et al., 2021)

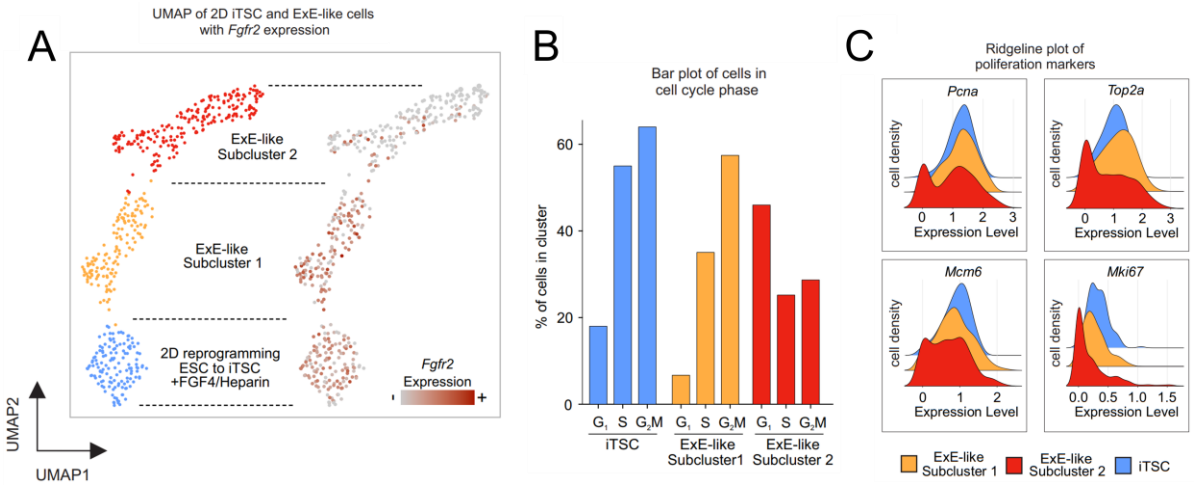

Figure 60 – Comparison of 2D monoculture induced iTSCs and ExE-like subclusters. A) UMAP representation of iTSCs generated by reprogramming in FGF4/Heparin supplemented 2D monoculture, and the two ExE-like subclusters. Cell clusters on the left side show general transcriptional clustering of the three iTSC/- ExE- like cell populations (blue = iTSCs; orange = ExE-like subcluster 1; red = ExE-like subcluster 2). The right side of the UMAP representation displays expression of *Fgfr2* across cells of all three cell clusters. Expression levels are indicated by color code, with red highlighting cells that display highest expression of *Fgfr2*. **B**) Bar plots showing percentage of iTSC and ExE-like cells that are situated in cell cycle phases G_1, S or G_2M, as assessed by Nestorowa et al., 2016. **C**) Ridgeline plots displaying expression of proliferation marker genes in ExE-like subcluster 1 and 2, as well as iTSCs. (Modified from Langkabel et al., accepted manuscript)

transcriptional character of the ExE-like cluster, GO term enrichment analysis performed using the DEGs of ExE-like subcluster 1 and 2 individually, revealed diverging biological functions with ExE-like subcluster 1 again showing a more TSC- / Placenta- related profile and ExE-like subcluster 2 displaying a more differentiated profile, that included enrichment in less embryogenesis- or stem cell fate- related gene sets (Figure 59). To further characterize the two ExE-like subclusters, they were compared to iTSCs, generated under FGF4/Heparin supplementation in 2D monoculture (Kaiser et al., 2020). UMAP representation revealed close, but not overlapping transcriptional profiles of ExE-like subcluster 1 and iTSCs, while cells of ExE-like subcluster 2 were found to cluster in furthest distance to iTSCs (Figure 60 A). Similarly, the expression of *Fgfr2* was found to be predominantly limited to cells of ExE-like subcluster 1 and iTSCs generated under FGF4 supplementation (Figure 60 A). The comparison of cell cycle stage distribution supported the observed stem cell characteristics of ExE-like subcluster 1, as the majority of cells were found to be in either S- or G_2M- phase, with few cells situated in G_1 phase (Figure 60 B). As such, their profile resembles that of iTSCs and are significantly different from cells of ExE-like subcluster 2 that include cells that are predominantly situated in G_1 phase, suggestive of decreased self-renewal capacity and a more differentiated cell fate (Figure 60 B) (Kubaczka et al., 2015). Analysis of the expression levels of proliferation marker genes *Pcna*, *Top2a*, *Mcm6* and *Mki67* further supported the observed proliferative stem cell characteristics of ExE-like subcluster 1, which displayed highly similar expression patterns of the four marker genes, compared to iTSCs obtained from reprogramming in FGF4/Heparin supplemented 2D monoculture (Figure 60 C). Exe-like subcluster 2 displayed a more heterogenous expression of

the proliferation marker genes, ranging from complete downregulation in some cells, to cells that displayed similar expression levels as iTSCs and cells of ExE-like subcluster 1 (Figure 60 C). Together, these findings strengthen the hypothesized bipartite character of the ExE-like cluster, with cells of ExE-like subcluster 1 being composed of highly proliferative TSCs and cells of ExE-like subcluster 2 that undergo differentiation and show decreased proliferative capacities, similar to the PrExE/DiExE cell populations observed during murine embryogenesis. This bipartite DiExE/PrExE-like character of the ExE-like compartment was further validated by IF staining using antibodies against phosphorylated ERK, as the ExE has been shown to exhibit a specific spatial and temporal pattern of pERK signaling during mouse embryogenesis (Corson et al., 2003). At E5.5 pERK can be detected throughout the ExE and the ectoplacental cone emerging from the DiExE (Corson et al., 2003). At this developmental stage pERK signaling is mediated either FGFR dependent (in the PrExE lining the epiblast) or FGFR independent (in the DiExE and the emerging ectoplacental cone) (Corson et al., 2003). Starting at E6.0 pERK activity is limited to a narrow band within the PrExE adjacent to the epiblast (FGFR dependent) and the ectoplacental cone (FGFR independent) emerging from the DiExE (Corson et al., 2003). In RtL-embryoids pERK signaling was detected in either a weak and diffuse distribution spanning the ExE-like compartment as a whole (Figure 52 D) or forming a pattern with the strongest activity of pERK at the most distal part of the ExE-like compartment and a weaker activity in ExE-like cells adjacent to the Epi-like compartment (Figure 61). As such, RtL-embryoids again show similarity to mouse embryos between E5.5 – E6.5, displaying similar spatial and temporal patterns of pERK signaling in the ExE-like compartment.

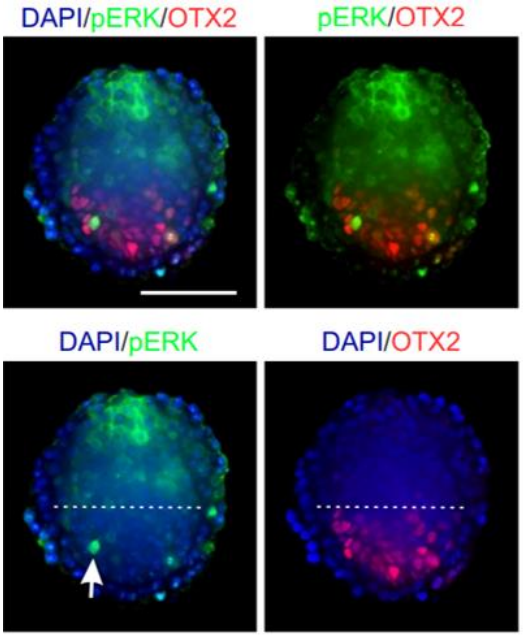

Figure 61 – IF staining visualizing pERK patterns in the ExE-like compartment. Photomicrographs of RtL-embryoids after IF staining using antibodies against pERK and OTX2. Strongest signals of pERK were observed in the most distal part of the ExE-like compartment and in the region adjacent to the Epi-like compartment. Dotted line shows border of ExE- and Epi- like compartments. (White Arrow indicates single pERK+/OTX2+ cell in the Epi-like compartment, as described in Figure 52 D). DAPI staining indicates nuclei. Scale bar = 100 µm. (Modified from Langkabel et al., accepted manuscript)

4.10 Signaling pathways between the three embryo-like cell types

The general ability to self-assemble into highly organized compartments, induction of an AVE-like signaling center, and initiation of PGC specification are all indicative of complex signaling pathways between the induced tissues. Hence, an unbiased analysis of ligand and receptor expression and interaction, was performed using the NicheNet algorithm (version 1.0.0, (Browaeys et al., 2020)) (Figure 62). NicheNet is a computational method that predicts ligand-target links between interacting cells, combining expression data of the input dataset with published models of ligand-to-target signaling pathways (Browaeys et al., 2020). Therefore, the NicheNet algorithm can be used to identify ligands acting on cells of the input dataset, trace the origin of expression of the respective ligands, predict potential receptors, their expression within

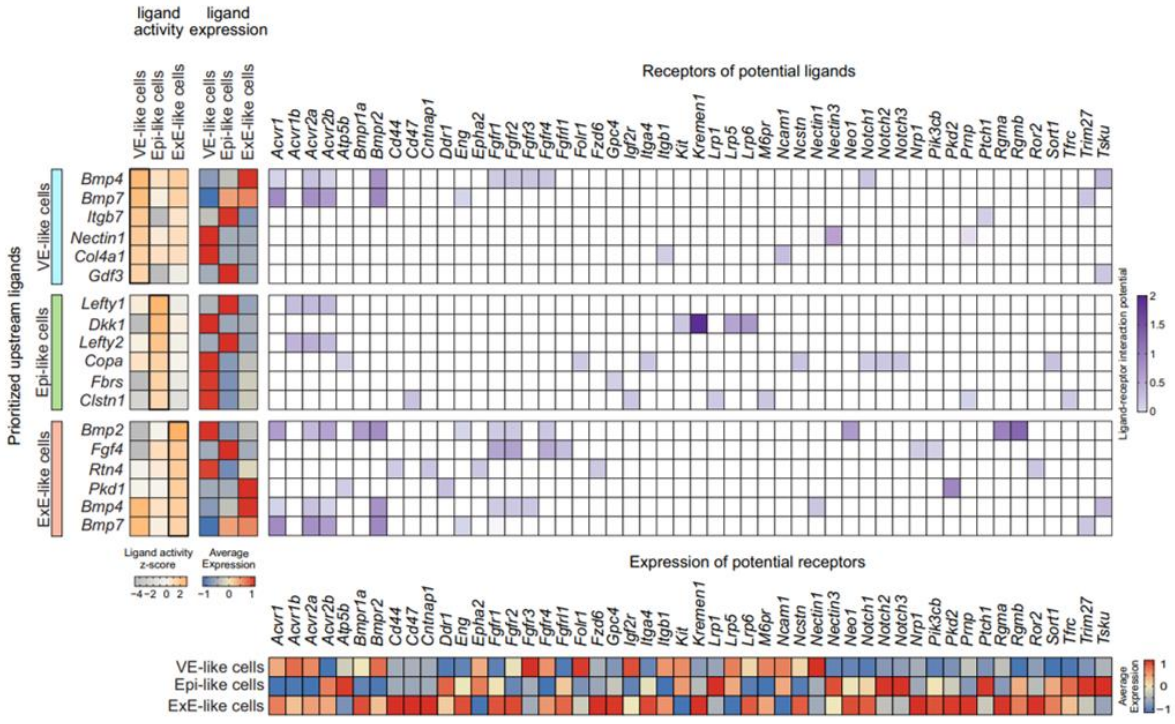

Figure 62 – NicheNet analysis performed on VE-, Epi-, and ExE-like cell clusters. Ligand-to-target interaction landscape of the three major compartments present in RtL-embryoids. Upper panels left: Prioritized upstream ligands showing ligands with highest activity in the respective cell clusters and their expression among the three clusters. Ligand activity z-score shows lowest activity in grey and highest activity in orange. Average gene expression in indicated in blue (lowest) to red (highest). Upper panel right: Receptors of potential ligands and respective predicted ligand-receptor interaction potential. Predicted ligand-receptor interaction potential is displaying from white (lowest to blue (highest). Lower panel: Expression of potential receptors in the three cell clusters. (This figure has been published in Langkabel et al., 2021)

the input datasets and the ligand-receptor interaction potential. Additionally, NicheNet allows for identification of potential target genes downstream of the ligand-receptor signaling cascades (Browaeys et al., 2020). Together, this complex bioinformatic analysis allows for identification, prediction and localization of ligand-to-receptor signaling cascades in the scRNA-Seq dataset of RtL-embryoids.

NicheNet analysis revealed BMP4, BMP7, ITGB7, NECTIN1, COL4A1 and GDF3 as the top 6 ligands showing highest activity on VE-like cells. *Bmp4* and *Bmp7* were found to be expressed in ExE-like cells, while *Itgb7* and *Gdf3* expression was found among Epi-like cells, and *Nectin* and *Col4a1* were found to be originating from the VE-like cells themselves. Regarding the expression of predicted receptors of the respective ligands, potential receptors of BMP signaling that were found to be expressed in VE-like cells included *Acvr1*, *Acvr1b*, *Acvr2a, Bmpr2, Fgfr2*, *Fgfr3* and *Fgfr4* (Figure 62). For ligands originating from the Epi-like cells and acting on VE-like cells, ITGB7 and GDF3, only weak ligand-receptor interaction potential with their respective receptors was detected and their expression was found predominantly in Epi-like cells. For ligands acting on and originating from the VE-like cells, *Nectin1* and *Col4a1*, their predicted receptors were found to be expressed in cells of the VE-like cluster, indicating autoregulatory functions of these ligands on the VE-like identity.

For ligands showing highest activity on Epi-like cells, LEFTY1, DKK1, LEFTY2, COPA, FBRS and CLSTN1 were identified. While expression of *Dkk1*, *Copa*, *Fbrs* and *Clstn1* was found to be predominantly restricted to VE-like cells, highest expression of *Lefty1* and *Lefty2* was detected in Epi-like cells. As previously demonstrated, *Lefty1* expression indicative of DVE/AVE formation could be detected within cells of the VE-like cluster as well, however, in the context of RtL-embryoids expression of *Lefty1* in the Epi-like cluster could be observed as well. The expression of predicted receptors for LEFTY1 and LEFTY2, *Acvr1b* and *Acvr2a*, was found among VE-like and ExE-like cells, however, LEFTY1/LEFTY2 predicted receptor *Acvr2b* was found to be expressed predominantly in Epi-like cells. ACVR2B is known as a key receptor and modulator of Nodal signaling and its role in maintaining a feedback inhibition of nodal signaling by Nodal itself and Lefty has been shown (Branford and Yost, 2002, Meno et al., 1999). Predicted receptors of DKK1 included KIT, KREMEN1, LRP5 and LRP6 of which only *Kit* and *Lrp5* were found to be expressed at moderate levels in Epi-like cells. Of note, highest ligand-receptor interaction potential for DKK1 was observed with KREMEN1, which was found to expressed predominantly in ExE-like cells and at baseline expression levels in Epi-like cells (Figure 62). The mechanism by which DKK1 mediated Wnt/β-catenin inhibitory signaling is mediated involves binding and antagonizing of DKK1 with LRP5/6, presumably by functionally cooperating with high-affinity DKK1 receptors KREMEN1 and KREMEN2 (Mao et al., 2002). Additionally, DKK1 expression has been demonstrated to be initiated in the mature PrE starting around E4.5, signaling the completion of PrE maturation, repressing WNT signaling and allowing for *Otx2* induction, rosette formation and pluripotency progression (Hoshino et al., 2015; Neagu et al., 2020). Hence, NicheNet analysis confirms the previous observations regarding *Otx2* induction, rosette formation and pluripotency

progression in Epi-like cells, which seems to be mediated, in part, by DKK1 signaling similar to the situation described for mouse embryogenesis (Neagu et al., 2020)

Of the predicted receptors for COPA*:* ATP5B, FOLR1, ITGA4, NCSTN, NOTCH1, NOTCH2, NOTCH3 and SORT1, several were found to be expressed in Epi-like cells, including *Atp5b*, *Itga4*, *Sort1* and all predicted Notch receptors. The only predicted receptor of the ligand FBRS, *Gpc4* was detected on base level expression in Epi-like cells, while of predicted receptors for CLSTN1, *Lrp1* and *Tfrc* were expressed on higher levels in Epi-like cells (Figure 62).

Ligands with highest activity on the ExE-like cells included BMP2, FGF4, RTN4, PKD1, BMP4 and BMP7 of which *Fgf4* was expressed on highest levels in cells of the Epi-like cluster, as previously observed when analyzing FGF signaling. *Bmp2* and *Rtn4* expression was detected in VE-like cells, while expression of *Pkd1* and *Bmp4* was found within ExE-like cells. Analysis of expression of potential receptors revealed high expression levels of all predicted BMP2 receptors, *Acvr1*, *Acvr2a*, *Acvr2b*, *Bmpr1a*, *Bmpr2*, *Eng*, *Fgfr1*, *Fgfr2*, *Fgfr4*, *Neo1*, *Rgma*, *Rgmb* among ExE-like cells. Predicted receptors for FGF4 included FGFR1, FGFR2, FGFR4 and FGFRL1, as well as NRP1 and PIK3CB, and the genes encoding for the respective receptors were detected to be expressed at high levels in ExE-like cells. For RTN4, predicted receptors included CD47, CNTNAP1, EPHA2, FZD6 and ROR2, of which all, except for *Epha2*, were found to be expressed at high levels in ExE-like cells. Of potential receptors for PKD1, only *Pkd2* was detected to be expressed at high levels in ExE-like cells. BMP4 and BMP7 were both predicted to interact with the previously mentioned BMP receptors ACVR1, ACVR2A, ACVR2B and BMPR2, all of which were detected to be expressed in ExE-like cells. Additionally, the genes encoding for predicted BMP4 receptors FGFR1 and FGFR2 were found to be expressed at high levels as well, while of additional predicted BMP7-specific receptors only *Eng* was found to be expressed at high levels in cells of the ExE-like cluster. Next the potential target genes of the prioritized ligands and their expression among VE-, Epi-, and ExE- like cells was analyzed. Of note, all respective potential target genes for all ligands were found to be highly expressed in cells of all three embryo-like compartments (Figure 63). For

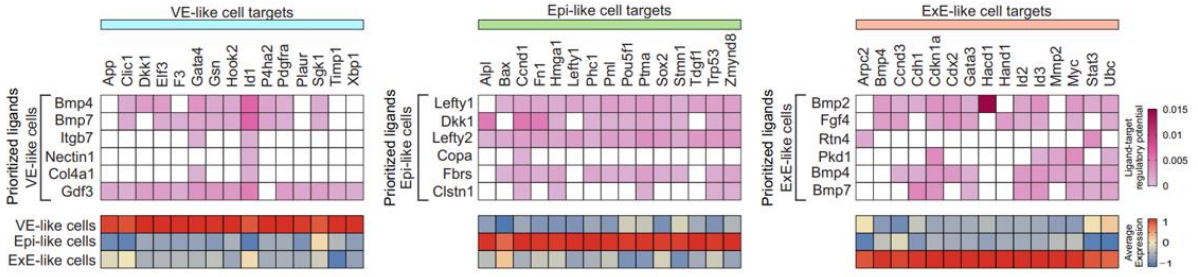

Figure 63 – NicheNet analysis of potential target genes of prioritized ligands. Upper panel: Potential target genes of the prioritized upstream ligands. Color scheme indicates ligand-target regulatory potential (white = lowest; purple = highest) as assessed by NicheNet analysis. Lower panel: Average expression of potential target genes. (This figure has been published in Langkabel et al., 2021)

ligands showing highest activity on VE-like cells, both, BMP4 and BMP7 showed high ligand-target regulatory potential with *Clic1*, *Elf3*, *Gata4*, *Gsn*, *Hook2*, *Id1*, *P4ha2*, *Pdgfra* and *Sgk1*, while BMP4 was also predicted to regulate *Dkk1*, and BMP7 displayed additionally regulatory potential on the expression of *F3*. ITGB7 and COL4A1 likewise exhibited regulatory potential for *Gata4* and *Id1*, while for NECTIN1 only *Id1* was identified as a potential target gene. GDF3 was predicted to have regulatory potential on all presented target genes, except for *P4ha2*.

For Epi-like cells, the top 3 ligands showing highest activity (LEFTY1, DKK1 and LEFTY2) showed regulatory potential for almost all predicted target genes, which included *Alpl*, *Bax*, *Ccnd1*, *Fn1*, *Hmga1*, *Lefty1*, *Phc1*, *Pml*, *Pou5f1* (*Oct3/4*), *Ptma*, *Sox2*, *Stmn1*, *Tdgf1*, *Trp53* and *Zmynd8*. For COPA, *Ccnd1* was identified as a potential target gene. FBRS was predicted to regulate expression of all target genes, except for *Alpl*, *Lefty1* and *Tdgf1*, while CLSTN1 showed regulatory potential on *Ccnd1*, *Hmga1*, *Ptma*, *Trp53* and *Zmynd8* (Figure 63).

Target genes regulated by the prioritized ligands acting on the ExE-like cells included *Arpc2*, *Bmp4*, *Ccnd3*, *Cdh1*, *Cdkn1a*, *Cdx2*, *Gata3*, *Hacd1*, *Hand1*, *Id2*, *Id3*, *Mmp2*, *Myc*, *Stat3* and *Ubc*. BMP2, the ligand showing highest activity on the ExE-like cells was predicted to regulate expression of all the predicted target genes, except for *Arpc2*, *Hand1* and *Mmp2*, showing highest predicted regulatory potential for *Hacd1*. FGF4 was predicted to regulate, among others, several of ExE marker genes, including *Bmp4*, *Cdx2*, *Gata3*, *Hand1* and *Id2*, again, highlighting its importance as a key regulator of the ExE-like cluster. The ligand RTN4 was predicted to regulate expression of *Arpc2* and *Stat3*, while ligand PKD1 was predicted to regulate expression of *Cdkn1a*, *Id3*, *Mmp2*, *Myc* and *Ubc*. BMP4 was predicted to regulate expression of *Ccnd3*, *Cdh1*, *Cdkn1a*, *Cdx2*, *Gata3*, *Id2*, *Id3*, *Mmp2*, *Myc*, *Stat3* and *Ubc*, while BMP7 demonstrated regulatory potential for the same target gene set as BMP4, except for *Ccnd3*, *Cdx2*, and *Mmp2* (Figure 63).

Together, NicheNet analysis confirmed the results of previous analysis, further supporting the observation, that LEFTY1 and DKK1 signaling secreted from the VE-like compartment is acting on the Epi-like compartment and functioning similar to that the mechanism described for mouse embryogenesis. Additionally, NicheNet analysis confirmed the observed FGF4 mediated signaling originating from the Epi-like compartment and its role in maintaining a TSC-fate in the ExE-like cluster, as all potential target genes of FGF4 were found to be highly expressed in cells of the ExE-like cluster, including *Bmp4*, *Cdx2*, *Gata3* and *Id2*. In conclusion, NicheNet analysis confirmed previously described observations of the complex signaling cascades between the three embryo-like compartments, in an unbiased, data-driven manner.

4.11 Stem cell derivation from RtL-embryoids

RtL-embryoids could potentially provide an alternative strategy to generate and derive embryo-like stem cell lineages that might be more similar to their natural embryo-derived equivalents, due to the complex intrinsic and instructive signaling in 3D co-culture, compared to traditional

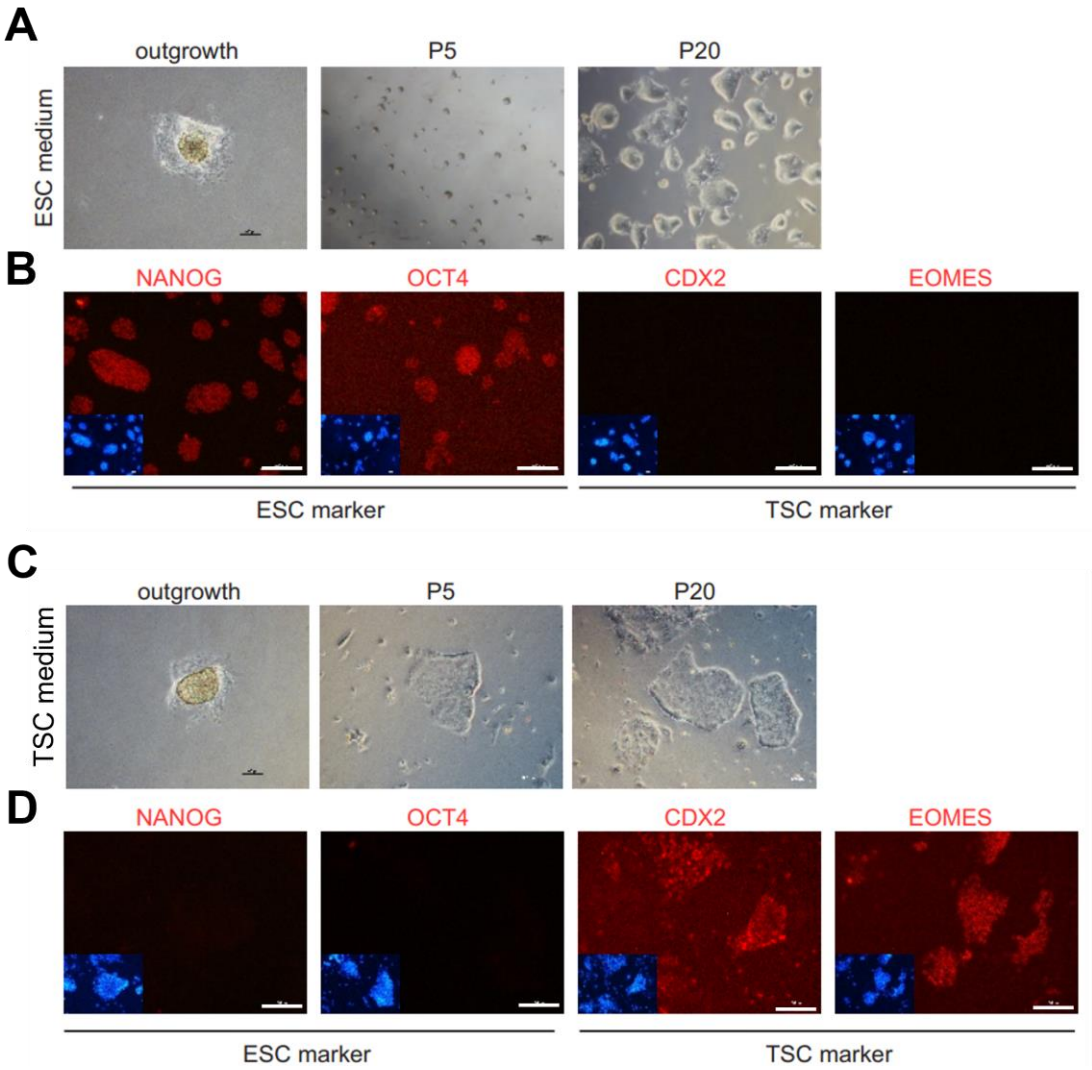

Figure 64 – Stem derivation from RtL-embryoids. Micrographs of stem cell derivation experiments for the isolation of 3D co-culture induced TSCs and ESCs from RtL-embryoids. **A)** Derivation of ESCs by outgrowth culture in 2i/LIF supplemented ESC medium, over the course of 2 days after seeding of RtL-embryoids until passage 20. **B)** IF staining against ESC marker (NANOG, OCT4) and TSC marker (CDX2, EOMES) performed on a RtL-embryoid derived ESC clone at passage 20. **C)** Derivation of iTSCs by outgrowth in FGF4/Heparin supplemented TSC medium, over the course of 2 days after seeding of RtL-embryoids until passage 20. **D)** IF staining against ESC marker (NANOG, OCT4) and TSC marker (CDX2, EOMES). Inlay images display Hoechst staining. Scale bars = 100 µm. (Modified from Langkabel et al., accepted manuscript)

2D monoculture induced stem cell identities. Therefore, it was next assessed if the three stem cell lineages that can be derived by blastocyst outgrowth from murine embryos could also be derived and propagated from RtL-embryoids. For the derivation of ESCs, RtL-embryoids were generated as described before, harvested, and transferred onto gelatin-coated cell culture dishes on which they were cultured in 2i/LIF supplemented ESC medium to support proliferation of ESCs (Figure

64 A). Once a cellular outgrowth had formed from the attached RtL-embryoids, cells were dissociated by incubation in Accutase for ~8 minutes and the single cell suspension was transferred onto a freshly prepared gelatin-coated cell culture dish. Once small colonies had formed, they were handpicked manually using a micropipette and resulting clones were further propagated individually. ESC clones derived from RtL-embryoids stably proliferated for >20 passages (P) and displayed characteristic morphology of 2i/LIF cultured ESCs (Figure 64 A). Assessment of marker expression on protein level by IF staining of an ESC clone at P20 revealed expression of ESC markers NANOG and OCT4 and absence of TSC markers CDX2 and EOMES (Figure 64 B). Similarly, iTSCs could be derived by outgrowth culture in FGF4/Heparin supplemented TS medium, that could be propagated for >20 passages and stained positive for TSC markers CDX2 and EOMES, while being devoid of ESC markers OCT4 and NANOG (Figure 64 C and D). Albeit testing different protocols for the derivation of XEN cells from murine embryos at pre- or post-implantation stages, iXEN cells could not be derived from RtL-embryoids, as they quickly differentiated and died off upon clone culture and expansion in XEN cell medium in 2D monoculture (Niakan et al., 2013; Lin et al., 2016). Nevertheless, these results demonstrate, that embryo-like stem cell lineages can be derived from RtL-embryoids, which potentially allows for more detailed studies of these stem cell identities generated by reprogramming in 3D co-culture.

4.12 Developmental potential of RtL-embryoids *in vivo*

Previous results indicated that RtL-embryoids closest mirror a developmental stage comparable to natural embryos around E4.5 – E5.5. As this would reflect the developmental timepoint at which the late blastocyst (E4.5) initiates implantation *in utero*, the developmental potential of RtL-embryoids was assessed *in vivo.* As Zhang et al. have demonstrated, ETX embryoids are able to implant *in utero* and initiate decidualization, despite showing a post implantation architecture

Figure 65 – Decidual reactions after transfer of RtL-embryoids in pseudopregnant foster mice. A) Isolated uterus of pseudopregnant foster mouse showing two sites of decidual tissue formation (white arrows) 7 days after transfer of RtL-embryoids. **B)** Uterus with natural implantation sites at 10.5 d.p.c. and **C)** at 11.5 d.p.c. Scale bars = 3 mm. (Parts of this figure have been published in Langkabel et al., 2021)

of the three embryo-like compartments and lacking tissues like the trophectoderm and the parietal endoderm that would naturally facilitate implantation during mouse embryogenesis (Zhang et al., 2019). To study the developmental potential of RtL-embryoids *in vivo*, RtL-embryoids were generated as described before using Kermit ESCs, 5F ESCs and iGATA6_mCherry ESCs, to allow for a preselection of correctly assembled structures (Figure 34). Female CB6F1 mice were mated with vasectomized males to generate pseudo-pregnant foster mice, which were then used for transfer of RtL-embryoids into the uterus at 2.5 d.p.c. The transferred aggregates were allowed to develop for a total of 7 days *in vivo*, before sacrificing the mice, isolating the uteri, and analysis for possible implantations. From 204 RtL-embryoids used for transplantation 11 implantation sites (5.39 %) were detected. Considering a developmental timepoint between E4.5 – E5.5 for RtL-embryoids at the time of transfer into the uterus and a further *in vivo* development for 7 days, the concepti should be comparable to 11.5 to 12.5 d.p.c. embryos assuming equal developmental potentials. Implantations of RtL-embryoids were more similar in size compared to natural implantations at 10.5 d.p.c., than the expected at 11.5 d.p.c. (Figure 65). Next, the implantation sites were dissected, and the structures obtained presented as elongated, cone-like structures of ~3 mm length and ~2 mm width (Figure 66 A). When compared to mouse concepti isolated at 10.5 or 11.5 d.p.c., structures obtained from RtL-embryoids presented almost completely homogenous in general tissue structure and neither placenta-like tissue, nor a yolk sac-like structure containing the embryo proper could be detected (Figure 66 B). Next, the isolated structures were micro surgically divided to analyze the decidual tissue for contribution of cells originating from RtL-embryoids. While, again, presenting rather homogenous in tissue structure, GFP signals originating from the center of the decidual tissue indicate, that Kermit ESCs from the Epi-like compartment of RtL-embryoids contribute to the decidual reaction (Figure 67). Of note, mCherry expression originating from descendants of iGATA6_mCherry ESC was not detectable in

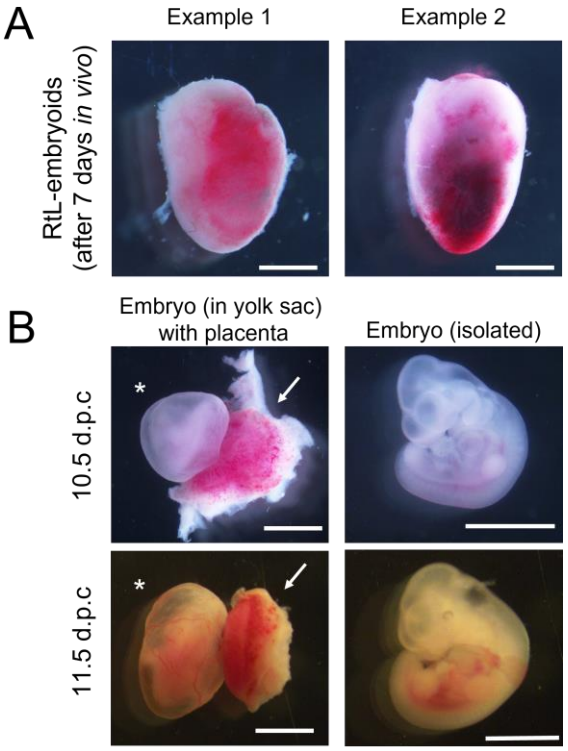

Figure 66 – Comparison of surgically isolated RtL-embryoids and murine concepti. A) Two examples of transferred RtL-embryoids isolated after 7 days culture *in vivo in utero*. Scale bars = 1 mm. **B)** Natural concepti isolated from the uterus of mice at 10.5 and 11.5 d.p.c. Left side: Embryo in yolk sac (indicated by asterisk) and placenta (indicated by arrow). Right side: Embryo isolated from yolk sac. Scale bars = 3 mm. (Parts of this figure have been published in Langkabel et al., 2021)

the surgically dissected structures. However, it cannot be excluded, that this missing fluorescence signal could be due to technical restrictions of the imaging setup and generally weak mCherry signals, compared to strong GFP signals. Together, these results are indicative of a drastically decreased or even completely ceased developmental potential *in vivo* of RtL-embryoids, compared to natural embryogenesis (Figure 66). However, as crucial tissues mediating implantation during embryogenesis, like TE derived TGCs and the parietal endoderm are not formed, and the developmental stage of RtL-embryoids reflects peri- to post-implantation stage characteristics, the observed 'implantations' should be regarded decidual tissue reactions resulting from mechanical stimuli of the uterus, rather than actual implantation sites, observed during embryogenesis.

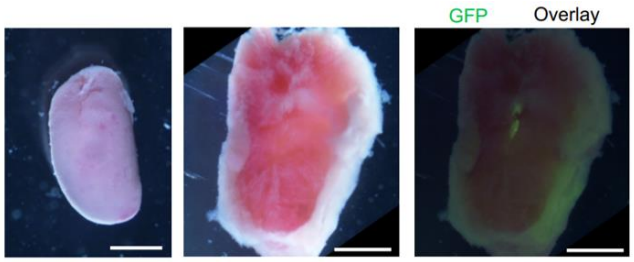

Figure 67 – RtL-embryoid isolated from pseudopregnant mice after 7 days *in utero*. Left: RtL-embryoid implantation isolated from pseudopregnant mice after 7 days development *in utero*. **Middle**: RtL-embryoid implantation surgically divided. **Right**: Detection of GFP signal in the center of divided structure. Scale bars = 1 mm. (This figure has been in Langkabel et al. 2021)

Parts of the chapters of the results section have been accepted for publication or have been published in:

Langkabel, J., Horne, A., Bonaguro, L., Holsten, L. Hesse, T., Knaus, A., Riedel, Y., Becker, M., Händler, K., Elmzzahi, T., Bassler, K., Reusch, N., Yeghiazarian, L.H., Pecht, T., Saglam, A., Ulas, T., Aschenbrenner, A.C., Kaiser, F., Kubaczka, C., Schultze, J.L. & Schorle, H. (**Accepted for publication**). Induction of Rosette-to-Lumen stage embryoids using reprogramming paradigms in ESCs. Nature Communications

Langkabel, J., Horne, A., Bonaguro, L., Hesse, T., Knaus, A., Riedel, Y., Händler, K., Bassler, K., Reusch, N., Yeghiazarian, L. H., Pecht, T., Aschenbrenner, A.C., Kaiser, F., Kubaczka, C., Schultze, J.L. & Schorle, H. (2021). Induction of peri-implantation stage synthetic embryos using reprogramming paradigms in ESCs. BioRxiv 2021.01.25.428068

Kaiser, F., Kubaczka, C., Graf, M., Langer, N., **Langkabel, J.**, Arévalo, L. & Schorle, H. (2020). Choice of factors and medium impinge on success of ESC to TSC conversion. Placenta *90*, 128-137.

5. Discussion

5.1 Generation of an *in vitro* embryo model based on reprogramming of ESCs

The goal of this thesis was the establishment of an organoid system that would allow for the generation of embryo-like structures from a solely ESC-based starting cell population, combining reprogramming paradigms and 3D cell culture. Reprogramming of 5F ESCs to iTSCs and iGATA6 ESCs to iXEN cells, in 3D co-culture with ESCs that remained in pluripotent state was demonstrated to result in self-organization into embryo-like structures that resemble murine embryos between E4.5 – E5.5. These structures, termed RtL-embryoids, were shown to undergo key hallmarks of embryogenesis, such as lumenogenesis, accompanied by a progression in pluripotency states as well as specification of PGC and DVE/AVE-like cells. Therefore, the protocol established and described in this study provides a novel strategy for the generation of embryo-like cell culture models, allowing for the generation of more than 700 RtL-embryoids in a single 12-well plate.

5.2 RtL-embryoids in the field of stem cell-based embryo models

The emerging field of embryo-related organoid culture systems provides advanced models to recreate embryogenesis and individual aspects of it in *in vitro* environments. Currently, this area of research is in active development by the scientific community and different terminologies have been proposed to correctly describe the embryo-like structures. As reviewed by Rossant and Tam, the term artificial or synthetic embryo has been used widely and to some degree too generic or even false, as the term 'synthetic' would require new genetic switches or synthetic pathways, that have been programmed into the starting cells (Rossant and Tam, 2021). The ground-breaking work of Rivron et al., Sozen et al., and Zhang et. al., that introduced and characterized blastoids and ETX embryoids relied on the self-organization properties of the three stem cell lineages, which can be isolated from blastocysts (Rivron et al., 2018a, Sozen et al., 2018, Zhang et al., 2019). Hence, emerging consensus is that such embryo-models should be termed *stem cell-based embryo models* (Hyun et al., 2020; Rivron et al., 2018b; Sozen et al, 2019; Sahu and Sharan, 2020; Rossant and Tam, 2021). In this context, the embryo model presented in this thesis would be regarded a 'synthetic, integrated stem cell-based embryo model', as the controllable, pre-programmed genetic switches used to induce cellular reprogramming are the key-prerequisite

for the protocol presented here. Furthermore, the method presented in this study relies on active, targeted manipulation of molecular pathways, rather than co-culture of the three blastocyst-derived stem cell lines, passively making use of their cell-lineage specific characteristics.

The embryo model presented here is based on reprogramming of ESC-fate to iTSC-fate, by controlled expression of *Cdx2*, *Tfap2c*, *Eomes*, *Gata3* and *Ets2*, a combination of trophoblast specific transgenes that can generate iTSCs showing key characteristics of blastocyst-derived trophoblast stem cells (Kaiser et al., 2020). Specifically, iTSCs obtained by cell fate conversion from 5 Factor ESCs displayed high expression levels of trophoblast-fate specific marker genes *CD40*, *Elf5* and *Eomes*, as well as demethylation of the *Elf5*- and methylation of the *Oct4*-promotor (Kaiser et al., 2020). Furthermore, we were able to demonstrate their ability to contribute to placental tissue upon blastocyst injection (Kaiser et al., 2020). In Kaiser et al., we also investigated ESC-iTSC cell fate conversion of other genetically modified cell lines, like the 4 Factor ESC line, carrying doxycycline inducible transgenes of *Tfap2c*, *Eomes*, *Gata3* and *Ets2*, or the iCDX2 ESC line, which relied on transgene expression of *Cdx2* alone (Kaiser et al., 2020). Both, iCDX2 ESCs and 4 Factor ESCs were demonstrated to require reprogramming in defined TX culture medium for complete cell fate lineage conversion, while 5 Factor ESCs were shown to undergo lineage conversion in serum-based TS medium (Kaiser et al., 2020). 5 Factor ESCs were chosen for cell fate conversion towards an iTSC-fate in the study presented here, as they would most likely allow for complete cellular reprogramming in serum based reconstructed embryo medium, as such a basal serum-based cell culture medium would be required for the 3D co-culture of different cell lineages (Zhang et al. 2019). Furthermore, addition of transgenic CDX2 was thought beneficial, as it induces downregulation of OCT4, thereby speeding up the exit from pluripotency and allowing for the other four transcription factors to induce the TSC transcription factor network (Kaiser et al. 2020).

The second reprogrammable ESC line used for the generation of the embryo model presented in this thesis are iGATA6 ESCs, which carry a doxycycline inducible *Gata6* transgene. Expression of *Gata6* in ESCs initiates reprogramming of pluripotent and differentiated cells to extraembryonic endoderm stem cells (Wamaitha et al., 2015; Ngondo et al., 2018). A short pulse of *Gata6* induction for 6 – 12 hours was demonstrated to be sufficient to stably induce an iXEN cell identity from mouse ESCs, by rapid repression of the pluripotency gene regulatory network in combination with the activation of an endoderm gene program (Wamaitha et al., 2015). Supporting this, RtL-embryoids presented here, displayed a clearly visible organization of descendants of iGATA6 ESCs into a sphere-like structure surrounding the two inner compartments already after 24 h of doxycycline induced transgene expression of *Gata6*. Interestingly, Amadei et al. have recently demonstrated that a doxycycline induced pulse of *Gata4*

in mouse ESCs for 5 hours and subsequent 3D co-culture with ESCs and TSCs leads to assembly into an iETX embryo model, which reflects natural embryogenesis more closely than their previously introduced ETX embryoids (Amadei et al., 2021; Sozen et al., 2018). Regarding terminology, these iETX embryoids could be described as 'synthetic integrated stem cell-based embryo models' as well, as they similarly rely on pre-programmed genetic switches to induce an endoderm lineage identity. Considering observations made during reprogramming of ESCs to iXEN cells (Wamaitha et al., 2015), self-organization into a functional VE-like layer in iETX embryoids (Amadei et al., 2021) and self-organization properties observed during the time-lapse experiments presented in this study, it can be assumed, that a short pulse of DOX-mediated transgene expression of *Gata4* or *Gata6* for less than 24 hours would be sufficient to generate a VE-like layer. However, while this reprogramming approach towards an endoderm lineage-fate is appropriate to generate a sphere-like compartment architecturally resembling a natural VE within 24 hours into the protocol, descendants of Kermit- and 5 Factor- ESCs remain in a random, salt-and-pepper distribution in the inner compartments at this timepoint. As previously demonstrated, the cell-fate conversion from 5 Factor ESCs to iTSCs requires doxycycline mediated transgene expression for a duration of 3 days to allow for complete reprogramming (Kaiser et al., 2020). Similarly, a complete self-organization of the inner cells into an ExE- and Epi-like compartment in RtL-embryoids was observed first after a total of 3 days of doxycycline supplementation. Supporting this observation, we were able to show that a shortened duration of DOX supplementation for only 48 h results in a decrease in self-organization efficiency to about 16 %. Hence, it can be assumed, that complete lineage conversion and self-organization of 5 Factor ESCs to an ExE-like tissue in RtL-embryoids requires the full duration of 3 days of transgene expression. As soon as the two inner cellular compartments have completely segregated, the boundary of ExE- and Epi-like compartments can provide a stem cell-fate enhancing environment that relies on NODAL-BMP signaling feedback loops, similar to the mechanism found in natural embryogenesis. In conventional reprogramming approaches in 2D monocultures, the generation of iTSCs from ESCs requires medium supplementation with FGF4 and heparin, in order to maintain the stem cell characteristics of TSCs (Tanaka et al., 1998). In the context of embryo-like models this signaling cascade is stimulated among others, by FGF4 originating from the Epi-like compartments, hence a structural rearrangement might be prerequisite for the stable propagation of iTSCs within the ExE-like compartment. Reprogramming of ESCs towards an iXEN cell fate using overexpression of *Gata6* however was demonstrated to function independently of exogenous factors, as the dual function of GATA6 as a repressor and activator potently drives ESC-to-iXEN cell conversion (Wamaitha et al., 2015). This could be interpretated as a possible explanation for differences in time needed reprogramming and self-organization of 5 Factor- and iGATA6- ESCs. Intrinsic signaling networks can be regarded

the main driving factor of natural embryogenesis during pre-implantation development, as the blastocyst is, at this developmental stage, still independent from maternal signaling. This changes upon implantation, when the first maternal-fetal interface is established and extrinsic signaling from the maternal environment becomes increasingly more important for post-implantation development. In the protocol presented in this study, RtL-embryoids remain structurally stable regarding their general architecture even during prolonged culture of up to 196 h, however, further development into more complex embryo-like structures seems to be hindered. Considering that general morphological appearance and scRNA-Seq suggest a developmental stage equivalent to E4.5 – E6.0 and therefore peri- to post- implantation characteristics, a supplementation with maternal signaling factors could prove beneficial for further development *in vitro*. Supporting this assumption, the embryo model presented by Amadei et al. is based on medium supplementation with sex hormones progesterone and β-estradiol, resulting in increased developmental potential *in vitro* (Amadei et al., 2021). For the method presented in this study, we opted for a basal medium, as this would provide a suitable growth environment for all induced cell lineages, while allowing for undisturbed signaling between the generated tissues. However, as we obtained structures that resemble peri- to post- implantation rather than pre-implantation stage embryos, future experiments should involve a more sophisticated culture medium composition, which can provide a more suitable environment for the respective induced developmental stages.

5.3 Cell fate lineage conversion in 3D co-culture vs 2D monoculture

The main difference of RtL-embryoids presented here and other embryo models such as blastoids and ETX embryoids lies in the simultaneous 3D co-culture and cell-fate reprogramming. As we and others have demonstrated successful cellular reprogramming towards alternative cell fates relies on a genome-wide changes in chromatin accessibility, combined with focused hyper-accessibility at critical chromatin loci (Schwarz et al., 2018). Hence, we hypothesized, that reprogramming in co-culture with other cell-fates could improve reprogramming efficiencies and quality of the resulting induced cell-fates, as genome-wide chromatin accessibility and hyper-accessibility at cell-lineage specific loci would render the cells undergoing reprogramming more susceptible towards signaling cues from the other cellular compartments within RtL-embryoids. Interestingly, the VE-like layer of iETX embryoids, obtained by reprogramming of ESCs to iXEN cells by *Gata4* expression was demonstrated to be more similar to its natural counterpart, compared to the VE-like layer of ETX embryoids, generated from blastocyst-derived XEN cells (Amadei et al., 2021). Therefore, embryo-like tissues generated by reprogramming approaches

seem to reflect characteristics of their natural equivalents more closely, which could be the result of genome-wide and loci specific chromatin (hyper)accessibility. As XEN cells are derived from the PrE of blastocysts, they represent a cell culture model of this lineage, however, it was previously demonstrated, that BMP signaling synergizes with laminin (*Lama1*), a major component of the extracellular matrix, to promote highly efficient conversion of XEN cells to a VE cell-fate (Paca et al., 2012; Niakan et al., 2013). Similarly, ESC-to-iXEN conversion by forced expression of *Gata6* did not result in the formation of a PrE-like tissue within a blastocyst-like structure in the approach presented here, but rather in formation of a VE-like compartment showing post-implantation characteristics. Among the highest differentially expressed genes of the VE-like cells we were able to detect *Lama1*, while the ExE-like compartment has been identified as a source of BMP signaling in RtL-embryoids presented here. Therefore, we hypothesized, that reprogramming of iGATA6 ESCs in 3D co-culture, directs reprogramming towards a VE-like character instead of an iXEN-identity. The comparison with scRNA-Seq datasets of murine embryos and RtL-embryoids did however reveal, that the presumed VE-like compartment was mainly enriched in PrE gene signatures and might only show morphological VE-like characteristics, while retaining a baseline PrE-like transcriptional profile. Interestingly, cells of the VE-like cluster did not show any overlap in transcriptional profiles compared to E4.5/E5.5 epiblast or ICM cells. Considering, that this cell population was not sorted by staining against lineage-specific cell surface markers, but instead by using a constitutive mCherry expression cassette, it can be assumed that VE-like cells in RtL-embryoids have converted towards an endoderm cell fate with high efficiency, leaving no transcriptional 'footprint' of the ESC-fate they were derived from. Conversely, 28.57% of cells of the ExE-like compartment did show a residual transcriptional 'footprint' of the ESC-fate they were derived from, indicating that these cells did not completely progress towards a TE/ExE-cellular identity. However, all ExE-like cells clustered closely according to their transcriptional profiles and all ExE-like cells displayed expression of trophoblast/placenta-specific marker genes. Therefore, it can be assumed, that 5 Factor ESCs in RtL-embryoid do undergo reprogramming towards a TE/ExE-like identity, albeit resulting in lower qualities of the induced cell fates, compared to ESC-to-iXEN cell conversion in RtL-embryoids.

The comparison of scRNA-Seq datasets of 3D co-culture and 2D monoculture induced cell fates revealed close, but not overlapping clustering in transcriptional profiles, for both VE- and ExE-like cells with iXEN cells or iTSCs, respectively. As this can be seen indicative of different reprogramming outcomes, we compared transcriptional signatures of 3D co-culture and 2D monoculture induced cells with the natural embryonic tissues they showed closest transcriptional clustering with in UMAP representation. Here, we found that 3D co-culture induced VE-like cells were highly enriched in both PrE and VE gene signatures of murine embryos.

2D monoculture induced iXEN cells did not show any significant enrichment in the PrE signature and a lower enrichment in the VE signature, albeit displaying higher mean expression of the genes included in this signature compared to 3D co-culture induced VE-like cells. This can be seen indicative of an induced developmental progression from a PrE to a VE cell fate of VE-like cells reprogrammed in 3D co-culture, which is absent in 2D monoculture induced iXEN cells. Similarly, the signature enrichment analysis of 3D co-culture induced Epi-like cells displayed an enrichment in E4.5 and E5.5 Epiblast signatures and a downregulation of genes in the ICM signature. As expected, ESC cultured in 2i/LIF supplemented monoculture were enriched in ICM and E4.5 Epiblast signatures. These results indicate that Epi-like cells in RtL-embryoids progress from a E4.5 to a E5.5 Epiblast-identity, accompanied by a downregulation of genes included in the ICM signature. The comparison of 3D co-culture induced ExE-like cells and iTSCs generated in FGF4/Heparin supplemented 2D monoculture revealed higher enrichment in the ExE gene signature for 2D monoculture induced iTSCs. However, these cells also displayed higher enrichment and mean expression levels of genes included in the E4.5 Epiblast signature, compared to 3D co-culture induced ExE-like cells. First, this result demonstrates that the transcriptional ESC 'footprint' is not the result of reprogramming in 3D co-culture, but rather an intrinsic problem of ESC-to-iTSC reprogramming by transgene overexpression. Second, lower enrichment and mean expression levels of gene included in the E4.5 Epiblast signature for 3D co-culture induced ExE-like cells indicate, that this co-culture reprogramming approach could potentially improve the quality of cell lineages conversion compared to traditional reprogramming in 2D monoculture.

Together, these results indicate different reprogramming outcomes of ESC-to-iTSC and ESC-to-iXEN cell conversions in 3D co-culture or 2D mono-culture protocols. Therefore, RtL-embryoids could potentially provide a novel source for the derivation of stem cell lineages, that might show higher resemblance to their natural equivalents due to reprogramming in complex embryo-like signaling environments. To allow for more a detailed analysis of the induced cell fates and test the possibility of rederivation of ESCs and iTSCs from RtL-embryoids, we applied outgrowth experiments by seeding aggregates in culture conditions supporting the respective stem cell fates. While we were able to rederive ESCs and iTSCs that stably proliferated for more than 20 passages and displayed respective marker expression on protein levels, we were unable to rederive iXEN cells from RtL-embryoids, albeit testing protocols for XEN cell derivation in both, pre- and post-implantation embryos (Niakan et al., 2013; Lin et al., 2016). Whether this was due to a technical problem or an inherent problem of the RtL-embryoid remains to be elucidated.

5.4 The visceral endoderm-like compartment of RtL-embryoids

Closer analysis of the individual embryo-like compartments revealed that the VE-like compartment is comprised of a fully polarized epithelial layer of GATA4+ cells, which displayed a noticeable bipartite behavior, both morphologically in long-term culture as well as in scRNA-Seq analysis. Considering its role in natural embryogenesis, where the VE is associated with nutrient uptake and transport before a placental maternal-embryonic circulation is established, the VE-like layer of RtL-embryoids could function similarly in the *in vitro* embryo model (Cross et al., 1994; Bielinska et al., 1999). This function is mediated by the VE endocytosis complex, which is, among others, based on the multiligand receptor CUBN, that forms a complex with AMN, LRP2 and DAB2, all of which were detected to be highly expressed in cells comprising the VE-like layer (Maurer et al., 2005; Perea-Gomez et al., 2019). Therefore, it can be assumed, that the function of the VE as a mediator of nutrient uptake and transport is reflected by the VE-like compartment in RtL-embryoids presented here. Assessment of expression of established VE marker genes, such as *Sox17*, *Spink1*, *Sox7*, *Gata4* and *Gata6* further confirmed the presumed identity of the VE-like layer and comparison to gene signatures obtained from PrE and VE revealed high similarity to these tissues (Brown et al., 2010; Mohammed et al. 2017). The VE is furthermore known to be distinguishable into two subpopulations representing either the VE surrounding the ExE (ExVE), or the Epi (EmVE) and a similar behavior could be observed in the VE-like compartment of RtL-embryoids. Mirroring the VE during natural embryogenesis, the VE-like layer displayed two transcriptionally similar, but diverging subpopulations of cells, which could be correlated with ExVE and EmVE signatures obtained from natural murine embryos (Cheng et al., 2019). Confirming this bipartite characteristic, the ExVE-like compartment displayed drastic morphological changes during long-term culture of the aggregates, showing cellular outgrowth, which was restricted to the ExVE-like structure, while the EmVE-like compartment remained consistent in its architecture. Apart from its role as an early mediator of nutrient uptake and transport, the VE is also known for its role as an important signaling center, which induces AP-axis formation, thereby facilitating formation of a body plan for the developing embryo. As previously described, this signaling center first becomes apparent when a subpopulation of cells at the most distal tip of the EmVE specify to become DVE cells, that secret antagonists of Wnt and Nodal signaling pathways (Yamamoto et al., 2009). The induction of this subpopulation relies on exposure to low levels of Nodal and simultaneous inhibition by BMP4 secreted from the ExE, which further restricts DVE specification to the distal part of the EmVE (Brennan et al., 2001; Yamamoto et al., 2009). DVE specification is controlled and maintained in part by EOMES and OTX2 that regulate expression of downstream DVE/AVE specification genes like *Lefty1* and *Dkk1* (Nowotschin et al., 2013; Perea-Gomez et al., 2001; Kimura-Yoshida et al., 2005). Upon

specification the DVE migrates towards the future anterior side of the developing embryo, where it localizes next to the AVE, which is thereby restricted to the anterior side from where the DVE/AVE complex continuously secrets Wnt/Nodal signaling pathway inhibitors like LEFTY1, CER1, DKK1 and HHEX (Hoshino et al., 2015). In RtL-embryoids presented in this thesis, scRNA-Seq revealed high expression of genes included in an AVE signature obtained from natural murine embryos within cells of the EmVE-like subpopulation and highest expression of DVE/AVE marker genes *Lefty1*, *Dkk1*, *Sfrp1* and *Sfrp5* (Cheng et al., 2019; Takaoka et al., 2011; Mukhopadhyay et al., 2001; Satoh et al., 2006; Finley et al., 2003). Additionally, we were able to localize the VE-like cells undergoing DVE/AVE specification by IF staining using antibodies against EOMES, OTX2 and LEFTY1, revealing that cells co expressing these highly specific DVE/AVE lineage markers were located predominantly in a distal and transitioning position within the EmVE-like compartment. However, as the comparison of localization of LEFTY1+ cells at day 4 and 5 did not show signs of any significant migratory potential of this DVE/AVE-like population, it seems that complete AP-axis formation is hindered or delayed in RtL-embryoids. Interestingly, analysis of aggregates, with poor ExE-like tissue contribution displayed LEFTY1+ cells across the EmVE-like compartment as a whole, albeit expression was still restricted to this subpopulation. Considering the importance of BMP signaling originating from the ExE to restrict specification of the DVE to the most distal tip of the EmVE, this result highlights the importance of this mechanism in spatial confinement of the DVE (Yamamoto et al., 2009). Additionally, this observation could explain the demand for a larger amount of 5 Factor ESCs within the mixed starting cell population, to achieve early embryo-like architecture and highest efficiency of correctly self-organized RtL-embryoids. Supporting these observations, ligand-receptor interaction potentials and potential downstream signaling targets analyzed using the NicheNet algorithm revealed BMP4, secreted by the ExE-like compartment, as the ligand displaying highest activity on VE-like cells.

5.5 The epiblast-like compartment of RtL-embryoids

Analysis of the Epi-like compartment of RtL-embryoids presented in this thesis revealed a high responsiveness to signaling from the VE-like compartment, as displayed by NicheNet algorithm. Here, LEFTY1, DKK1, LEFTY2, COPA, FBRS and CLSTN1 were identified as ligands with highest activity on the Epi-like cluster, all of which are related to the VE lineage, again highlighting the importance of the VE-like compartment as signaling center for the Epi-like compartment. Of note, *Lefty1* and *Lefty2*, as assessed by NicheNet, were detected to be highly expressed in cells of the Epi-like cluster and displayed only low expression levels in VE-like cells. However, *Lefty1* expression in the VE is restricted to single cells and could therefore be lost in heatmap

representation, and both LEFTY1 and LEFTY2 are known to control the balance between self-renewal and pluripotent differentiation in mESCs, hence, their high expression within ESCs comprising the Epi-like compartment can be explained and was previously observed in other embryo models as well (Kim et al., 2014; Sozen et al., 2018). The receptor of LEFTY1 and LEFTY2, ACVR2B, a known key receptor and modulator of Nodal signaling (Branford and Yost, 2002; Meno et al., 1999), was found to be expressed in cells of the Epi-like compartment, and Nodal expression was detected in a heterogenous manner within the Epi-like cell population, indicative of a gradient of gene expression regulation. Together, these observations strengthen the assumption, that the Lefty1-Nodal feedback inhibition loop present in murine embryos is also established in RtL-embryoids. Contributing to this, gene signature enrichment analysis of anterior-, transition- and posterior- epiblast gene sets obtained from natural murine embryos revealed high similarity to the anterior gene signature and only minor enrichment in transition-, and posterior- epiblast signatures. Considering the limited migratory potential of the DVE/AVE-like population in the EmVE-like compartment, this low or absent enrichment of Epi-like cells in transition-, and posterior epiblast signatures could be the results of missing or weak Wnt/Nodal signaling inhibition from DVE/AVE-like cells in a truly anterior position within the VE-like compartment.

The comparison with scRNA-Seq datasets of murine embryos revealed highest resemblance to E4.5 and E5.5 Epi cells, and in murine embryos this developmental progression is known to be accompanied by the transition from naïve- to primed-pluripotency in Epi cells (Neagu et al., 2020). This progression is mediated by a switch of transcription factor programs regulating naïve- (KLF4+, NANOG+,ESRRB+,OTX2+, OCT6-) and primed- (KLF4-, NANOG-, ESRRB-, OTX2+, OCT6+) pluripotency (Neagu et al., 2020). Therefore, we analyzed RtL-embryoids for presence or absence of the respective pluripotency markers on gene and protein levels. We were able to detect a tripartite transcriptional character of the Epi-like cluster, including subpopulations of cells representing either a naïve- or primed-pluripotency character, indicating a progression in pluripotency states in the Epi-like compartment of RtL-embryoids. Downregulation of KLF4, and ESRRB, as well as upregulation of OTX2 and OCT6 during rosette to lumen progression was detected by IF staining, however RtL-embryoids displayed a delay in pluripotency progression, as we additionally detected a failure of downregulation of naïve-pluripotency marker NANOG. Supporting the presumed delay in pluripotency progression we were able to detect pERK pulses in single cells of the Epi-like compartment, that were absent in RtL-embryoids at rosette stage and only detectable at lumen stage. This is in contrast to the situation described during mouse embryogenesis, where pERK pulses can be detected first at rosette stage, which then increase in frequency at lumen stage (Neagu et al., 2020). Contributing to this, expression of primed pluripotency factors *Fox2a*, *Cer1* and *T* was not detectable in the dataset or by IF staining,

indicating, that RtL-embryoids initiate progression from naïve- to primed pluripotency, but fail to adopt a complete primed pluripotency state, possibly due to developmental roadblocks before *T* induction and subsequent EMT of Epi cells. Again, one possible explanation for this cease in pluripotency progression and failure to induce expression of *T*, could be seen in missing or weak signaling from the DVE/AVE-like population in a truly anterior position, that might be insufficient to induce a posterior epiblast identity, EMT and subsequent PS formation in the Epi-like compartment.

As PGC specification is first initiated prior to gastrulation at E6.25 (Ohinata et al., 2009), the expression of marker genes for this developmental hallmark was assessed among Epi-like cells, revealing a subpopulation of Epi-like cells, showing expression of PGC marker genes *Nanos3*, *Kit*, *Dppa3* (*Stella*) and *Tfap2c* (Mintz and Russel, 1957; Payer et al., 2003; Suzuki et al., 2008; Weber et al., 2010). The corresponding signaling molecules responsible for initiation of PGC specification, *Bmp4*, *Bmp8b* were detected to be highly expressed in ExE-like subcluster 1, while expression of *Bmp2* was restricted to the VE-like cluster, as expected in natural embryogenesis (Lawson et al., 1999; Ying et al., 2000; Ying and Zhao, 2001; Ohinata et al., 2009). Interestingly, Ohinata et al, have demonstrated that the competence of epiblast cells to commit to the germ cell fate is restricted between E5.5 and E6.5, correlating with the determined developmental stage represented by RtL-embryoids (Ohinata et al., 2009). However, as the comparison with scRNA-Seq datasets of natural mouse embryos did not show any Epi-like subpopulation overlapping in transcriptional profiles with the annotated natural PGCs, the PGC-like subpopulation in Epi-like cells could follow a different route of specification. It has previously been demonstrated that Epi-like cells can be directed towards a PGC-like cell fate in response to exposure to BMP and WNT signaling (Hayashi et al., 2011). Similarly, BMP and WNT signaling within the RtL-embryoid could force a subset of Epi-like cells towards adopting a PGC-like fate, functioning similar to the instructive signaling paradigms described during natural embryogenesis, but without fully committing to this cellular identity and failing to adopt a complete transcriptional program of PGCs.

5.6 The extraembryonic ectoderm-like compartment of RtL-embryoids

As described before, the ExE-like cluster was found to be composed of two transcriptionally diverging subpopulations, both of which displayed a general ExE-like transcriptional profile, however certain marker genes were detected to be highly restricted to either of the

subpopulations. As previously demonstrated when assessing DVE/AVE and PGC specification, the expression of *Bmp4* and *Bmp8b* was detected highly restricted to ExE-like subcluster 1. As this observation hinted towards a transcriptional architecture present at the ExE-Epi boundary in mouse embryos, we assessed the expression of FGF ligands and receptors among cells of the tissues comprising the RtL-embryoid. Mirroring natural embryogenesis, *Fgf4* expression was detected in cells of the Epi-like cluster, while expression of its receptor *Fgfr2* was found predominantly in cells of ExE-like subcluster 1. TSC marker genes downstream of FGFR2 like *Elf5*, *Eomes* and *Cdx2* were detected to be expressed in this subcluster as well, with *Elf5* expression being highly restricted to ExE-like subcluster 1. Supporting these observations, the comparison with the scRNA-Seq dataset from iTSCs generated in FGF4/ Heparin supplemented 2D monoculture revealed high resemblance with cells of ExE-like subcluster 1 in UMAP representation, cell cycle stages and expression of proliferation marker genes. Together, these results support our hypothesis that ExE-like subcluster 1 identifies as the stem cell niche within the ExE-like compartment, similar to the PrExE described at the Epi/ExE border in natural murine embryos. Supporting this observation, DEG genes specific for ExE-like subcluster 1 included *Gjb3*, *Gjb5*, *Phlda2*, *Utf1*, *Elf5*, *Hand1* and *Lad1*, all of which have been previously identified as progenitor trophoblast marker genes (Nelson et al., 2016). Additionally, GO term enrichment analysis performed individually using the differentially expressed genes of each of the ExE-like subclusters, revealed enrichment in 'placenta development' related gene sets for ExE-like subcluster 1. As ExE-like subcluster 1 could be identified as the stem cell niche within the ExE-like compartment, we hypothesized, that ExE-like subcluster 2 could represent a more differentiated section within the ExE-like compartment, as observed during natural embryogenesis, where the most distal part the ExE further differentiates, giving rise to the ectoplacental cone and ultimately the fetal part of the placenta. Contrary to results of GO term enrichment analysis performed on ExE-like subcluster 1, ExE-like subcluster 2 was detected to be enriched in less placenta-related gene sets, that were mainly involved in negative regulation of cellular differentiation. Interestingly, assessment of distribution of proliferation marker expression and cell cycle stages, again highlighted the bipartite character of the ExE-like cluster, with ExE-like subcluster 1 displaying typical characteristics of proliferating stem cells, while ExE-like subcluster 2 showed a more differentiated behavior and decreased capacity for self-renewal. Supporting the presumptive differentiating character of ExE-like subcluster 2, the expression of 'inhibitor of differentiation (*Id2*), a known regulator of placental differentiation was found to be expressed relatively homogenous among cell of ExE-like subcluster 1, while showing a decreasing, heterogenous character in gene expression levels in cells of ExE-like subcluster 2 (Selesniemi et al, 2016). As demonstrated by Selesniemi et al., ID2 mediates TGF-β-induced differentiation of labyrinthine trophoblast cells, as high expression levels of *Id2* prevents such a

differentiation, while decreased expression resulted in trophoblast differentiation (Selesniemi et al., 2016). However, while still showing a general trophoblast- / ExE- related transcriptional profile, indicated by close clustering in UMAP and expression of general ExE-related marker genes, the set of DEGs of ExE-like subcluster 2 could not be correlated with a specific, differentiated ExE-like cell fate. In addition to the transcriptional analysis, we also analyzed the observed bipartite character of the ExE-like compartment morphologically using IF staining against pERK, which has been demonstrated to exhibit a specific temporal and spatial signaling pattern during mouse embryogenesis (Corson et al., 2003). We were able to detect pERK signaling patterns similar to those found in the PrExE and DiExE of mouse embryos between E5.5 and E6.5, confirming the hypothesized bipartite character of the ExE-like compartment.

Considering that the DiExE and the EPC emerging from it would contribute to and build the maternal-fetal interface after implantation *in utero* it can be assumed, that specific maternal signaling cues are missing, as such an interface is not established in the *in vitro* cultured RtL-embryoid. Another key factor to consider regarding interpretation of scRNA-Seq data of the ExE-like cluster is the cell sorting strategy applied prior to sequencing. While expression GFP in Kermit ESCs and mCherry in VE-like cells remained constant throughout the protocol and allowed for identification of correctly assembled structures, ExE-like cells were identified and labelled by cell surface staining of CD40, providing a potentially less reliable method of identification compared to labelling by constitutive fluorescent marker expression. However, as Rugg-Gunn et al. have demonstrated, cell surface staining against CD40 can be used for identification and sorting of TS-cells from mouse embryos by flow cytometry (Rugg-Gunn et al., 2012). It has to be mentioned though, that CD40 was additionally identified as a cell surface marker of EpiSCs by Rugg-Gunn et al., however, they also demonstrated that flow cytometry using different marker combinations for cells of the different embryonic tissues can still result in reliably sorting of TS cells using staining against CD40 (Rugg-Gunn et al., 2012). In the approach used for analysis of the ExE-like compartment in this study, exclusion of GFP+ and mCherry+ cells combined with detection and sorting of CD40+ cells, similarly allowed for enrichment of a TS-like population by flow cytometry. Nevertheless, it has to be considered, that CD40+ ExE-like cells could downregulate CD40 expression upon differentiation, which would therefore have been excluded from sorting and subsequent analysis by scRNA-Seq. The sorting strategy applied in this study was chosen due to technical constraints, as enrichment of correctly assembled structures prior to cell sorting was performed using an inverted microscope that provided space for pipetting and handpicking, as well as a laser for detection of either GFP or mCherry with respective excitation wavelengths. For future analysis of the ExE-like compartment a more sophisticated method of

cell labelling for FACS should be performed, to allow for inclusion of all cells comprising the placental tissues, including differentiated, CD40 negative TSC daughter cell lineages.

5.7 Developmental potential of RtL-embryoids *in vivo*

As previously discussed, RtL-embryoids presented in this study can reflect specific hallmarks of natural murine embryogenesis between ~E4.5 – ~E6.0 and gene signature comparison confirmed similarity with these developmental stages. In natural mouse embryogenesis, implantation of the blastocyst into the uterus is initiated around E4.5 (Reviewed in Saiz et al., 2015). This process is mediated primarily by primary trophoblast giant cells, which differentiate from the mural TE, while the polar TE remains multipotent, giving rise to the ExE (Reviewed in Sutherland, 2003 and Hu & Cross, 2010). As the transcriptional profiles of the RtL-embryoid presented here resemble their natural equivalents between ~ E4.5 – E6.0, their potential for initiation of implantation and developmental progression *in vivo* was assessed. Therefore, correctly self-organized RtL-embryoids were transferred into the uterus of pseudopregnant foster mice, at 2.5 d.p.c. after mating with vasectomized males. RtL-embryoids were left to develop *in utero* for a total of 7 days, before sacrificing the foster mice, isolation of the uterus and analysis for possible implantation sites. Considering their transcriptional resemblance to natural murine embryos around E4.5, a developmental potential comparable to that of natural mouse embryogenesis would have resulted in implantation sites and concepti showing similarity to murine embryos around E11.5, with a fully developed placenta and the embryo located within the yolk sac. However, implantation efficiency was low (5.39 %), and the isolated concepti did not display signs of placental tissues or yolk sac formation. Instead, the isolated structures presented as elongated tissues, that, upon microsurgical dissection, displayed GFP-positive cells located in the center of a rim-like structure within the decidual reaction. As such, the isolated tissue still resembled implantations at E5.5 more closely, than the expected E11.5 developmental stage, indicative of a drastically decreased or even ceased developmental potential compared to their natural equivalent. As Kermit ESCs can be regarded the only source of GFP signals within the transferred structures and the foster mice, it can be assumed, that the isolated structures are indeed originating from the transferred RtL-embryoids.

Considering the importance of the TE for implantation in natural murine blastocysts, and the observation that descendants of 5 Factor ESCs assemble into an ExE-like compartment in RtL-embryoids it can be concluded, that implantation in the system presented here does not follow implantation paradigms of natural embryogenesis. In general, the model system presented here

can generate induced tissues that represent certain characteristics of Epi, VE and ExE, however, several embryonic tissues are not generated and lacking in this model, such as the Reichert's membrane, a basement membrane located between PE and primary TGCs, thereby building the outermost layer of the developing embryo. Together, post-implantation architecture with ExE-like instead of TE-like compartment, absence of TGC-, PE- and Reichert's membrane- layers, low efficiencies of implantation *in utero* and drastically limited developmental potential, suggest that RtL-embryoids are unable to implant *in utero* following natural implantation paradigms. It is long known that mechanical stimulation of the uterine surface in pseudopregnant rodents can induce artificial decidualization, leading to formation and proliferation of decidual tissue, called deciduomata (Krehbiel et al., 1937, Velardo et al., 1953). Therefore, it has to be considered, that the process of transferring RtL-embryoids into the uterus of pseudopregnant could have triggered an artificial decidualization, leading to formation of decidual tissue surrounding the transferred structures. Interestingly, the importance of BMP2 for uterine decidual response during implantation in mice has been demonstrated previously by Lee et al., who observed complete infertility in female mice carrying a uterine tissue-specific knockout of *Bmp2* (Lee et al., 2007). Additionally, Lee et al., were able to show that an administration of recombinant human BMP2 can partially rescue this defect, suggesting that acute BMP2 action is sufficient for uterine function (Lee et al., 2007). In RtL-embryoids presented in this study, *Bmp2* expression was detected in VE-like cells, which comprise the outermost layer of the transferred structures and are therefore in contact with the uterine surface. This could provide an environment further supporting a decidual reaction in addition to the mechanical stimulus during uterine transfer.

5.8 Evaluation of performance of the RtL-embryoid model

In summary, we were able to demonstrate that RtL-embryoids presented in this thesis can be used as a tool to recreate specific characteristics and hallmarks of natural embryogenesis in an *in vitro* environment. However, the system as presented here displayed a number of limitations. In RtL-embryoids specification of a DVE/AVE-like subpopulation of EmVE-like cells was observed, however this subpopulation displayed limited migratory potential, failing to establish an AP-axis within the Epi-like compartment. Similar, Epi-like cells were demonstrated to initiate the transition from naïve- to primed-pluripotency, however failing to adopt a state of completely primed pluripotency and do not progress to EMT and PS formation.

'Integrated stem cell-based embryo models' like ETX embryoids and 'synthetic integrated stem cell-based embryo models' like iETX reflect natural embryogenesis more closely, showing

increased developmental potential *in vitro* that progresses from AP-axis formation to EMT and PS formation (Sozen et al., 2018; Amadei et al., 2021). As previously discussed, Amadei et al. also demonstrated that reprogramming approaches in iETX embryoids resulted in increased similarity to natural murine embryos compared to ETX embryoids (Amadei et al., 2021). Similarly depending on reprogramming of ESCs to a VE-like structure and assembly of an Epi-like compartment from non-reprogrammed ESCs, the main difference between RtL-embryoids presented in this thesis and iETX embryoids lies in the origin of cells comprising the ExE-like compartment. In iETX embryoids the ExE-like tissue is comprised of blastocyst-derived TSCs, which can aggregate and self-organize with the likewise blastocyst-derived ESCs immediately upon co-culture in a 3D environment (Amadei et al., 2021). Additionally, reprogramming of ESCs towards an endoderm identity in iETX embryoids is initiated prior to co-culture with TSCs and ESCs, thereby likely priming the respective cell fate earlier, again allowing for fast self-assembly into embryo-like structures (Amadei et al., 2021). In RtL-embryoids, the conversion of cell fate lineages is achieved simultaneously and in co-culture, which in the case of ESC-iTSC reprogramming requires a total of 3 days of transgene expression. Therefore, the additional time needed for complete lineage conversion in a multifactorial reprogramming approach can be seen as a key limiting factor for the developmental potential. Further research is needed to identify factors that could decrease the time needed for complete ESC-iTSC cell fate conversion, in order to possibly enhance the developmental potential of RtL-embryoids generated by reprogramming in 3D co-culture.

In conclusion, the system presented here in this study can be regarded a first approximation towards a fully functional embryo model induced by reprogramming paradigms, that can recreate specific embryonic signaling environments, developmental hallmarks during embryogenesis and potentially allow for the isolation and study of rare stem cell lineages such as DVE/AVE- and PGC-like cells.

6. Outlook

The protocol presented here offers a general proof-of-principle assay for the generation of embryo-like organoids by reprogramming of ESCs, however, the effect of different culture media compositions on efficiency and developmental potential of RtL-embryoids was not analyzed. As Amadei et al. demonstrated, medium supplementation with sex hormones progesterone and β-estradiol are beneficial to support an increased developmental potential of iETX embryoids *in vitro* (Amadei et al., 2021). Additionally, Aguilera-Castrejon et al. recently presented improved culture conditions that can support embryogenesis from pre-gastrulation to late organogenesis *ex utero* (Aguilera-Castrejon et al., 2021). Therefore, different culture media compositions should be tested for the generation of RtL-embryoids, to potentially enhance their developmental potential *in vitro*.

The comparison of reprogramming outcomes of induced stem cell fates in 2D monoculture and 3D co-culture revealed differences in the transcriptional profiles and should be completed with additional epigenetic analysis. A comparison of the methylation patterns could be used to characterize reprogramming outcomes in more detail and would reveal as to how far and efficiently epigenetic lineage barriers have been overcome during lineage conversion. The RtL-embryoid model provides a tool to generate induced stem cell lineages, that are derived in signaling environments similar to those present during natural embryonic development. Therefore, the RtL-embryoid could potentially provide a source of stem cells that are more similar to their natural equivalents, compared to induced stem cells obtained from traditional 2D monoculture reprogramming. Chromatin ImmunoPrecipitation and subsequent DNA-Sequencing (ChIP-Seq) could be performed at different timepoints during the protocol presented here to identify pioneer factors and their DNA binding targets during cellular reprogramming in 3D co-culture. This could potentially allow for the identification of previously undescribed transcription factor interactions and might therefore enhance reprogramming efficiencies and/or the quality of the induced cell fates.

Ultimately, the question if such an inducible embryo-model can be generated from naïve human ESC, iPSCs or human fibroblasts should be, and has been addressed recently (Yu et al., 2021 and Liu et al., 2021). Such human embryo models would enhance our understanding and knowledge of early human embryogenesis and diseases involved in specific developmental processes. Application of a cellular reprogramming approach allows for the generation of such organoid model system without the need for human embryo-derived stem cells.

7. Bibliography

Aguilera-Castrejon, A., Oldak, B., Shani, T., Ghanem, N., Itzkovich, C., Slomovich, S., Tarazi, S., Bayerl, J., Chugaeva, V., Ayyash, M., Ashouokhi, S., Sheban, D., Livnat, N., Lasman, L., Viukov, S., Zerbib, M., Addadi, Y., Rais, Y., Cheng, S., Stelzer, Y., Keren-Shaul, H., Shlomo, R., Massarwa, R., Novershtern, N., Maza, I. & Hanna, J.H. (2021) Ex utero mouse embryogenesis from pre-gastrulation to late organogenesis. Nature. doi: 10.1038/s41586-021-03416-3. Advance online publication. PMID: 33731940.

Amadei, G., Lau, K., De Jonghe, J., Gantner, C. W., Sozen, B., Chan, C., Zhu, M., Kyprianou, C., Hollfelder, F., & Zernicka-Goetz, M. (2021). Inducible Stem-Cell-Derived Embryos Capture Mouse Morphogenetic Events In Vitro. Developmental cell, 56(3), 366–382.e9.

Arnold, S. J., Hofmann, U. K., Bikoff, E. K., & Robertson, E. J. (2008). Pivotal roles for eomesodermin during axis formation, epithelium-to-mesenchyme transition, and endoderm specification in the mouse. Development, 135(3), 501–511.

Assémat, E., Vinot, S., Gofflot, F., Linsel-Nitschke, P., Illien, F., Châtelet, F., Verroust, P., Louvet-Vallée, S., Rinninger, F., & Kozyraki, R. (2005). Expression and role of cubilin in the internalization of nutrients during the peri-implantation development of the rodent embryo. Biology of reproduction, 72(5), 1079–1086.

Bardot, E. S., & Hadjantonakis, A. K. (2020). Mouse gastrulation: Coordination of tissue patterning, specification, and diversification of cell fate. Mechanisms of development, 163, 103617.

Beccari, L., Moris, N., Girgin, M., Turner, D. A., Baillie-Johnson, P., Cossy, A. C., Lutolf, M. P., Duboule, D., & Arias, A. M. (2018). Multi-axial self-organization properties of mouse embryonic stem cells into gastruloids. Nature, 562(7726), 272–276.

Beck, F., Erler, T., Russell, A., & James, R. (1995). Expression of Cdx-2 in the mouse embryo and placenta: possible role in patterning of the extra-embryonic membranes. Developmental dynamics: an official publication of the American Association of Anatomists, 204(3), 219–227.

Beck, S., Le Good, J. A., Guzman, M., Ben Haim, N., Roy, K., Beermann, F., & Constam, D. B. (2002). Extraembryonic proteases regulate Nodal signaling during gastrulation. Nature cell biology, 4(12), 981–985.

Bedzhov, I., & Zernicka-Goetz, M. (2014). Self-organizing properties of mouse pluripotent cells initiate morphogenesis upon implantation. Cell, 156(5), 1032–1044.

Ben-Haim, N., Lu, C., Guzman-Ayala, M., Pescatore, L., Mesnard, D., Bischofberger, M., Naef, F., Robertson, E. J., & Constam, D. B. (2006). The nodal precursor acting via activin receptors induces mesoderm by maintaining a source of its convertases and BMP4. Developmental cell, 11(3), 313–323.

Bessonnard, S., De Mot, L., Gonze, D., Barriol, M., Dennis, C., Goldbeter, A., Dupont, G., & Chazaud, C. (2014). Gata6, Nanog and Erk signaling control cell fate in the inner cell mass through a tristable regulatory network. Development (Cambridge, England), 141(19), 3637-3648

Bielinska, M., Narita, N., & Wilson, D. B. (1999). Distinct roles for visceral endoderm during embryonic mouse development. The International journal of developmental biology, 43(3), 183–205.

Boroviak, T., Loos, R., Bertone, P., Smith, A., & Nichols, J. (2014). The ability of inner-cell-mass cells to self-renew as embryonic stem cells is acquired following epiblast specification. Nature cell biology, 16(6), 516–528.

Branford, W. W., & Yost, H. J. (2002). Lefty-dependent inhibition of Nodal- and Wnt-responsive organizer gene expression is essential for normal gastrulation. Current biology: CB, 12(24), 2136–2141.

Brennan, J., Lu, C. C., Norris, D. P., Rodriguez, T. A., Beddington, R. S., & Robertson, E. J. (2001). Nodal signaling in the epiblast patterns the early mouse embryo. Nature, 411(6840), 965–969.

Browaeys, R., Saelens, W., & Saeys, Y. (2020). NicheNet: modeling intercellular communication by linking ligands to target genes. Nat Methods. 17, 159-162.

Brown, K., Legros, S., Artus, J., Doss, M. X., Khanin, R., Hadjantonakis, A. K., & Foley, A. (2010). A comparative analysis of extra-embryonic endoderm cell lines. PloS one, 5(8), e12016.

Buhl, S., Egert, A., Schorle, H., & Woynecki, T. (2009). Induced blastocyst-like structures, methods of reproduction and uses of the same (European Union Patent No. EP2088191A1). https://patents.google.com/patent/EP2088191A1/en?q=induced&q=blastocyst&q=mouse&oq=induced+blastocyst+mouse

Cano, A., Pérez-Moreno, M. A., Rodrigo, I., Locascio, A., Blanco, M. J., del Barrio, M. G., Portillo, F., & Nieto, M. A. (2000). The transcription factor snail controls epithelial-mesenchymal transitions by repressing E-cadherin expression. Nature cell biology, 2(2), 76–83.

Chávez, D. J., Enders, A. C., & Schlafke, S. (1984). Trophectoderm cell subpopulations in the periimplantation mouse blastocyst. The Journal of experimental zoology, 231(2), 267–271.

Chazaud, C., Yamanaka, Y., Pawson, T., & Rossant, J. (2006). Early lineage segregation between epiblast and primitive endoderm in mouse blastocysts through the Grb2-MAPK pathway. Developmental cell, 10(5), 615–624.

Chen, G., Schell, J. P., Benitez, J. A., Petropoulos, S., Yilmaz, M., Reinius, B., Alekseenko, Z., Shi, L., Hedlund, E., Lanner, F., Sandberg, R., & Deng, Q (2016). Single-cell analyses of X Chromosome inactivation dynamics and pluripotency during differentiation. Genome Research. 26, 1342–1354.

Cheng, S., Pei, Y., He, L., Peng, G., Reinius, B., Tam, P., Jing, N., & Deng, Q. (2019). Single-Cell RNA-Seq Reveals Cellular Heterogeneity of Pluripotency Transition and X Chromosome Dynamics during Early Mouse Development. Cell reports, 26(10), 2593–2607.e3.

Christodoulou, N., Kyprianou, C., Weberling, A., Wang, R., Cui, G., Peng, G., Jing, N., & Zernicka-Goetz, M. (2018). Sequential formation and resolution of multiple rosettes drive embryo remodelling after implantation. Nature cell biology, 20(11), 1278–1289.

Christodoulou, N., Weberling, A., Strathdee, D., Anderson, K. I., Timpson, P., & Zernicka-Goetz, M. (2019). Morphogenesis of extra-embryonic tissues directs the remodelling of the mouse embryo at implantation. Nature communications, 10(1), 3557.

Ciruna, B. G., Schwartz, L., Harpal, K., Yamaguchi, T. P., & Rossant, J. (1997). Chimeric analysis of fibroblast growth factor receptor-1 (Fgfr1) function: a role for FGFR1 in morphogenetic movement through the primitive streak. Development (Cambridge, England), 124(14), 2829–2841.

Ciruna, B., & Rossant, J. (2001). FGF signaling regulates mesoderm cell fate specification and morphogenetic movement at the primitive streak. Developmental cell, 1(1), 37–49.

Corson, L.B., Yamanaka, Y., Lai, K.M. & Rossant, J. (2003). Spatial and temporal patterns of ERK signaling during mouse embryogenesis. Development, 130, 4527 – 4537.

Costello, I., Pimeisl, I. M., Dräger, S., Bikoff, E. K., Robertson, E. J., & Arnold, S. J. (2011). The T-box transcription factor Eomesodermin acts upstream of Mesp1 to specify cardiac mesoderm during mouse gastrulation. Nature cell biology, 13(9), 1084–1091.

Copp A. J. (1979). Interaction between inner cell mass and trophectoderm of the mouse blastocyst. II. The fate of the polar trophectoderm. Journal of embryology and experimental morphology, 51, 109–120.

Cross, J. C., Werb, Z., & Fisher, S. J. (1994). Implantation and the placenta: key pieces of the development puzzle. Science (New York, N.Y.), 266(5190), 1508–1518.

Donnison, M., Broadhurst, R., & Pfeffer, P. L. (2015). Elf5 and Ets2 maintain the mouse extraembryonic ectoderm in a dosage dependent synergistic manner. Developmental biology, 397(1), 77–88.

Downs, K. M., Hellman, E. R., McHugh, J., Barrickman, K., & Inman, K. E. (2004). Investigation into a role for the primitive streak in development of the murine allantois. Development (Cambridge, England), 131(1), 37–55.

Evans, M.J., and Kaufman, M.H. (1981). Establishment in culture of pluripotential cells from mouse embryos. Nature 292, 154-156.

Finley, K. R., Tennessen, J., & Shawlot, W. (2003). The mouse secreted frizzled-related protein 5 gene is expressed in the anterior visceral endoderm and foregut endoderm during early post-implantation development. Gene expression patterns, 3(5), 681–684.

Fiorenzano, A., Pascale, E., D'Aniello, C., Acampora, D., Bassalert, C., Russo, F., Andolfi, G., Biffoni, M., Francescangeli, F., Zeuner, A., Angelini, C., Chazaud, C., Patriarca, E. J., Fico, A., & Minchiotti, G. (2016). Cripto is essential to capture mouse epiblast stem cell and human embryonic stem cell pluripotency. Nature communications, 7, 12589.

Gao, H., Gao, R., Zhang, L., Xiu, W., Zang, R., Wang, H., Zhang, Y., Chen, J., Gao, Y., & Gao, S. (2019). Esrrb plays important roles in maintaining self-renewal of trophoblast stem cells (TSCs) and reprogramming somatic cells to induced TSCs. Journal of molecular cell biology, 11(6), 463–473.

Guzman-Ayala, M., Ben-Haim, N., Beck, S., & Constam, D. B. (2004). Nodal protein processing and fibroblast growth factor 4 synergize to maintain a trophoblast stem cell microenvironment. Proceedings of the National Academy of Sciences of the United States of America, 101(44), 15656–15660.

Hayashi, K., Ohta, H., Kurimoto, K., Aramaki, S. & Saitou, M. (2011). Reconstitution of the mouse germ cell specification pathway in culture by pluripotent stem cells. Cell, 146(4), 519–532

Hoffman, J.A., Wu, C.I., & Merrill, B.J. (2013). Tcf7l1 prepares epiblast cells in gastrulating mouse embryos for lineage specification. Development (Cambridge, England), 140(8) 1665-1675.

Hoshino, H., Shioi, G., & Aizawa, S. (2015). AVE protein expression and visceral endoderm cell behavior during anterior-posterior axis formation in mouse embryos: Asymmetry in OTX2 and DKK1 expression. Developmental biology, 402(2), 175–191.

Hu, D., & Cross, J. C. (2010). Development and function of trophoblast giant cells in the rodent placenta. The International journal of developmental biology, 54(2-3), 341–354.

Huang, D., Guo, G., Yuan, P., Ralston, A., Sun, L., Huss, M., Mistri, T., Pinello, L., Ng, H. H., Yuan, G., Ji, J., Rossant, J., Robson, P., & Han, X. (2017). The role of Cdx2 as a lineage specific transcriptional repressor for pluripotent network during the first developmental cell lineage segregation. Scientific reports, 7(1), 17156.

Huelsken, J., Vogel, R., Brinkmann, V., Erdmann, B., Birchmeier, C., & Birchmeier, W. (2000). Requirement for beta-catenin in anterior-posterior axis formation in mice. The Journal of cell biology, 148(3), 567–578.

Hyun, I., Munsie, M., Pera, M. F., Rivron, N. C., & Rossant, J. (2020). Toward Guidelines for Research on Human Embryo Models Formed from Stem Cells. Stem cell reports, 14(2), 169–174.

Kaiser, F., Kubaczka, C., Graf, M., Langer, N., Langkabel, J., Arévalo, L., & Schorle, H. (2020). Choice of factors and medium impinge on success of ESC to TSC conversion. Placenta, 90, 128–137.

Kemp, C., Willems, E., Abdo, S., Lambiv, L., & Leyns, L. (2005). Expression of all Wnt genes and their secreted antagonists during mouse blastocyst and postimplantation development. Developmental dynamics: an official publication of the American Association of Anatomists, 233(3), 1064–1075.

Keramari, M., Razavi, J., Ingman, K. A., Patsch, C., Edenhofer, F., Ward, C. M., & Kimber, S. J. (2010). Sox2 is essential for formation of trophectoderm in the preimplantation embryo. PloS one, 5(11), e13952.

Kim, D. K., Cha, Y., Ahn, H. J., Kim, G., & Park, K. S. (2014). Lefty1 and lefty2 control the balance between self-renewal and pluripotent differentiation of mouse embryonic stem cells. Stem cells and development, 23(5), 457–466.

Kimura-Yoshida, C., Nakano, H., Okamura, D., Nakao, K., Yonemura, S., Belo, J.A., Aizawa, S., Matsui, Y., and Matsuo, I. (2005). Canonical Wnt signaling and its antagonist regulate anterior-posterior axis polarization by guiding cell migration in mouse visceral endoderm. Dev. Cell 9, 639-650.

Kinder, S. J., Tsang, T. E., Quinlan, G. A., Hadjantonakis, A. K., Nagy, A., & Tam, P. P. (1999). The orderly allocation of mesodermal cells to the extraembryonic structures and the anteroposterior axis during gastrulation of the mouse embryo. Development (Cambridge, England), 126(21), 4691–4701.

Knox, K., Leuenberger, D., Penn, A. A., & Baker, J. C. (2011). Global hormone profiling of murine placenta reveals Secretin expression. Placenta, 32(11), 811–816.

Krehbiel, R.H. (1937). Cytological studies of the decidual reaction in the rat during early pregnancy and in the production of deciduomata. Physiological Zoology 10(2),212–233

Kubaczka, C., Senner, C., Araúzo-Bravo, M. J., Sharma, N., Kuckenberg, P., Becker, A., Zimmer, A., Brüstle, O., Peitz, M., Hemberger, M., & Schorle, H. (2014). Derivation and maintenance of murine trophoblast stem cells under defined conditions. Stem cell reports, 2(2), 232–242.

Kubaczka, C., Senner, C. E., Cierlitza, M., Araúzo-Bravo, M. J., Kuckenberg, P., Peitz, M., Hemberger, M., & Schorle, H. (2015). Direct Induction of Trophoblast Stem Cells from Murine Fibroblasts. Cell stem cell, 17(5), 557–568.

Kumar, A., Lualdi, M., Lyozin, G. T., Sharma, P., Loncarek, J., Fu, X. Y., & Kuehn, M. R. (2015). Nodal signaling from the visceral endoderm is required to maintain Nodal gene expression in the epiblast and drive DVE/AVE migration. Developmental biology, 400(1), 1–9.

Kunath, T., Arnaud, D., Uy, G. D., Okamoto, I., Chureau, C., Yamanaka, Y., Heard, E., Gardner, R. L., Avner, P., & Rossant, J. (2005). Imprinted X-inactivation in extra-embryonic endoderm cell lines from mouse blastocysts. Development, 132(7), 1649–1661.

Kwon, G. S., Viotti, M., & Hadjantonakis, A. K. (2008). The endoderm of the mouse embryo arises by dynamic widespread intercalation of embryonic and extraembryonic lineages. Developmental cell, 15(4), 509–520.

Lancaster, M. A., Renner, M., Martin, C. A., Wenzel, D., Bicknell, L. S., Hurles, M. E., Homfray, T., Penninger, J. M., Jackson, A. P., & Knoblich, J. A. (2013). Cerebral organoids model human brain development and microcephaly. Nature, 501(7467), 373–379.

Langkabel, J., Horne, A., Bonaguro, L., Hesse, T., Knaus, A., Riedel, Y., Händler, K., Bassler, K., Reusch, N., Yeghiazarian, L. H., Pecht, T., Aschenbrenner, A.C., Kaiser, F., Kubaczka, C., Schultze, J.L. & Schorle, H. (2021). Induction of peri-implantation stage synthetic embryos using reprogramming paradigms in ESCs. BioRxiv 2021.01.25.428068

Lawson, K. A., Dunn, N. R., Roelen, B. A., Zeinstra, L. M., Davis, A. M., Wright, C. V., Korving, J. P., & Hogan, B. L. (1999). Bmp4 is required for the generation of primordial germ cells in the mouse embryo. Genes & development, 13(4), 424–436.

Lee, K. Y., Jeong, J. W., Wang, J., Ma, L., Martin, J. F., Tsai, S. Y., Lydon, J. P., & DeMayo, F. J. (2007). Bmp2 is critical for the murine uterine decidual response. Molecular and cellular biology, 27(15), 5468–5478.

Lim, C. Y., Tam, W. L., Zhang, J., Ang, H. S., Jia, H., Lipovich, L., Ng, H. H., Wei, C. L., Sung, W. K., Robson, P., Yang, H., & Lim, B. (2008). Sall4 regulates distinct transcriptional circuitries in different blastocyst-derived stem cell lineages. Cell stem cell, 3(5), 543-554

Lin, J., Khan, M., Zapiec, B., & Mombaerts, P. (2016). Efficient derivation of extraembryonic endoderm stem cell lines from mouse postimplantation embryos. Sci Rep. 6, 39457.

Liu, X., Tan, J. P., Schröder, J., Aberkane, A., Ouyang, J. F., Mohenska, M., Lim, S. M., Sun, Y., Chen, J., Sun, G., Zhou, Y., Poppe, D., Lister, R., Clark, A. T., Rackham, O., Zenker, J., & Polo, J. M. (2021). Modelling human blastocysts by reprogramming fibroblasts into iBlastoids. Nature, 10.1038/s41586-021-03372-y. Advance online publication.

Malleshaiah, M., Padi, M., Rué, P., Quackenbush, J., Martinez-Arias, A., & Gunawardena, J., (2016). Nac1 Coordinates a Sub-network of Pluripotency Factors to Regulate Embryonic Stem Cell Differentiation. Cell reports, 14(5), 1181-1194.

Mao, B., Wu, W., Davidson, G., Marhold, J., Li, M., Mechler, B.M., Delius, H., Hoppe, D., Stannek, P., Walter, C., Glinka, A. & Niehrs, C. (2002). Kremen proteins are Dickkopf receptors that regulate Wnt/beta-catenin signaling. Nature, 417, 664-667.

Maurer, M. E., & Cooper, J. A. (2005). Endocytosis of megalin by visceral endoderm cells requires the Dab2 adaptor protein. Journal of cell science, 118(Pt 22), 5345–5355.

McCracken, K. W., Catá, E. M., Crawford, C. M., Sinagoga, K. L., Schumacher, M., Rockich, B. E., Tsai, Y. H., Mayhew, C. N., Spence, J. R., Zavros, Y., & Wells, J. M. (2014). Modelling human development and disease in pluripotent stem-cell-derived gastric organoids. Nature, 516(7531), 400–404.

Meno, C., Gritsman, K., Ohishi, S., Ohfuji, Y., Heckscher, E., Mochida, K., Shimono, A., Kondoh, H., Talbot, W. S., Robertson, E. J., Schier, A. F., & Hamada, H. (1999). Mouse Lefty2 and zebrafish antivin are feedback inhibitors of nodal signaling during vertebrate gastrulation. Molecular cell, 4(3), 287–298.

Mintz, B., and Russel, E.S. (1957). Gene-induced embryological modifications of primordial germ cells in the mouse. The Journal of experimental zoology, 134(2), 207–237.

Mohammed, H., Hernando-Herraez, I., Savino, A., Scialdone, A., Macaulay, I., Mulas, C., Chandra, T., Voet, T., Dean, W., Nichols, J., Marioni, J. C., & Reik, W. (2017). Single-Cell Landscape of Transcriptional Heterogeneity and Cell Fate Decisions during Mouse Early Gastrulation. Cell reports, 20(5), 1215–1228.

Morgani, S. M., Metzger, J. J., Nichols, J., Siggia, E. D., & Hadjantonakis, A. K. (2018). Micropattern differentiation of mouse pluripotent stem cells recapitulates embryo regionalized cell fate patterning. eLife, 7, e32839.

Mukhopadhyay, M., Shtrom, S., Rodriguez-Esteban, C., Chen, L., Tsukui, T., Gomer, L., Dorward, D. W., Glinka, A., Grinberg, A., Huang, S. P., Niehrs, C., Izpisúa Belmonte, J. C., & Westphal, H. (2001). Dickkopf1 is required for embryonic head induction and limb morphogenesis in the mouse. Developmental cell, 1(3), 423–434.

Neagu, A., van Genderen, E., Escudero, I., Verwegen, L., Kurek, D., Lehmann, J., Stel, J., Dirks, R., van Mierlo, G., Maas, A., Eleveld, C., Ge, Y., den Dekker, A. T., Brouwer, R., van IJcken, W., Modic, M., Drukker, M., Jansen, J. H., Rivron, N. C., Baart, E. B., Marks, H. & Ten Berge, D. (2020). In vitro capture and characterization of embryonic rosette-stage pluripotency between naive and primed states. Nature Cell Biology, 22, 534–545.

Nelson, A. C., Mould, A. W., Bikoff, E. K., & Robertson, E. J. (2016). Single-cell RNA-seq reveals cell type-specific transcriptional signatures at the maternal-fetal interface during pregnancy. Nature communications, 7, 11414.

Nestorowa, S., Hamey, F. K., Pijuan Sala, B., Diamanti, E., Shepherd, M., Laurenti, E., Wilson, N. K., Kent, D. G., & Göttgens, B. (2016). A single-cell resolution map of mouse hematopoietic stem and progenitor cell differentiation. Blood, 128(8), e20–e31.

Ngondo, R. P., Cirera-Salinas, D., Yu, J., Wischnewski, H., Bodak, M., Vandormael-Pournin, S., Geiselmann, A., Wettstein, R., Luitz, J., Cohen-Tannoudji, M., & Ciaudo, C. (2018). Argonaute 2 Is Required for Extra-embryonic Endoderm Differentiation of Mouse Embryonic Stem Cells. Stem cell reports, 10(2), 461–476.

Niakan, K. K., Schrode, N., Cho, L. T., & Hadjantonakis, A. K. (2013). Derivation of extraembryonic endoderm stem (XEN) cells from mouse embryos and embryonic stem cells. Nature protocols, 8(6), 1028–1041.

Nichols, J., Zevnik, B., Anastassiadis, K., Niwa, H., Klewe-Nebenius, D., Chambers, I., Schöler, H., & Smith, A. (1998). Formation of pluripotent stem cells in the mammalian embryo depends on the POU transcription factor Oct4. Cell, 95(3), 379–391.

Niwa, H., Burdon, T., Chambers, I., & Smith, A. (1998). Self-renewal of pluripotent embryonic stem cells is mediated via activation of STAT3. Genes & development, 12(13), 2048–2060.

Nowotschin, S., Costello, I., Piliszek, A., Kwon, G.S., Mao, C.A., Klein, W.H., Robertson, E.J. & Hadjantonakis, A.K. (2013). The T-box transcription factor Eomesodermin is essential for AVE induction in the mouse embryo. Genes & development. 27, 997-1002.

Ohinata, Y., Ohta, H., Shigeta, M., Yamanaka, K., Wakayama, T., & Saitou, M. (2009). A signaling principle for the specification of the germ cell lineage in mice. Cell, 137(3), 571–584.

Paca, A., Séguin, C. A., Clements, M., Ryczko, M., Rossant, J., Rodriguez, T. A., & Kunath, T. (2012). BMP signaling induces visceral endoderm differentiation of XEN cells and parietal endoderm. Developmental biology, 361(1), 90–102.

Payer, B., Saitou, M., Barton, S. C., Thresher, R., Dixon, J. P., Zahn, D., Colledge, W. H., Carlton, M. B., Nakano, T., & Surani, M. A. (2003). Stella is a maternal effect gene required for normal early development in mice. Current biology: CB, 13(23), 2110–2117.

Peitz, M., Jäger, R., Patsch, C., Jäger, A., Egert, A., Schorle, H., & Edenhofer, F. (2007). Enhanced purification of cell-permeant Cre and germline transmission after transduction into mouse embryonic stem cells. Genesis, 45, 508–517.

Perea-Gomez, A., Lawson, K. A., Rhinn, M., Zakin, L., Brûlet, P., Mazan, S., & Ang, S. L. (2001) Otx2 is required for visceral endoderm movement and for the restriction of posterior signals in the epiblast of the mouse embryo. Development. 128, 753–765

Perea-Gomez, A., Vella, F. D., Shawlot, W., Oulad-Abdelghani, M., Chazaud, C., Meno, C., Pfister, V., Chen, L., Robertson, E., Hamada, H., Behringer, R. R., & Ang, S. L. (2002). Nodal antagonists in the anterior visceral endoderm prevent the formation of multiple primitive streaks. Developmental cell, 3(5), 745–756.

Perea-Gomez, A., Cases, O., Lelièvre, V., Pulina, M. V., Collignon, J., Hadjantonakis, A. K., & Kozyraki, R. (2019). Loss of Cubilin, the intrinsic factor-vitamin B12 receptor, impairs visceral endoderm endocytosis and endodermal patterning in the mouse. Scientific reports, 9(1), 10168.

Pijuan-Sala, B., Griffiths, J. A., Guibentif, C., Hiscock, T. W., Jawaid, W., Calero-Nieto, F. J., Mulas, C., Ibarra-Soria, X., Tyser, R., Ho, D., Reik, W., Srinivas, S., Simons, B. D., Nichols, J., Marioni, J. C., & Göttgens, B (2019). A single-cell molecular map of mouse gastrulation and early organogenesis. Nature. 566, 490–495.

Posfai, E., Petropoulos, S., de Barros, F., Schell, J. P., Jurisica, I., Sandberg, R., Lanner, F., & Rossant, J. Position- and Hippo signaling-dependent plasticity during lineage segregation in the early mouse embryo (2017). Elife. 6, e22906.

Posfai, E., Schell, J. P., Janiszewski, A., Rovic, I., Murray, A., Bradshaw, B., Yamakawa, T., Pardon, T., El Bakkali, M., Talon, I., De Geest, N., Kumar, P., To, S. K., Petropoulos, S., Jurisicova, A., Pasque, V., Lanner, F., & Rossant, J (2021). Evaluating totipotency using criteria of increasing stringency. Nature Cell Biology. 23, 49–60

Richardson, L., Venkataraman, S., Stevenson, P., Yang, Y., Moss, J., Graham, L., Burton, N., Hill, B., Rao, J., Baldock, R. A., & Armit, C. (2014). EMAGE mouse embryo spatial gene expression database: 2014 update. Nucleic acids research, 42(Database issue), D835–D844.

Rivera-Pérez, J. A., & Magnuson, T. (2005). Primitive streak formation in mice is preceded by localized activation of Brachyury and Wnt3. Developmental biology, 288(2), 363–371.

Rivera-Pérez, J. A., & Hadjantonakis, A. K. (2014). The Dynamics of Morphogenesis in the Early Mouse Embryo. Cold Spring Harbor perspectives in biology, 7(11), a015867.

Rivron, N. C., Frias-Aldeguer, J., Vrij, E. J., Boisset, J. C., Korving, J., Vivié, J., Truckenmüller, R. K., van Oudenaarden, A., van Blitterswijk, C. A., & Geijsen, N. (2018a). Blastocyst-like structures generated solely from stem cells. Nature, 557(7703), 106–111.

Rivron, N., Pera, M., Rossant, J., Martinez Arias, A., Zernicka-Goetz, M., Fu, J., van den Brink, S., Bredenoord, A., Dondorp, W., de Wert, G., Hyun, I., Munsie, M., & Isasi, R. (2018b). Debate ethics of embryo models from stem cells. Nature, 564(7735), 183–185.

Rossant, J., & Tam, P.P. (2009). Blastocyst lineage formation, early embryonic asymmetries and axis patterning in the mouse. Development (Cambridge, England), 136(5), 701-713.

Rossant, J., & Tam, P. (2021). Opportunities and Challenges with Stem Cell-Based Embryo Models. Stem cell reports, S2213-6711(21)00082-5. Advance online publication.

Rossi, G., Manfrin, A., & Lutolf, M. P. (2018). Progress and potential in organoid research. Nature reviews. Genetics, 19(11), 671–687.

Rugg-Gunn, P. J., Cox, B. J., Lanner, F., Sharma, P., Ignatchenko, V., McDonald, A. C., Garner, J., Gramolini, A. O., Rossant, J., & Kislinger, T. (2012). Cell-surface proteomics identifies lineage-specific markers of embryo-derived stem cells. Developmental cell, 22(4), 887–901.

Sahu, S., & Sharan, S. K. (2020). Translating Embryogenesis to Generate Organoids: Novel Approaches to Personalized Medicine. iScience, 23(9), 101485.

Saitou, M., Barton, S. C., & Surani, M. A. (2002). A molecular programme for the specification of germ cell fate in mice. Nature, 418(6895), 293–300.

Saitou, M., & Yamaji, M. (2012). Primordial germ cells in mice. Cold Spring Harbor perspectives in biology, 4(11), a008375.

Saiz, N., Plusa, B., & Hadjantonakis, A. K. (2015). Single cells get together: High-resolution approaches to study the dynamics of early mouse development. Seminars in cell & developmental biology, 47-48, 92–100.

Sasai Y. (2013). Next-generation regenerative medicine: organogenesis from stem cells in 3D culture. Cell stem cell, 12(5), 520–530.

Sato, M., Kimura, T., Kurokawa, K., Fujita, Y., Abe, K., Masuhara, M., Yasunaga, T., Ryo, A., Yamamoto, M., & Nakano, T. (2002). Identification of PGC7, a new gene expressed specifically in preimplantation embryos and germ cells. Mechanisms of development, 113(1), 91–94.

Sato, T., Vries, R. G., Snippert, H. J., van de Wetering, M., Barker, N., Stange, D. E., van Es, J. H., Abo, A., Kujala, P., Peters, P. J., & Clevers, H. (2009). Single Lgr5 stem cells build crypt-villus structures in vitro without a mesenchymal niche. Nature, 459(7244), 262–265

Satoh, W., Gotoh, T., Tsunematsu, Y., Aizawa, S., & Shimono, A. (2006). Sfrp1 and Sfrp2 regulate anteroposterior axis elongation and somite segmentation during mouse embryogenesis. Development (Cambridge, England), 133(6), 989–999.

Schröter, C., Rué, P., Mackenzie, J.P., & Martinez Arias, A. (2015). FGF/MAPK signaling sets the switching threshold of a bistable circuit controlling cell fate decisions in embryonic stem cells. Development (Cambridge, England), 142(24), 4205-4216

Schwarz, B. A., Cetinbas, M., Clement, K., Walsh, R. M., Cheloufi, S., Gu, H., Langkabel, J., Kamiya, A., Schorle, H., Meissner, A., Sadreyev, R. I., & Hochedlinger, K. (2018). Prospective Isolation of Poised iPSC Intermediates Reveals Principles of Cellular Reprogramming. Cell stem cell, 23(2), 289–305.e5.

Selesniemi, K., Albers, R.E. & Brown, T.L. (2016). Id2 mediates differentiation of labyrinthine placental progenitor cell line, SM10. Stem Cell Dev. 25(13):959-74

Simian, M., Hirai, Y., Navre, M., Werb, Z., Lochter, A., & Bissell, M. J. (2001). The interplay of matrix metalloproteinases, morphogens and growth factors is necessary for branching of mammary epithelial cells. Development (Cambridge, England), 128(16), 3117–3131.

Silva, J., Barrandon, O., Nichols, J., Kawaguchi, J., Theunissen, T. W., & Smith, A. (2008). Promotion of reprogramming to ground state pluripotency by signal inhibition. PLoS biology, 6(10), e253.

Smith, A.G. (1991). Culture and differentiation of embryonic stem cells. Journal of Tissue Culture Methods 13, 89-94.

Soudais, C., Bielinska, M., Heikinheimo, M., MacArthur, C.A., Narita, N., Saffitz, J.E., Simon, M.C., Leiden, J.M., & Wilson, D.B. (1995). Targeted mutagenesis of the transcription factor GATA-4 gene in mouse embryonic stem cells disrupts visceral endoderm differentiation in vitro. Development (Cambridge, England), 121(11), 3877-3888

Sozen, B., Amadei, G., Cox, A., Wang, R., Na, E., Czukiewska, S., Chappell, L., Voet, T., Michel, G., Jing, N., Glover, D. M., & Zernicka-Goetz, M. (2018). Self-assembly of embryonic and two extra-embryonic stem cell types into gastrulating embryo-like structures. Nature cell biology, 20(8), 979–989.

Sozen, B., Cox, A. L., De Jonghe, J., Bao, M., Hollfelder, F., Glover, D. M., & Zernicka-Goetz, M. (2019). Self-Organization of Mouse Stem Cells into an Extended Potential Blastoid. Developmental cell, 51(6), 698–712.e8.

Sutherland A. (2003). Mechanisms of implantation in the mouse: differentiation and functional importance of trophoblast giant cell behavior. Developmental biology, 258(2), 241–251

Suzuki, H., Tsuda, M., Kiso, M., & Saga, Y. (2008). Nanos3 maintains the germ cell lineage in the mouse by suppressing both Bax-dependent and -independent apoptotic pathways. Developmental biology, 318(1), 133–142.

Takahashi, K., & Yamanaka, S. (2006). Induction of pluripotent stem cells from mouse embryonic and adult fibroblast cultures by defined factors. Cell, 126(4), 663–676.

Takaoka, K., Yamamoto, M., & Hamada, H. (2011). Origin and role of distal visceral endoderm, a group of cells that determines anterior-posterior polarity of the mouse embryo. Nature cell biology, 13(7), 743–752.

Takaoka, K., & Hamada, H. (2012). Cell fate decisions and axis determination in the early mouse embryo. Development (Cambridge, England), 139(1), 3–14.

Tamai, Y., Ishikawa, T., Bösl, M. R., Mori, M., Nozaki, M., Baribault, H., Oshima, R. G., & Taketo, M. M. (2000). Cytokeratins 8 and 19 in the mouse placental development. The Journal of cell biology, 151(3), 563–572.

Tanaka, S., Kunath, T., Hadjantonakis, A. K., Nagy, A., & Rossant, J. (1998). Promotion of trophoblast stem cell proliferation by FGF4. Science (New York, N.Y.), 282(5396), 2072–2075.

Turner, D. A., Baillie-Johnson, P., & Martinez Arias, A. (2016). Organoids and the genetically encoded self-assembly of embryonic stem cells. BioEssays : news and reviews in molecular, cellular and developmental biology, 38(2), 181–191.

Varlet, I., Collignon, J., & Robertson, E. J. (1997). nodal expression in the primitive endoderm is required for specification of the anterior axis during mouse gastrulation. Development (Cambridge, England), 124(5), 1033–1044.

Velardo, J.T., Dawson, A.B., Olsen, A.G. & Hisaw, F.L. (1953). Sequence of histological changes in the uterus and vagina of the rat during prolongation of pseudopregnancy associated with the presence of deciduomata. The American journal of anatomy, 93(2), 272–305.

Viotti, M., Nowotschin, S., & Hadjantonakis, A. K. (2014). SOX17 links gut endoderm morphogenesis and germ layer segregation. Nature cell biology, 16(12), 1146–1156.

Wamaitha, S. E., del Valle, I., Cho, L. T., Wei, Y., Fogarty, N. M., Blakeley, P., Sherwood, R. I., Ji, H., & Niakan, K. K. (2015). Gata6 potently initiates reprograming of pluripotent and differentiated cells to extraembryonic endoderm stem cells. Genes & development, 29(12), 1239–1255.

Weber, S., Eckert, D., Nettersheim, D., Gillis, A. J., Schäfer, S., Kuckenberg, P., Ehlermann, J., Werling, U., Biermann, K., Looijenga, L. H., & Schorle, H. (2010). Critical function of AP-2 gamma/TCFAP2C in mouse embryonic germ cell maintenance. Biology of reproduction, 82(1), 214–223.

Wickham, H. (2016). ggplot2: Elegant Graphics for Data Analysis. Springer.

Winnier, G., Blessing, M., Labosky, P. A., & Hogan, B. L. (1995). Bone morphogenetic protein-4 is required for mesoderm formation and patterning in the mouse. Genes & development, 9(17), 2105–2116.

Xenopoulos, P., Kang, M., & Hadjantonakis, A. K. (2012). Cell lineage allocation within the inner cell mass of the mouse blastocyst. Results and problems in cell differentiation, 55, 185–202.

Yamamoto, M., Beppu, H., Takaoka, K., Meno, C., Li, E., Miyazono, K., & Hamada, H. (2009). Antagonism between Smad1 and Smad2 signaling determines the site of distal visceral endoderm formation in the mouse embryo. The Journal of cell biology, 184(2), 323–334.

Yang, J., Ryan, D. J., Wang, W., Tsang, J. C., Lan, G., Masaki, H., Gao, X., Antunes, L., Yu, Y., Zhu, Z., Wang, J., Kolodziejczyk, A. A., Campos, L. S., Wang, C., Yang, F., Zhong, Z., Fu, B., Eckersley-Maslin, M. A., Woods, M., Tanaka, Y., Chen, X., Wilkinson, A.C., Bussel, J., White, J., Ramirez-Solis, R., Reik, W., Göttgens, B., Teichmann, S.A., Tam, P.P.L., Nakauchi, H., Zou, X., Lu, L. & Liu, P. (2017). Establishment of mouse expanded potential stem cells. Nature, 550(7676), 393–397.

Ying, Y., Liu, X. M., Marble, A., Lawson, K. A., & Zhao, G. Q. (2000). Requirement of Bmp8b for the generation of primordial germ cells in the mouse. Molecular endocrinology (Baltimore, Md.), 14(7), 1053–1063.

Ying, Y., & Zhao, G. Q. (2001). Cooperation of endoderm-derived BMP2 and extraembryonic ectoderm-derived BMP4 in primordial germ cell generation in the mouse. Developmental biology, 232(2), 484–492.

Ying, Q. L., Nichols, J., Chambers, I., & Smith, A. (2003). BMP induction of Id proteins suppresses differentiation and sustains embryonic stem cell self-renewal in collaboration with STAT3. Cell, 115(3), 281–292.

Ying, Q. L., Wray, J., Nichols, J., Batlle-Morera, L., Doble, B., Woodgett, J., Cohen, P., & Smith, A. (2008). The ground state of embryonic stem cell self-renewal. Nature, 453(7194), 519–523.

Yoshimizu, T., Sugiyama, N., De Felice, M., Yeom, Y.I., Ohbo, K., Masuko, K., Obinata, M., Abe, K., Schöler, H.R., & Matsui, Y. (1999). Germline-specific expression of the Oct-4/green fluorescent protein (GFP) transgene in mice. Development, growth & differentiation, 41(6), 675-684.

Yu, L., Wei, Y., Duan, J., Schmitz, D. A., Sakurai, M., Wang, L., Wang, K., Zhao, S., Hon, G. C., & Wu, J. (2021). Blastocyst-like structures generated from human pluripotent stem cells. Nature, 10.1038/s41586-021-03356-y. Advance online publication.

Zhang, S., Chen, T., Chen, N., Gao, D., Shi, B., Kong, S., West, R. C., Yuan, Y., Zhi, M., Wei, Q., Xiang, J., Mu, H., Yue, L., Lei, X., Wang, X., Zhong, L., Liang, H., Cao, S., Belmonte, J., Wang, H. & Han, J. (2019). Implantation initiation of self-assembled embryo-like structures generated using three types of mouse blastocyst-derived stem cells. Nature communications, 10(1), 496.

Zheng, Y., Xue, X., Shao, Y., Wang, S., Esfahani, S. N., Li, Z., Muncie, J. M., Lakins, J. N., Weaver, V. M., Gumucio, D. L., & Fu, J. (2019). Controlled modelling of human epiblast and amnion development using stem cells. Nature, 573(7774), 421–425.

8. Appendix

8.1 Efficiencies of self-organization into RtL-embryoids

Day 4 into protocol (DOX STOP)	**Replicates**			
	1. Replicate n #	2. Replicate n #	3. Replicate n #	Mean %
ESCs + iTSCs + iXEN (Correct assembly)	60	45	67	14.74%
ESCs + iTSCs + iXEN (incorrect assembly)	76	84	72	19.91%
ESCs + iTSCs	97	115	121	28.48%
ESCs + iXEN	26	30	38	8.02%
iTSCs + iXEN	27	34	20	6.97%
ESCs only	25	23	29	6.59%
iTSCs only	51	44	39	11.53%
iXEN only	11	15	18	3.75%
Total n	373	390	404	
Day 5 into protocol (24h after DOX STOP)	**Replicates**			
	1. Replicate n #	2. Replicate n #	3. Replicate n #	Mean %
ESCs + iTSCs + iXEN (Correct assembly)	54	65	71	24.41%
ESCs + iTSCs + iXEN (incorrect assembly)	15	28	26	8.76%
ESCs + iTSCs	49	52	60	20.76%
ESCs + iXEN	30	42	38	14.14%
iTSCs + iXEN	16	11	21	6.18%
ESCs only	12	18	18	6.13%
iTSCs only	40	32	45	15.16%
iXEN only	8	15	12	4.46%
Total n	224	263	291	

8.2 TOP 50 DEGs of the VE-like cell cluster

Gene ID	P value	Average logFC	Pct.1	Pct.2	P value adjusted
Cubn	2,38E-192	1,458161853	0,994	0,025	7,13E-188
Srgn	7,70E-188	3,257015436	1	0,053	2,31E-183
Dab2	1,43E-181	2,110047312	0,994	0,068	4,28E-177
Col4a2	5,43E-179	1,422532041	1	0,101	1,63E-174
Pdgfra	1,01E-176	0,557315507	0,949	0,029	3,04E-172
Col4a1	1,15E-175	2,705913844	1	0,121	3,45E-171
Amn	6,12E-175	1,745080302	0,956	0,048	1,83E-170
Flrt3	2,85E-174	0,923423302	0,965	0,053	8,55E-170
Habp2	2,93E-172	1,04348861	0,895	0,002	8,77E-168
Npl	3,63E-167	2,086244699	1	0,18	1,09E-162
Sox7	3,86E-167	0,674267346	0,905	0,025	1,16E-162
Sox17	4,93E-166	0,943741356	0,886	0,008	1,48E-161
Lama1	1,65E-165	1,342843999	0,984	0,149	4,94E-161
Myo7a	1,25E-156	0,758091201	0,93	0,076	3,73E-152
Klb	7,00E-152	0,447029261	0,854	0,026	2,10E-147
Gata4	3,48E-150	1,158542357	0,997	0,203	1,04E-145
Gata6	3,79E-150	0,529952411	0,908	0,067	1,14E-145
Tfec	1,80E-146	1,104687879	0,794	0,005	5,40E-142
Pth1r	4,72E-146	0,940643648	0,943	0,124	1,41E-141
Rhpn1	1,08E-145	0,765027985	0,863	0,054	3,25E-141
Serpinh1	1,52E-145	1,592508758	1	0,474	4,55E-141
Aqp8	7,71E-144	1,421926473	0,857	0,04	2,31E-139
Bend5	2,98E-143	1,032242959	0,921	0,093	8,93E-139
Tfpi	4,05E-143	1,758289766	0,978	0,249	1,21E-138
Gdpd5	4,61E-142	0,575569739	0,86	0,059	1,38E-137
Sparc	6,71E-142	3,053837896	1	0,635	2,01E-137
Retreg1	1,89E-141	0,849111673	0,93	0,138	5,66E-137
Lrp2	5,20E-141	0,903554867	0,997	0,406	1,56E-136
Lrpap1	4,68E-140	2,47270886	1	0,789	1,40E-135
Rab3il1	9,09E-140	0,89187912	0,911	0,104	2,72E-135
Ifi30	7,26E-139	1,94060443	0,997	0,568	2,18E-134
Lamb1	6,32E-138	1,664386759	0,997	0,477	1,89E-133
Amot	5,73E-136	0,58598522	0,93	0,159	1,72E-131
Lamp1	5,39E-135	1,422095968	1	0,972	1,62E-130
Ctsl	2,49E-134	2,120346285	1	0,963	7,45E-130
Ctsz	2,43E-133	1,723488517	1	0,848	7,27E-129
Ctsh	3,96E-133	1,480063333	0,917	0,132	1,19E-128
Nrg1	8,14E-132	0,659156096	0,813	0,042	2,44E-127
Hkdc1	3,60E-131	0,451419673	0,781	0,026	1,08E-126
Calr	6,75E-131	1,470346097	1	0,952	2,02E-126
P4hb	9,94E-129	1,254001547	1	0,946	2,98E-124
Vamp8	2,34E-128	1,560033799	0,997	0,577	7,01E-124

Rcn3	1,04E-127	1,345278336	0,994	0,413	3,12E-123
Dpp4	4,07E-127	0,800868727	0,816	0,056	1,22E-122
Htra1	3,41E-126	1,270086275	0,924	0,159	1,02E-121
Ctsc	3,43E-126	1,514454283	0,975	0,311	1,03E-121
Ankrd33b	2,77E-124	0,505092807	0,876	0,101	8,31E-120
P4ha2	1,44E-123	1,405117488	0,917	0,235	4,31E-119
Mttp	4,18E-123	0,42881684	0,838	0,101	1,25E-118
Lgmn	5,97E-123	1,667793812	0,997	0,704	1,79E-118
Kdelr3	1,04E-122	1,356439046	0,965	0,255	3,11E-118

8.3 TOP 50 DEGs of the Epi-like cell cluster

Gene ID	P value	Average logFC	Pct.1	Pct.2	P value adjusted
Tdgf1	1,26E-188	2,090870202	0,968	0,012	3,77E-184
Fgf4	3,32E-165	0,712740314	0,868	0,002	9,95E-161
Gdf3	9,91E-157	0,911678851	0,884	0,038	2,97E-152
Igfbp2	3,45E-152	1,878476805	0,977	0,169	1,03E-147
Pla2g1b	2,05E-147	1,91643519	0,8	0,008	6,13E-143
Tdgf1-ps1	4,64E-138	1,224929848	0,748	0	1,39E-133
Cmah	1,09E-136	0,668156993	0,997	0,627	3,26E-132
Trh	2,32E-136	1,943800257	0,752	0,006	6,96E-132
Platr10	1,92E-135	1,108131529	0,91	0,141	5,76E-131
Nanog	6,32E-131	1,477013583	0,932	0,28	1,89E-126
Pou5f1	3,99E-127	1,519242045	1	0,499	1,20E-122
Gsta4	4,19E-126	1,537608786	0,987	0,444	1,25E-121
Chchd10	6,92E-126	1,871709427	1	0,922	2,07E-121
Phc1	2,30E-125	0,823812829	0,961	0,335	6,88E-121
Ifitm3	1,43E-124	1,799876419	0,958	0,283	4,28E-120
Mkrn1	1,44E-123	1,396693571	1	0,908	4,32E-119
Dppa5a	1,53E-123	1,884110114	0,994	0,68	4,59E-119
Enpp3	6,76E-120	0,884853968	0,774	0,066	2,02E-115
Zfp985	1,60E-118	0,840508656	0,974	0,504	4,79E-114
Fam60a	2,14E-107	1,106677146	1	0,905	6,42E-103
Pipox	3,97E-107	0,71801652	0,648	0,018	1,19E-102
Snrpn	2,15E-106	1,243790054	0,994	0,77	6,43E-102
AC154630.1	3,57E-106	0,536448671	0,887	0,266	1,07E-101
Slc7a3	4,32E-104	1,277658135	0,961	0,496	1,29E-99
Utf1	5,24E-104	1,255844216	0,994	0,59	1,57E-99
Hsf2bp	1,02E-103	0,887626515	0,745	0,083	3,05E-99
Ldhb	1,44E-103	1,660153992	0,981	0,531	4,32E-99
Olfr1388	1,18E-100	0,463760672	0,8	0,152	3,53E-96
Ifitm2	1,49E-100	1,095339858	1	0,848	4,47E-96
Eno1	5,20E-100	0,751362847	1	0,997	1,56E-95
Pkm	4,67E-99	0,716242495	1	1	1,40E-94

Nphs1	3,07E-98	0,643508724	0,652	0,051	9,20E-94
Mymx	4,10E-98	1,022043426	0,661	0,051	1,23E-93
Col18a1	4,36E-98	0,606720816	0,884	0,198	1,31E-93
Ccnd1	5,36E-98	0,478483221	0,671	0,055	1,61E-93
Wiz	1,43E-97	0,458589156	0,961	0,639	4,28E-93
Cobl	2,64E-97	0,464519576	0,697	0,072	7,92E-93
Rbpms2	4,31E-97	1,032338464	0,997	0,811	1,29E-92
Zfp980	3,40E-96	0,530620169	0,871	0,286	1,02E-91
Set	4,34E-95	0,650115784	1	1	1,30E-90
Jam2	5,76E-95	0,777658195	0,652	0,055	1,73E-90
Nr0b1	3,10E-88	1,094584704	0,81	0,214	9,30E-84
Fn1	2,29E-87	0,780718711	0,958	0,522	6,85E-83
Sep1	1,07E-86	1,108776098	0,687	0,117	3,20E-82
Hsp90aa1	5,26E-86	0,706266854	1	1	1,57E-81
Msh6	2,58E-85	0,677607593	0,99	0,811	7,74E-81
Lefty2	3,11E-85	1,129877276	0,729	0,109	9,31E-81
Rif1	2,27E-84	0,60133054	1	0,848	6,80E-80
Trp53	3,34E-84	0,846102494	0,997	0,9	1,00E-79
Zfp990	4,90E-84	0,779756173	0,981	0,693	1,47E-79
Sox2	6,05E-83	0,520088868	0,887	0,29	1,81E-78

8.4 TOP 50 DEGs of the ExE-like cell cluster

Gene ID	P value	Average logFC	Pct.1	Pct.2	P value adjusted
Id2	7,84E-121	1,938235849	0,949	0,394	2,35E-116
Sct	1,39E-110	2,580514037	0,708	0,043	4,16E-106
Cdx2	4,82E-107	0,476109701	0,649	0,014	1,44E-102
Pla2g7	2,92E-105	2,195055116	0,726	0,08	8,75E-101
F11r	6,90E-97	1,277670856	0,964	0,611	2,07E-92
Selenbp1	1,87E-96	1,742380913	0,613	0,024	5,61E-92
Cldn3	7,65E-94	1,143334609	0,658	0,061	2,29E-89
Ak2	2,71E-93	0,818039044	0,997	0,974	8,11E-89
Ahnak	1,65E-91	0,408288687	0,905	0,314	4,95E-87
Errfi1	4,44E-89	0,671290577	0,798	0,213	1,33E-84
Psap	2,51E-85	0,976617354	0,991	0,848	7,52E-81
Sorl1	1,65E-84	1,121398265	0,872	0,326	4,96E-80
Lgals1	5,23E-84	1,528707814	0,92	0,541	1,57E-79
Anxa3	5,53E-84	1,047453577	0,58	0,037	1,66E-79
Rnf128	7,73E-83	0,763151522	0,798	0,206	2,32E-78
Krt19	4,00E-81	1,241753835	0,586	0,046	1,20E-76
Gata3	3,18E-79	0,570500896	0,557	0,034	9,51E-75
Smagp	2,76E-78	1,062249744	0,863	0,365	8,27E-74
Igf2	1,20E-77	1,770678876	0,789	0,282	3,58E-73
Cadm1	1,99E-75	1,011832464	0,851	0,341	5,96E-71

Tspan1	4,24E-73	1,210691141	0,476	0,013	1,27E-68
Bex1	1,33E-69	1,120599957	0,955	0,784	3,98E-65
Ifi35	9,36E-69	0,481587249	0,512	0,035	2,80E-64
Tifa	3,07E-68	0,715772487	0,473	0,024	9,21E-64
Nupr1	4,59E-68	1,642761688	0,92	0,549	1,38E-63
Tpm1	8,46E-67	0,938612399	0,973	0,728	2,54E-62
Tmsb4x	2,11E-66	1,376653347	0,961	0,722	6,32E-62
Bex3	1,10E-65	0,725207064	0,997	0,997	3,30E-61
Rassf4	3,07E-65	0,522280732	0,509	0,046	9,19E-61
Mid1	8,48E-65	0,623129733	0,914	0,541	2,54E-60
Wls	4,85E-63	0,784802402	0,771	0,301	1,45E-58
Epcam	8,27E-62	0,743560885	0,973	0,8	2,48E-57
Jak1	4,07E-60	0,689115454	0,917	0,613	1,22E-55
Dhrs3	5,54E-60	1,101150997	0,548	0,091	1,66E-55
Blnk	5,79E-59	0,751473701	0,542	0,094	1,74E-54
Cnn2	2,21E-58	0,736684921	0,783	0,32	6,63E-54
Trap1a	4,98E-57	0,710009393	0,938	0,798	1,49E-52
Cdh1	1,00E-56	0,561098754	0,97	0,792	3,01E-52
Myl12a	1,17E-56	0,539645148	0,997	0,981	3,52E-52
Tes	6,97E-56	0,55257958	0,777	0,322	2,09E-51
Gpx3	8,62E-56	1,847749015	0,881	0,51	2,58E-51
Cldn4	1,60E-54	1,544684272	0,774	0,411	4,79E-50
Arpc2	2,57E-54	0,534719525	0,994	0,976	7,69E-50
S100a6	1,39E-53	0,630699524	0,399	0,024	4,16E-49
Myc	4,68E-52	0,482492566	0,592	0,139	1,40E-47
Fgfr1	7,51E-52	0,416133128	0,854	0,395	2,25E-47
Tceal9	5,63E-51	0,61990065	0,988	0,97	1,69E-46
Lrrfip1	1,60E-50	0,609351604	0,86	0,55	4,79E-46
Arpc1b	2,75E-50	0,751490903	0,949	0,87	8,23E-46
Cystm1	2,16E-49	0,790853064	0,997	0,824	6,49E-45
Ptp4a2	6,09E-49	0,66575018	0,997	0,997	1,83E-44

8.5 TOP 50 DEGs in ExVE-like cluster / VE-like subcluster 1

Gene ID	P value	Average logFC	Pct.1	Pct.2	P value adjusted
P4ha2	1,22E-29	1,07605289	0,979	0,734	3,65E-25
Lama1	9,41E-25	0,68135179	1	0,937	2,82E-20
Lamc1	1,54E-22	0,80406447	1	0,962	4,61E-18
Fabp3	1,58E-22	0,69837775	1	0,987	4,75E-18
Sat1	9,67E-21	0,98211502	0,975	0,848	2,90E-16
Hs3st1	3,90E-20	0,75117304	0,89	0,367	1,17E-15
Tpm4	2,46E-19	0,67062245	0,996	0,949	7,37E-15
Tmsb10	3,92E-19	0,7273032	0,996	0,899	1,17E-14
Nostrin	2,11E-18	0,69460301	0,835	0,253	6,31E-14

Pdlim4	1,94E-17	0,81060194	0,886	0,468	5,82E-13
Lamb1	5,25E-16	0,61489414	1	0,987	1,57E-11
Plaur	3,28E-15	0,68760602	0,958	0,646	9,81E-11
Glipr2	8,50E-15	0,67273869	0,958	0,646	2,55E-10
Anxa2	4,54E-14	0,68888112	0,733	0,241	1,36E-09
Cd9	7,56E-14	0,51600672	1	0,975	2,27E-09
Dppa5a	9,50E-14	0,45478361	1	1	2,85E-09
Htra1	3,53E-13	0,6351775	0,966	0,797	1,06E-08
Plod2	4,02E-13	0,42285959	0,979	0,861	1,21E-08
S100a10	4,84E-13	0,57771807	0,97	0,899	1,45E-08
Spp1	5,12E-13	1,22692943	0,818	0,43	1,53E-08
Tagln2	2,24E-12	0,53533041	0,953	0,62	6,71E-08
Pth1r	1,36E-11	0,4602295	0,953	0,911	4,06E-07
Atox1	1,44E-11	0,48676593	0,975	0,962	4,30E-07
Gsn	1,90E-11	0,43671554	0,852	0,468	5,70E-07
2200002D01Rik	4,02E-11	0,55571342	0,864	0,57	1,20E-06
Mgst3	4,93E-11	0,46740108	0,979	0,975	1,48E-06
Col4a1	1,41E-10	0,41556662	1	1	4,23E-06
B2m	2,72E-10	0,51267487	0,962	0,873	8,16E-06
Tax1bp3	4,20E-10	0,41817231	0,962	0,899	1,26E-05
Cryab	4,72E-10	0,49971897	0,458	0,076	1,41E-05
Serpinb6c	6,54E-10	0,4427219	0,805	0,43	1,96E-05
Rhox5	6,93E-10	0,45112663	0,979	0,949	2,08E-05
Gjb5	7,57E-10	0,44320018	0,75	0,38	2,27E-05
S100a11	9,38E-10	0,59802774	0,792	0,519	2,81E-05
Echdc2	4,24E-09	0,46199404	0,958	0,835	0,00012693
Prr13	5,65E-09	0,45005852	0,97	0,873	0,00016917
F3	1,07E-08	0,56315013	0,746	0,519	0,00032083
Ccnd3	1,21E-08	0,42375675	0,894	0,696	0,0003616
Dok2	1,33E-08	0,43854813	0,61	0,203	0,00039924
Dnmt3l	4,04E-08	0,40628113	0,928	0,81	0,00121144
Dut	5,07E-08	0,44473568	0,843	0,671	0,00152041
Dkkl1	5,87E-08	0,46376974	0,775	0,519	0,00175915
Fam213a	7,36E-08	0,46825754	0,847	0,684	0,00220464
Aqp8	8,11E-08	0,44023009	0,911	0,696	0,0024289
Tk1	1,09E-07	0,40610206	0,873	0,684	0,00326436
Lgals3	3,05E-07	0,49289781	0,568	0,253	0,00914883
Tmsb4x	1,67E-06	0,49212918	0,758	0,532	0,05010779
S100g	1,36E-05	0,56639482	0,686	0,481	0,40624359
1500009L16Rik	3,95E-05	0,41129899	0,686	0,43	1
AC123832.2	0,00017866	0,45301348	0,852	0,772	1
Arhgef40	0,00021491	0,54958648	0,775	0,595	1

8.6 TOP 50 DEGs in EmVE-like cluster / VE-like subcluster 2

Gene ID	P value	Average logFC	Pct.1	Pct.2	P value adjusted
Has2	6,11E-27	0,4431484	0,734	0,148	1,83E-22
Fdps	1,12E-24	1,28550803	0,949	0,729	3,36E-20
Amot	3,00E-24	0,6345051	1	0,907	8,99E-20
Fdft1	1,44E-22	0,89174782	0,949	0,589	4,31E-18
Tspan13	1,71E-22	0,55557722	0,937	0,449	5,12E-18
Hmgcs1	3,19E-22	0,87578089	0,949	0,716	9,57E-18
Msmo1	3,49E-22	1,14480791	0,975	0,814	1,05E-17
Slc7a7	4,11E-22	0,82549988	0,949	0,585	1,23E-17
Slc40a1	4,21E-22	0,59546909	0,696	0,182	1,26E-17
Apoe	3,43E-21	0,71724843	1	1	1,03E-16
Ctsc	1,10E-20	0,90441336	1	0,966	3,30E-16
Hmgb3	2,26E-20	0,90181825	0,899	0,568	6,76E-16
Idi1	6,04E-20	0,58420745	0,835	0,356	1,81E-15
Sqle	7,18E-20	0,68577886	0,924	0,619	2,15E-15
Mvd	1,11E-19	0,89566957	0,899	0,492	3,32E-15
Scd1	2,34E-19	0,46690397	0,962	0,742	7,00E-15
Car4	2,75E-19	1,05807443	1	0,852	8,25E-15
Acat2	1,02E-18	0,94709307	0,937	0,809	3,04E-14
Eml1	7,33E-18	0,82145091	0,861	0,441	2,20E-13
2610528J11Rik	8,91E-18	0,61258711	0,405	0,038	2,67E-13
Dhcr7	9,71E-18	0,66133573	0,835	0,386	2,91E-13
Gcat	2,78E-17	0,49454132	1	0,945	8,32E-13
Tm7sf2	7,06E-17	0,63159128	0,646	0,195	2,12E-12
Reep6	1,33E-16	0,57538726	0,684	0,229	3,99E-12
Apob	5,68E-16	0,57270562	0,354	0,03	1,70E-11
Agpat3	1,62E-15	0,52085736	0,861	0,517	4,85E-11
Hmga1	4,06E-15	0,68328915	0,911	0,564	1,22E-10
Utf1	1,05E-14	0,54982426	0,987	0,775	3,14E-10
Lefty2	2,36E-14	0,62639603	0,354	0,038	7,06E-10
Tfec	6,14E-14	0,67069661	0,949	0,742	1,84E-09
Fhl1	8,92E-14	0,51021866	0,987	0,915	2,67E-09
Pcyt2	1,35E-13	0,64235471	0,987	0,754	4,06E-09
Slc9a3r1	1,75E-13	0,49996725	0,987	0,966	5,25E-09
Abcg2	2,02E-13	0,47550913	0,911	0,581	6,07E-09
Dab2	4,12E-13	0,41465532	0,987	0,996	1,24E-08
Slc39a4	4,83E-13	0,45522632	0,924	0,636	1,45E-08
Cyp26a1	5,79E-13	0,65209343	0,734	0,347	1,73E-08
Aldh1l1	6,21E-13	0,41446532	0,861	0,475	1,86E-08
Lss	6,91E-13	0,66779253	0,861	0,576	2,07E-08
Apoc2	1,04E-12	0,77139078	0,253	0,013	3,10E-08
Adk	1,29E-12	0,56650844	0,937	0,686	3,86E-08
Tmem9	1,52E-12	0,62879173	0,797	0,441	4,56E-08

H2-K1	2,04E-12	0,81602683	0,785	0,458	6,12E-08
Aldoc	2,68E-12	0,42103898	0,367	0,059	8,03E-08
Soat2	3,64E-12	0,61232748	0,873	0,631	1,09E-07
Bin2	4,27E-12	0,42013135	0,582	0,212	1,28E-07
Rab4a	4,32E-12	0,55034449	0,924	0,839	1,29E-07
Ass1	5,09E-12	0,58296122	0,911	0,589	1,53E-07
Fasn	1,10E-11	0,61889733	0,987	0,936	3,30E-07
Cited1	1,71E-11	0,81995217	0,899	0,801	5,11E-07
Hmgcr	1,77E-11	0,46940895	0,937	0,805	5,29E-07

8.7 Quantification of LEFTY1+ cell location in RtL-embryoids

Day 4 into protocol (DOX STOP)	**Replicates**			
	1. Replicate n #	2. Replicate n #	3. Replicate n #	Mean %
Distal Position	44	39	45	34.13%
Transition Position	31	48	42	32.27%
Anterior Position	5	2	7	3.73%
No LEFTY1+ cells in VE	17	10	11	10.13%
Random location within EmVE (but restricted to EmVE)	22	25	17	17.07%
Random location within EmVE and ExVE	6	1	3	2.67%
Total n	125	125	125	
Day 5 into protocol (24h after DOX STOP)	**Replicates**			
	1. Replicate n #	2. Replicate n #	3. Replicate n #	Mean %
Distal Position	40	45	51	36.00%
Transition Position	46	33	39	31.47%
Anterior Position	10	5	4	5.07%
No LEFTY1+ cells in VE	10	14	13	9.87%
Random location within EmVE (but restricted to EmVE)	16	20	10	12.27%
Random location within EmVE and ExVE	3	8	8	5.07%
Total n	125	125	125	

8.8 TOP 50 DEGs in Epi-like subcluster 1

Gene ID	P value	Average logFC	Pct.1	Pct.2	P value adjusted
Dppa5a	9,54E-18	0,69758379	0,995	0,991	2,86E-13
Zfp42	1,53E-14	0,78950835	0,99	0,835	4,57E-10
Sept1	7,93E-14	0,91570378	0,836	0,435	2,38E-09
Tcl1	5,89E-12	0,8256145	0,836	0,461	1,77E-07
Stmn2	1,15E-10	0,63203457	0,821	0,548	3,46E-06
Nr0b1	1,49E-10	0,77253538	0,887	0,678	4,47E-06
Fn1	2,09E-10	0,55219816	0,985	0,913	6,28E-06
Ldhb	4,94E-10	0,77484502	0,985	0,974	1,48E-05
Spp1	1,19E-09	1,00246612	0,959	0,765	3,56E-05
Tsc22d1	2,11E-09	0,58146706	0,99	0,965	6,31E-05
Chchd10	2,11E-09	0,47969929	1	1	6,31E-05
Cd9	3,86E-09	0,53674547	0,969	0,939	0,00011579
Mybl2	4,36E-09	0,49649051	0,995	0,983	0,00013057
Fstl1	8,69E-09	0,56687882	0,862	0,574	0,00026039
Cobl	9,21E-09	0,4481945	0,785	0,548	0,00027591
Hspb1	1,18E-08	0,52429834	0,969	0,8	0,00035246
Tdh	1,53E-08	0,55033709	0,99	0,852	0,00045846
Slc25a36	4,71E-08	0,46482852	0,979	0,974	0,00140995
Mymx	9,10E-08	0,55344112	0,774	0,47	0,00272549
Hexb	1,67E-07	0,53438434	0,846	0,687	0,00500025
Zfp57	3,66E-07	0,44265309	0,918	0,791	0,01096833
Asns	3,66E-07	0,44584491	0,969	0,991	0,01097914
Halr1	3,73E-07	0,57017328	0,6	0,278	0,01116328
Ephx2	7,21E-07	0,44147857	0,549	0,261	0,02159709
2210409E12Rik	7,25E-07	1,07698316	0,328	0,087	0,02171479
Apoe	9,81E-07	0,59871611	0,995	1	0,0293965
Idh2	2,89E-06	0,451659	0,985	0,957	0,08665396
Jam2	3,04E-06	0,61161255	0,728	0,522	0,09119072
Nfkbia	5,64E-06	0,57447288	0,703	0,53	0,16906367
Ly6g6e	9,38E-06	0,44068208	0,226	0,035	0,28111435
Lrrc2	9,59E-06	0,45733278	0,656	0,435	0,28726647
Ass1	1,31E-05	0,499399	0,831	0,722	0,39321266
Nanog	1,44E-05	0,4321896	0,954	0,896	0,43225319
Pgpep1	4,46E-05	0,43721883	0,754	0,557	1
Lefty2	0,00016838	0,78314139	0,769	0,661	1
Lgals3	0,00021175	0,41381082	0,492	0,27	1
Hsd17b14	0,0003353	0,50268864	0,687	0,522	1
Tmem39a	0,00049566	0,5830818	0,81	0,748	1
AC156560.2	0,00678299	0,63343801	0,697	0,548	1
AC153532.1	0,00761757	0,42052764	0,549	0,417	1

8.9 TOP 50 DEGs in Epi-like subcluster 2

Gene ID	P value	Average logFC	Pct.1	Pct.2	P value adjusted
Dnmt3b	6,24E-24	1,39219801	0,957	0,614	1,87E-19
Fgf15	2,30E-23	1,0166139	0,812	0,183	6,89E-19
Car4	8,46E-23	1,79249087	0,754	0,191	2,53E-18
Kif1a	5,43E-19	0,42569606	0,449	0,041	1,63E-14
Enpp2	3,76E-15	0,91687368	0,58	0,141	1,13E-10
Emb	1,55E-14	0,79879286	1	0,88	4,64E-10
Fgf5	1,74E-14	0,52187507	0,464	0,079	5,23E-10
Pim2	1,63E-13	1,48798248	0,638	0,266	4,87E-09
Krt18	5,72E-13	0,59396507	0,493	0,112	1,71E-08
Gnas	1,01E-12	1,01533744	0,957	0,763	3,01E-08
Dnmt3a	9,13E-12	1,03108346	0,957	0,83	2,74E-07
Gja1	9,76E-12	0,73983101	0,942	0,776	2,92E-07
Slc16a3	1,21E-11	0,56305506	0,783	0,373	3,62E-07
Cldn6	1,70E-11	0,84105974	0,754	0,349	5,08E-07
Limd2	6,90E-11	0,7567607	0,87	0,606	2,07E-06
Plekha1	8,46E-11	0,64537351	0,899	0,618	2,54E-06
Car14	6,36E-10	0,49029653	0,42	0,104	1,91E-05
Cthrc1	6,64E-09	0,54788246	0,391	0,095	0,00019904
Utf1	1,00E-08	0,56170272	1	0,992	0,00029992
Lss	2,05E-08	0,78293551	0,87	0,631	0,00061559
Otx2	4,08E-08	0,5857029	0,797	0,469	0,00122089
Card19	7,62E-08	0,5963044	0,507	0,212	0,00228263
Hes6	9,60E-08	0,89627884	0,71	0,386	0,00287682
Gpx3	1,11E-07	0,49438713	0,594	0,253	0,00332485
Ldha	1,26E-07	0,6809564	0,986	0,925	0,00376949
Pitx2	2,77E-07	0,51009792	0,594	0,266	0,00830169
Adk	2,78E-07	0,53128779	0,971	0,838	0,00832608
Laptm4b	3,45E-07	0,52331547	0,957	0,826	0,01033591
Mdk	5,19E-07	0,57276789	0,986	0,921	0,01555422
Cbr3	5,48E-07	0,42845496	0,58	0,282	0,01641865
Sycp3	9,74E-07	0,41393348	0,551	0,27	0,02916719
Soat1	1,43E-06	0,46385294	0,841	0,585	0,04293031
Tmem54	1,56E-06	0,46401182	0,217	0,041	0,04668655
Gsto1	5,56E-06	0,464511	0,783	0,49	0,16655456
Map1b	6,62E-06	0,41587413	0,913	0,73	0,19832924
Ssbp3	8,72E-06	0,4318016	0,725	0,498	0,26124104
Bst2	1,01E-05	0,68135554	0,783	0,564	0,30385282
Snhg14	1,10E-05	0,63594224	1	0,954	0,32995639
Zcrb1	1,17E-05	0,48303712	0,754	0,568	0,35196789
Fdft1	1,63E-05	0,47578305	0,928	0,851	0,48966176
Fdps	2,39E-05	0,48534834	0,986	0,954	0,71613482
Rbpms	3,12E-05	0,43668407	0,957	0,88	0,93433189

Dhps	3,72E-05	0,41201482	0,812	0,585	1
Gclm	3,96E-05	0,59533661	0,841	0,759	1
Ddx18	4,07E-05	0,4878203	0,942	0,817	1
Mtch1	5,64E-05	0,5419557	0,812	0,622	1
Gstt2	5,72E-05	0,46705481	0,826	0,539	1
Fam162a	6,53E-05	0,50739368	0,884	0,714	1
Dcxr	7,44E-05	0,68513537	0,638	0,444	1
Adi1	8,78E-05	0,47029928	0,739	0,556	1
Tmem5	0,0001567	0,48423244	0,594	0,373	1

8.10 TOP 50 DEGs in Epi-like subcluster 3

Gene ID	P value	Average logFC	Pct.1	Pct.2	P value adjusted
Sfmbt2	2,59E-26	0,69811216	0,826	0,148	7,75E-22
Klhl13	4,09E-22	1,20189106	0,978	0,333	1,23E-17
Rhox6	1,26E-21	0,60897263	0,435	0,019	3,78E-17
Slc25a4	1,28E-20	1,61681292	1	0,943	3,84E-16
Tfap2c	7,76E-19	0,81426247	0,935	0,299	2,32E-14
Nup62cl	4,44E-18	1,73448448	0,935	0,398	1,33E-13
Fhl1	8,42E-17	0,7816431	0,891	0,326	2,52E-12
Rhox5	2,89E-16	2,30053432	0,609	0,11	8,65E-12
Cox4i1	3,79E-16	0,83715483	1	1	1,14E-11
Crip1	1,69E-15	1,57135497	0,891	0,455	5,07E-11
Dppa3	1,43E-14	2,01010951	0,739	0,288	4,28E-10
Bmp4	1,78E-14	1,03375727	0,435	0,061	5,33E-10
Cpsf4l	6,17E-14	0,81609435	0,826	0,277	1,85E-09
Mgarp	2,20E-13	0,66815243	0,543	0,106	6,58E-09
Ak4	2,84E-13	0,66307669	0,739	0,235	8,52E-09
Rasgrp2	3,28E-13	1,20635461	0,87	0,413	9,83E-09
Gpx1	9,11E-13	0,8767025	1	0,992	2,73E-08
Lgals1	1,06E-12	1,26261495	0,87	0,428	3,16E-08
Sfn	1,05E-11	0,69323506	0,717	0,239	3,13E-07
Fth1	1,19E-11	0,85475689	1	1	3,56E-07
B4galt1	1,98E-11	0,43817369	0,935	0,629	5,92E-07
Mt1	2,02E-11	1,53478178	0,957	0,803	6,04E-07
Mylpf	2,68E-11	1,40309705	0,978	0,659	8,03E-07
Gjb3	2,74E-11	0,84367327	0,913	0,436	8,21E-07
Skp1a	9,60E-11	0,7050513	1	0,992	2,88E-06
Hmgn5	1,14E-10	0,8690238	0,848	0,545	3,41E-06
Rhox9	1,20E-10	0,49332744	0,304	0,034	3,60E-06
Eif2s2	3,57E-10	0,8451493	1	1	1,07E-05
Zfp706	3,91E-10	0,75877148	1	0,981	1,17E-05
Mt2	4,08E-10	1,15764958	0,957	0,837	1,22E-05
Sms	6,91E-10	0,8048788	0,957	0,773	2,07E-05

Fabp3	1,50E-09	1,24437953	0,978	0,833	4,51E-05
Rbm47	1,72E-09	0,43168074	0,826	0,549	5,14E-05
Tpm1	3,68E-09	0,74850913	0,848	0,53	0,00011029
Calml4	4,05E-09	0,48482657	0,283	0,038	0,00012128
Tfpi	7,04E-09	0,63494788	0,457	0,121	0,00021104
Sod2	8,40E-09	0,49414464	1	0,958	0,00025159
Vangl1	8,56E-09	0,85397003	0,87	0,511	0,00025652
Etfb	1,85E-08	0,69421609	1	0,924	0,00055439
Naprt	2,47E-08	0,49974675	0,5	0,174	0,00073912
Cd63	2,59E-08	0,6485158	1	0,913	0,00077649
Ctnnal1	2,71E-08	0,75482369	0,848	0,527	0,00081165
Galk1	2,81E-08	0,69205879	0,978	0,848	0,00084288
AU018091	3,08E-08	0,41093733	0,957	0,629	0,00092411
Hmces	5,21E-08	0,81423128	0,935	0,739	0,00156002
Sms-ps	1,02E-07	0,76380439	0,826	0,481	0,00305298
Ssc4d	1,14E-07	0,43685418	0,326	0,068	0,0034188
Krt42	3,11E-07	0,76583744	0,652	0,269	0,00932297
Serpinb6a	4,23E-07	0,46801938	0,761	0,39	0,01268264
H2afy	4,98E-07	0,53555965	0,935	0,686	0,0149168
Nkain4	6,90E-07	0,65534835	0,37	0,098	0,02066195

8.11 TOP 50 DEGs in ExE-like subcluster 1

Gene ID	P value	Average logFC	Pct.1	Pct.2	P value adjusted
Gjb3	5,35E-50	1,29425167	0,978	0,193	1,60E-45
Utf1	1,58E-49	1,32377141	0,843	0,05	4,75E-45
Rhox5	1,34E-45	2,45770288	0,963	0,317	4,01E-41
Dnmt3b	1,67E-44	0,73795244	0,925	0,228	5,01E-40
Gjb5	1,76E-42	0,82950952	0,91	0,173	5,28E-38
Wnt7b	2,28E-42	0,49294148	0,709	0,01	6,82E-38
Bmp8b	1,02E-41	0,67535262	0,769	0,069	3,04E-37
Dusp9	3,37E-41	0,68208164	0,903	0,193	1,01E-36
Ddah1	1,28E-37	1,08202033	0,896	0,386	3,84E-33
Car2	2,94E-37	1,58173737	0,858	0,188	8,81E-33
Reep6	2,80E-36	0,66778673	0,776	0,099	8,39E-32
Morc4	3,60E-36	1,00815745	0,925	0,351	1,08E-31
Hand1	7,46E-36	1,0844107	0,664	0,04	2,23E-31
Cldn3	7,82E-36	1,12777721	0,948	0,465	2,34E-31
Gldc	9,69E-36	0,49711753	0,836	0,178	2,90E-31
Nup62cl	1,71E-35	1,32925149	0,978	0,485	5,11E-31
Plet1	2,41E-35	1,232512	0,724	0,094	7,21E-31
Anp32b	3,00E-35	0,80100142	1	0,98	8,99E-31
Tinagl1	7,72E-34	1,05457923	0,881	0,218	2,31E-29
Slc38a4	1,58E-33	0,72609503	0,866	0,287	4,75E-29

Dppa5a	2,13E-32	1,63814283	0,754	0,134	6,38E-28
Sfn	5,82E-32	0,81508402	0,724	0,114	1,74E-27
Alpl	4,96E-31	0,4981665	0,679	0,079	1,49E-26
Fbxo21	7,49E-31	0,72747179	0,993	0,683	2,24E-26
Hsp90aa1	2,40E-30	0,62276053	1	1	7,18E-26
Bmp4	1,93E-29	1,08244215	0,649	0,089	5,77E-25
Uchl5	2,34E-29	0,91849861	1	0,936	7,01E-25
Slc29a1	2,73E-29	0,78219472	0,888	0,282	8,17E-25
Sfmbt2	3,52E-29	0,55178658	0,873	0,391	1,06E-24
Hat1	6,40E-29	1,02253287	1	0,807	1,92E-24
Dppa4	8,43E-29	0,83278845	0,851	0,297	2,52E-24
Elf5	1,98E-28	0,89850211	0,672	0,139	5,95E-24
Fgfr2	3,16E-28	0,6739111	0,843	0,262	9,46E-24
Bcat1	7,23E-28	0,9212237	0,91	0,515	2,17E-23
Fdps	1,23E-27	1,00429236	1	0,767	3,67E-23
Cbs	1,28E-27	0,42603039	0,687	0,104	3,83E-23
Gtpbp4	2,58E-27	1,23593904	0,993	0,955	7,74E-23
Cct6a	3,03E-26	0,70802081	1	0,995	9,08E-22
Ndrg1	1,28E-25	0,68612505	0,597	0,079	3,83E-21
Slc2a1	1,32E-25	0,96240952	0,993	0,738	3,94E-21
Foxh1	1,35E-25	0,42977313	0,522	0,03	4,04E-21
Ezr	1,58E-25	0,64801178	0,993	0,847	4,73E-21
Rhox9	3,37E-25	1,24340616	0,769	0,223	1,01E-20
Snf8	5,15E-25	1,12537302	0,978	0,827	1,54E-20
Htra1	6,18E-25	0,65745817	0,567	0,064	1,85E-20
Srm	1,03E-24	0,68220821	1	0,802	3,10E-20
Gart	2,20E-24	0,51300911	0,993	0,703	6,60E-20
Apoc1	2,25E-24	0,84227403	0,739	0,243	6,74E-20
Ncl	2,71E-24	0,50016109	1	1	8,13E-20
Ran	3,20E-24	0,45904837	1	0,995	9,58E-20
Zfp131	6,84E-24	1,03917774	0,985	0,906	2,05E-19

8.12 TOP 50 DEGs in ExE-like subcluster 2

Gene ID	P value	Average logFC	Pct.1	Pct.2	P value adjusted
Pla2g7	7,29E-50	2,2929047	0,985	0,336	2,18E-45
Gpc3	1,40E-45	1,58819033	0,97	0,299	4,21E-41
Smim14	4,33E-35	1,18254127	0,95	0,597	1,30E-30
Pdpn	5,10E-35	1,24951243	0,98	0,649	1,53E-30
Tcf7l2	2,90E-34	0,90958804	0,99	0,784	8,70E-30
Mdk	9,47E-34	1,46434129	0,95	0,672	2,84E-29
Tifa	7,62E-33	0,95355792	0,748	0,06	2,28E-28
Cadm1	1,15E-32	1,07477484	0,955	0,694	3,46E-28
Dazap2	1,32E-32	0,98211818	0,965	0,731	3,95E-28

Hmga2	4,49E-32	0,55161589	0,851	0,276	1,34E-27
Map1lc3b	7,50E-32	0,91317876	0,995	0,978	2,25E-27
Dst	1,04E-31	0,54191571	0,995	0,828	3,12E-27
Tspan7	1,09E-31	1,25865635	0,827	0,299	3,26E-27
Psme2	1,19E-30	1,06387129	0,975	0,866	3,57E-26
Actg1	1,45E-30	0,7499885	1	1	4,34E-26
Itm2b	1,20E-29	0,93161459	0,98	0,91	3,59E-25
Ifitm1	2,46E-29	1,95120247	0,812	0,246	7,37E-25
Nupr1	4,52E-29	1,43703721	0,975	0,836	1,35E-24
Sod1	6,12E-29	0,52202188	1	1	1,83E-24
Gpx3	1,34E-28	2,04417272	0,941	0,791	4,01E-24
Gabarap	3,20E-28	0,96931892	0,921	0,716	9,60E-24
Slc39a1	4,08E-28	0,5915831	1	0,993	1,22E-23
Calm1	6,28E-28	0,7027382	1	1	1,88E-23
Myl6	4,29E-27	0,57941641	1	1	1,29E-22
Rragd	8,86E-27	0,66288465	0,842	0,336	2,66E-22
Wls	1,17E-26	0,82252815	0,911	0,56	3,51E-22
B2m	1,52E-26	1,51493566	0,916	0,731	4,54E-22
Fam213a	1,73E-26	1,09556098	0,926	0,619	5,17E-22
Atp1b1	1,82E-26	0,91784214	0,896	0,552	5,47E-22
Lgr4	2,18E-26	0,56670791	0,921	0,664	6,53E-22
Prdx2	4,01E-26	0,67401028	1	0,993	1,20E-21
Cd47	8,43E-26	0,89693545	0,851	0,388	2,53E-21
Selenbp1	9,92E-26	1,55033537	0,822	0,299	2,97E-21
Qdpr	2,02E-25	1,1678035	0,95	0,933	6,06E-21
Dhrs3	4,21E-25	1,24793831	0,752	0,239	1,26E-20
Scpep1	8,19E-25	0,91143314	0,995	0,873	2,45E-20
Hoxa9	9,06E-25	0,49926595	0,624	0,067	2,72E-20
Smagp	1,50E-24	0,8804039	0,941	0,746	4,48E-20
Scrn1	5,14E-24	0,66996105	0,693	0,142	1,54E-19
Hoxa11os	1,01E-23	1,11962637	0,554	0,015	3,03E-19
Gnas	2,02E-23	0,68356819	0,955	0,791	6,06E-19
Tspan1	2,07E-23	1,41309978	0,683	0,164	6,19E-19
Btg1	2,44E-23	0,49040461	0,881	0,53	7,30E-19
Hoxa10	3,20E-23	0,49531325	0,594	0,052	9,58E-19
Ociad2	5,37E-23	0,91790216	0,639	0,119	1,61E-18
Sorl1	7,55E-23	1,02546988	0,936	0,776	2,26E-18
Jak1	1,55E-22	0,64467868	0,96	0,851	4,65E-18
Rcn1	2,04E-22	0,60997468	0,832	0,448	6,12E-18
Lamp2	2,95E-22	0,65144797	0,866	0,634	8,84E-18
Map1b	9,71E-22	0,70113545	0,896	0,59	2,91E-17
Spp1	2,59E-21	2,56589822	0,723	0,261	7,77E-17

9. Publications

Langkabel, J., Horne, A., Bonaguro, L., Holsten, L. Hesse, T., Knaus, A., Riedel, Y., Becker, M., Händler, K., Elmzzahi, T., Bassler, K., Nico, R., Yeghiazarian, L.H., Pecht, T., Saglam, A., Ulas, T., Aschenbrenner, A.C., Kaiser, F., Kubaczka, C., Schultze, J. L. & Schorle, H. (**Accepted for publication**). Induction of Rosette-to-Lumen stage embryoids using reprogramming paradigms in ESCs. Nat Comm.

Langkabel, J., Horne, A., Bonaguro, L., Hesse, T., Knaus, A., Riedel, Y., Händler, K., Bassler, K., Reusch, N., Yeghiazarian, L. H., Pecht, T., Aschenbrenner, A.C., Kaiser, F., Kubaczka, C., Schultze, J.L. & Schorle, H. (2021). Induction of peri-implantation stage synthetic embryos using reprogramming paradigms in ESCs. BioRxiv 2021.01.25.428068. DOI: 10.1101/2021.01.25.428068

Kaiser, F., Hartweg, J., Jansky, S., Pelusi, N., Kubaczka, C., Sharma, N., Nitsche, D., **Langkabel, J.**, & Schorle, H. (2020). Persistent Human KIT Receptor Signaling Disposes Murine Placenta to Premature Differentiation Resulting in Severely Disrupted Placental Structure and Functionality. Int J Mol Sci. 21, 5503. DOI: 10.3390/ijms21155503

Kaiser, F., Kubaczka, C., Graf, M., Langer, N., **Langkabel, J.**, Arévalo, L., & Schorle, H. (2020). Choice of factors and medium impinge on success of ESC to TSC conversion. Placenta, 90, 128–137. DOI: 10.1016/j.placenta.2019.12.017

Schwarz, B. A., Cetinbas, M., Clement, K., Walsh, R. M., Cheloufi, S., Gu, H., **Langkabel, J.**, Kamiya, A., Schorle, H., Meissner, A., Sadreyev, R. I., & Hochedlinger, K. (2018). Prospective Isolation of Poised iPSC Intermediates Reveals Principles of Cellular Reprogramming. Cell stem cell, 23, 289–305.e5. DOI: 10.1016/j.stem.2018.06.013

10. Acknowledgements

Zuerst möchte ich meinem Doktorvater Prof. Dr. Hubert Schorle danken, der es mir ermöglicht hat, die Forschung für meine Dissertation in seinem Labor durchzuführen. Insbesondere möchte ich mich für das entgegengebrachte Vertrauen bedanken, das es mir ermöglicht hat, meine Ideen und das Projekt selbstständig und frei voranzutreiben und umzusetzen.

Darüber hinaus gilt mein Dank Prof. Dr. Marieta Toma für ihre freundliche Bereitschaft das Korreferat zu übernehmen. Ebenso danke ich Priv.-Doz. Dr. Reinhard Bauer und Prof. Dr. Pavel Kroupa für die Zusage zur Prüfungskommission als fachnaher und als fachfremder Gutachter.

Ein besonderes Dankeschön möchte ich an Arik Horne richten, für eine außerordentlich erfolgreiche wissenschaftliche Kooperation im Rahmen dieses Projektes. Intensive Diskussionen bis spät in die Nacht, tage- und nächtelange Auswertungen der bioinformatischen Datensätze und Figure Designs, die sich wortwörtlich über Wände zogen, haben dieses Projekt zu dem gemacht was es heute ist.

Auch bei meinen Kolleginnen und Kollegen der Pathologie möchte ich mich herzlich bedanken, für eine sehr freundschaftliche und angenehme Arbeitsatmosphäre. Gaby Beine möchte ich danken, dass sie mir mit viel mehr als Rat und Tat beiseite gestanden hat und mich durch alle Höhen und Tiefen der Arbeiten in diesem Projekt begleitet und unterstützt hat. Lena Arévalo, Gina Merges, Franziska Kaiser, Sina Jostes, Kai Funke und Simon Schneider möchte ich dafür danken, dass jedes experimentelle Problem von allen leidenschaftlich diskutiert und zumeist auch dadurch gelöst werden konnte. Angela Egert und Andrea Jäger danke ich für die Hilfe bei Zellkultur- und Mausarbeiten.

Meiner Familie danke ich für ihre Liebe und Unterstützung während dieser spannenden Phase meines Lebens. Judith möchte ich für ihre unerschöpfliche Geduld, Verständnis und Unterstützung danken.